BIOACTIVE CALCIUM PHOSPHATE COATINGS ON ZIRCONIA CERAMICS

Martin Štefanič

Doctoral Dissertation

Jožef Stefan International Postgraduate School

Ljubljana, Slovenia, June 2013

Evaluation Board:

Prof. Dr. Darko Makovec, Chairman, Jožef Stefan Institute, Jamova cesta 39, 1000 Ljubljana

Asst. Prof. Dr. Danjela Kuščer Hrovatin, Member, Jožef Stefan Institute, Jamova cesta 39, 1000 Ljubljana

Prof. Dr. Mihael Drofenik, Member, University of Maribor, Faculty of Chemistry and Chemical Engineering, Smetanova ulica 17, 2000 Maribor

MEDNARODNA PODIPLOMSKA ŠOLA JOŽEFA STEFANA
JOŽEF STEFAN INTERNATIONAL POSTGRADUATE SCHOOL

Martin Štefanič

BIOACTIVE CALCIUM PHOSPHATE COATINGS ON ZIRCONIA CERAMICS

Doctoral Dissertation

BIOAKTIVNE KALCIJEVE FOSFATNE PREVLEKE NA KERAMIKI IZ CIRKONIJEVEGA OKSIDA

Doktorska disertacija

Supervisor: Prof. Dr. Tomaž Kosmač

Co-supervisor: Asst. Prof. Kristoffer Krnel

Ljubljana, Slovenia, June 2013

Index

Abstract

This doctoral thesis describes the synthesis and characterization of calcium phosphate (CaP) coatings on zirconia ceramics. The main application of coated zirconia is in medicine, particularly in the area of dental bone implants. Due to the favourable biological characteristics of CaP, it can be expected that the application of CaP coatings on zirconia bone implants will improve the quality of the bone-implant interface and increase the lifetime of the zirconia implants.

The first part of my research was dedicated to the development of a biomimetic synthesis procedure for the deposition of CaP coatings on zirconia and to the characterization of the coating's composition and formation. The developed synthesis procedure involved two steps. In the first step, zirconia substrates were immersed in the supersaturated CaP solution with a pH = 7.4 and after 1 hour of soaking a thin (200 nm) calcium hydroxyapatite (HA) seeding layer formed on the zirconia substrates via three stages: i) precipitation of amorphous CaP; ii) precipitation of octacalcium phosphate (OCP); iii) transformation of OCP to HA. The subsequent immersion of these coated zirconia substrates in a fresh solution with a similar composition but a lower pH (pH = 7.0) led to the rapid growth of the biomimetic CaP coating with a lamellar topography (second step). After 11 hours of immersion in the second solution (pH=7.0) the thickness of the biomimetic CaP coating was 12 µm. The biomimetic CaP coating was composed of two compositionally distinct layers. The lower layer was composed of HA nanoparticles with an average size of 6 nm, while the upper layer was composed of lamellar octacalcium phosphate (OCP) monocrystals. The thickness of the biomimetic CaP coating increased with the immersion time in the second solution. The test of bioactivity with the simulated body fluid confirmed that the biomimetic CaP coatings are bioactive. Moreover, the results of different mechanical tests indicate, that the prepared biomimetic CaP coatings possess relatively low adhesion to the substrate, which could be a limiting factor for their application in clinics.

In the second part of my research I studied the influence of the thermal processing of biomimetic CaP coatings on their composition, dissolution rate and, in particular, on their

bonding strength to the zirconia substrate. Heating at 600 °C did not have any influence on the topography of coatings, but it promoted the phase transformation of the OCP crystals to HA and calcium pyrophosphate (CPP). The adhesion of the as-treated coating was only slightly higher compared to the biomimetic CaP coating. The dissolution rate of the coating heated at 600 °C was higher than the biomimetic CaP coatings. After heating the biomimetic CaP coatings at 800 °C and 900 °C they were composed of β-tricalcium phosphate (β-TCP) and β-CPP and after heating at 1100 °C and 1200 °C the β-TCP was the only phase present in the coating. When the coatings that were prepared by heating between 800 in 1200 °C were sonicated in an ultra-sound bath for a short period of time a majority of the coating was removed with only a thin β-TCP coating remaining on the zirconia substrate. As-prepared thin β-TCP coatings were the focus of my further research. The heating temperature influenced the topography and the thickness of thin β-TCP coatings, as well as their dissolution rate in a physiological solution. Moreover, various mechanical tests showed that thin β-TCP coatings possess excellent mechanical strengths and therefore the potential for applications in clinics.

Povzetek

Doktorsko delo obravnava sintezo in karakterizacijo kalcijevih fosfatnih (CaP) prevlek na površini gosto sintrane keramike iz cirkonijevega dioksida (ZrO_2). Glavna aplikacija tako modificirane keramike je v medicini na področju dentalnih keramičnih kostnih vsadkov. Zaradi primernih bioloških lastnosti je pričakovati, da bodo CaP prevleke izboljšale kakovost spoja med kostjo in vsadkom in posledično podaljšale življenjsko dobo keramičnih vsadkov.

Prvi del raziskav sem namenil razvoju biomimetičnega postopka za sintezo CaP prevlek na ZrO_2 podlagah in karakterizaciji sestave in zgradbe prevlek. Razvit sintezni postopek je vključeval dve stopnji. V prvi stopnji sinteze sem ZrO_2 substrate potopil v prenasičeno CaP raztopino s pH = 7.4 in po 1 h namakanja se je na njihovi površini tvoril tanek (200 nm) sloj kalcijevega hidroksiapatita (HA). Precipitacija HA je potekla v treh stopnjah: i) precipitacija amorfnega CaP; ii) precipitacija oktakalcijevega fosfata (OCP); iii) transformacija OCP v HA. V drugi stopnji sinteze sem ZrO_2 substrate s HA nanosi prenesel v svežo raztopino s podobno sestavo in pH = 7.0 (druga stopnja sinteze). Po 11 urah namakanja v tej raztopini se je na površinah ZrO_2 substratov tvorila 12 µm debela prevleka z lamelarno topografijo, ki je bila sestavljena iz dveh plasti. Spodnja plast je bila sestavljena iz HA nanodelcev s povprečno velikostjo 6 nm, zgornja plast pa je bila sestavljena iz lamelarnih OCP monokristalov. Debelina biomimetičnih CaP prevlek je naraščala s časom namakanja v drugi raztopini (pH = 7.0). Test bioaktivnosti s simulirano telesno tekočino je potrdil, da so prevleke bioaktivne, različni mehanski testi pa so pokazali, da je adhezija biomimetičnih prevlek relativno slaba, kar bi lahko omejevalo njihovo nadaljnjo uporabo v kliniki.

V drugem delu raziskav sem študiral vpliv termične obdelave biomimetičnih CaP prevlek na sestavo prevlek in na njihovo hitrost raztapljanja v fiziološki raztopini, največ pozornosti pa sem namenil izboljšanju adhezije CaP prevlek na ZrO_2 podlagah. Žganje pri 600 °C ni vplivalo na topografijo prevlek, prišlo pa je do fazne transformacije OCP kristalov v HA in kalcijev pirofosfat (CPP). Adhezija teh prevlek je bila nekoliko izboljšana v primerjavi z biomimetičnimi CaP prevlekami. Prevleke, obdelane pri

temperaturi 600 °C, so bile bolj topne v fiziološki raztopini kakor biomimetične CaP prevleke. Po žganju biomimetičnih CaP prevlek pri temperaturi 800 °C in 900 °C so bile prevleke sestavljene iz β-trikalcijevega fosfata (β-TCP) in CPP, po žganju pri 1100 °C in 1200 °C pa so bile sestavljene le še iz β-TCP. Če sem prevleke, ki so bile žgane v temperaturnem območju med 800 in 1200 °C, za kratek čas obdelal v ultrazvočni kopeli, je bila večina prevlek odstranjenih in na substratu je ostala le še tanka (500 nm–2 μm) prevleka, sestavljena iz β-TCP. Tako pripravljene β-TCP prevleke sem študiral v nadaljnjih raziskavah. Ugotavljal sem vpliv temperature žganja na topografijo in hitrost raztapljanja β-TCP prevlek v fiziološki raztopini. Z različnimi mehanskimi testi sem pokazal, da imajo β-TCP prevleke zelo dobro adhezijo, kar kaže na možnost njihove uporabe v kliniki.

Abbreviations

ACP = Amorphous calcium phosphate
AFM = Atomic force microscopy
ATZ = Alumina toughened zirconia
CaP = Calcium phosphate
CPP = Calcium pyrophosphate
CDHA = Calcium-deficient hydroxyapatite
FTIR = Fourier transform infrared spectroscopy
HA = Hydroxyapatite
NGIA = Near grazing incidence angle
NMR = Nuclear magnetic resonance
OCP = Octacalcium phosphate
PBS = Phosphate buffer saline
R_a = Average surface roughness
S_{dr} = Developed surface area ratio
SEM = Scanning electron microscopy
TEM = Transmission electron microscopy
TF-XRD = Thin-film X-ray diffraction
XPS = X-ray photoelectron spectroscopy
XRD = X-ray diffraction
Y-TZP = Yttria stabilized polycrystalline tetragonal zirconia
ZrO_2 = Zirconium dioxide
ZTA = Zirconia toughened alumina
β-CPP = Beta-calcium pyrophosphate
β-TCP = Beta-tricalcium phosphate

1 Introduction

1.1 Biomaterials

Biomaterial research is a multidisciplinary field that has grown exponentially during the past decades. It is a relatively “young” science existing only just a half century. A biomaterial can be defined as “material intended to interface with biological systems to evaluate, treat, augment, or replace any tissue, organ or function of the body” [1]. Biomaterials are in daily use in various fields of medicine and pharmacy. An important prerequisite for biomaterials to properly perform their function is the biocompatibility. Understanding and assessing the biocompatibility of materials is one of the key fields in the science of biomaterials. Various definitions have been proposed to describe the phenomena of biocompatibility. A commonly used definition is “the ability of a material to perform with an appropriate host response in a specific application” [1]. The subject of biomaterials resides at a multidimensional interface between chemistry, chemical engineering, materials science, mechanics, surface science, bioengineering, biology, and medicine, with considerable input from ethicists, government-regulated standards organizations, and entrepreneurs. Although medical implant materials have been used for at least 2500 years (some historians trace sutures back 32,000 years), most early medical implants were doomed to failure because important concepts relating to infection, materials, and the biological reaction to materials were not yet established [2]. The modern era of medical implants might be traced back to the end of 19th century and the beginning of 20th century when first in vivo experiments aimed at assessing the bioactivity of metals in animals were performed. Important milestones in the field were reached after World War II, when different novel biomaterials have been developed, such as polymeric intraocular lenses, metallic hip implant, vascular graft, kidney dialysis system, and the heart valve. These first biomaterials developed in an era before principles for medical materials were established, proved feasibility, saved lives, and evolved the foundations for the rapid development of the area of biomaterials later in the 20th century [1].

On the basis of the evolution of biomaterials research and their clinical availability during the last 60 years, three different generations of biomaterials seem to be clearly marked [3]: bioinert materials (first generation), bioactive and biodegradable materials (second generation), and materials designed to stimulate specific cellular responses at the molecular and genetic level (third generation). These three generations should not be interpreted as chronological, but conceptual, since each generation represents an evolution on the requirements and properties of the materials involved. This means that at present, research and development is still devoted to biomaterials that, according to their properties, could be considered to be of the first or the second generation. The materials that each new generation brings in do not necessarily override the use of those of a previous one [4].

Biomaterials can be classified by various criteria. According to their composition biomaterials can be classified as follows: 1) metals, 2) polymers, 3) ceramics, 4) composites and 5) biological materials [1]. Groups 1)–4) are synthetic materials while 5) are of biological origin. The biomaterials of biological origin can be further divided into four categories: 1) tissue transplants, 2) blood products, 3) processed human or animal originated products, such as demineralized bone matrix and 4) hybrid products.

1.2 Biomaterials for bone applications

No foreign material placed within a living body can be completely compatible to the biological surroundings with the notable exception of autografts, which are retrieved from the body itself. Any other foreign substance initiates a specific host-tissue response. With respect to bone-repairing materials, several classifications have been proposed based on their biocompatibility to bone [5–6]. A common property of these classifications is division of bone biomaterials to:

Bioinert materials. They are characterized by a distant osteogenesis with the formation of a thick fibrous tissue layer at the interface between the implant and the bone.

Bioactive materials. They exhibit improved biocompatibility and osseointegration and are characterized by the establishment of direct chemical bonds with the bone tissue and by the formation of a very tight and strong interface (direct osteogenesis). Such property is highly desirable for bone implants.

Typical representatives of both groups of bone biomaterials are listed in the Table 1.

.

Table 1. Typical representatives of bioinert and bioactive materials.

Bioinert materials	*Metals (Titanium and its alloys, Co-Cr-Mo alloys, stainless steel)* *Ceramics (zirconia, alumina, silicon nitride)* *Polymers (*poly(methyl methacrylate) *(PMMA), Polyether ether ketone (PEEK) polyethylene, polylactic acid etc.)*
Bioactive materials	Silicon based bio-glasses and glass-ceramics Calcium phosphates

The following mechanism was proposed to describe the phenomenon of bioactivity of implants after implantation in the bone tissue [7]:

- Local environment in the tissue around the implant becomes acidic because of the activity of immune cells and osteoclasts.
- Dissolution and re-precipitation of the material and subsequent formation of a hydroxyapatite layer on the surface of material. Proteins from surroundings adhere to newly formed apatite and attract cells and enable their adhesion and activity.
- Cells synthesize extracellular matrix (ECM) with adhesive proteins and collagen fibers, which start to mineralize.
- Incorporation of collagen fibers into the hydroxyapatite structure which enables strong connection between the bone and the material.

All bioactive materials are osteoconductive. Osteoconductivity is a property of a biomaterial that it serves as a scaffold for bone cells and promotes their proliferation, migration and differentiation. Moreover, newly formed bone tissue follows the shape of an osteoconductive material [8]. Some materials possess osteoinductive ability, i.e., they can induce de novo bone formation in an area where there is no vital bone, such as when implanted into the muscle tissue. Osteoinductivity is a highly desirable property for bone-repairing implants [9].

After implantation of a biomaterial into the organism a sequence of events occurs, which are summarized in Figure 1. At the initial step, proteins respond to the implant surface and form a thin film on the surface within few seconds. Cells adhere on the protein film and they proliferate and eventually organize themselves into various types of complex tissues. Therefore, the adsorption of proteins plays an important role at the tissue-implant interface. These proteins come from blood and tissue fluids at the wound site [10].

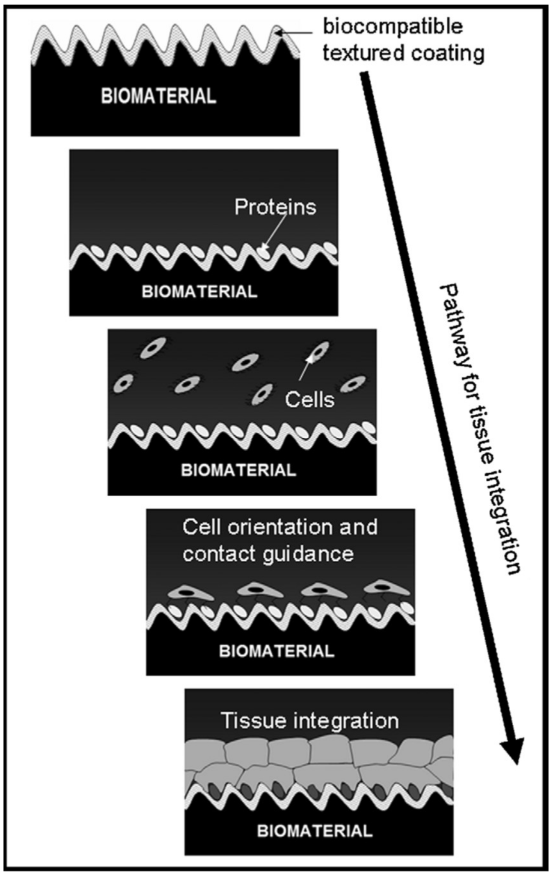

Figure 1. Illustration of the sequential reactions that take place after the implantation of a biomaterial into a living body [11].

1.3 Bioceramics

Ceramics are defined as nonmetallic, inorganic solids. They are prepared by the action of heat and subsequent cooling. Ceramic materials may have a crystalline or partly crystalline structure, or may be amorphous (e.g., a glass) [12]. During the evolution of the biomaterial science, ceramics have also been used for the repair of the human body due to the fact that they are biocompatible and possess some highly desirable characteristics for some applications, such as high hardness, flexural strength, abrasion resistance, corrosion resistance, aesthetic quality, bioactivity etc. Ceramics used for this purposes are called bioceramics. First in vivo report on the use of ceramics was in 1920 when Albee et al. [13] showed that calcium phosphate material could induce osteogenesis, and therefore he proposed their use in bone repair. Most clinical applications of bioceramics are related to the repair of the skeletal system, which is composed of bones, joints and teeth. Bioceramics are produced in a variety of forms and compositions and serve many different functions in repair of the body, which are summarized in Figure 2 [5].

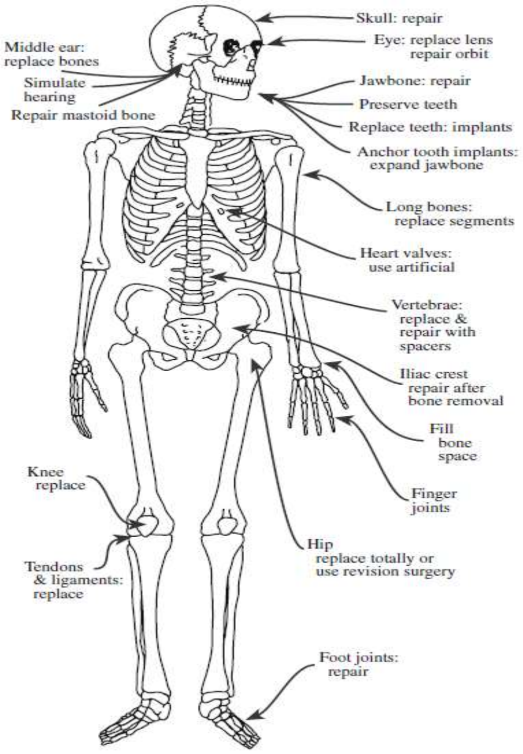

Figure 2. Illustration of the clinical uses of bioceramics for repair of the human body [14].

The use of ceramics in medicine is constantly increasing. Ceramic materials, which are mostly used in clinics, are zirconia, alumina and their composites (zirconia-toughened alumina (ZTA) and alumina-toughened zirconia (ATZ)), calcium phosphates and some glasses and glass-ceramics. These bioceramics possess different physico-chemical properties and are consequently used in different applications. In Table 2, the mechanical properties of different bioceramics are given.

Table 2. Mechanical properties of different bioceramics used in clinics [15].

Material	Toughness (K_{IC}; MPa $m^{1/2}$)	Flexural strength (MPa)	Vickers hardness
Alumina	4.2	400–600	2000
Zirconia	5.4	1000	1300
Hydroxyapatite	0.9	60	500
Tricalcium phosphate	1.3	60	900

The most widely used load bearing bioceramics in clinics are zirconia, alumina and their composites. They possess high mechanical strength and are biocompatible due to their chemical stability and undergo little or no chemical change during long-term exposure to the physiological environment. The surface inertness makes them an ideal candidate in situations where no interactions with the surrounding tissues are desirable, as in the case of dental abutments, crowns and bridges. On the other hand, chemical inertness can turn out as a drawback in the situations where strong interactions with the tissue are desirable, for example in the case of bone implants. As a result of surface inertness, there is no initiation of new bone formation around the implant. Rather than that, soft and non-adherent fibrous layer develops at the bone-implant interface. The main mechanism for the fixation of such ceramic implants in the bone thus remains mechanical interlocking, which is achieved by tissue ingrowth into undulating surface and surface irregularities. In some cases, the fibrous capsule can become several hundred micrometers thick and the implant can start loosening. Implant loosening sooner or later inevitably leads to clinical failure for a variety of reasons which includes fracture of the implant or the bone adjacent to the implant [7]. Such detrimental consequences, which have origins in the bioinert nature of the ceramic surface, can be circumvented by modifying the surface of inert bioceramics.

1.4 Surface modifications of load bearing bioceramics

Various studies have clearly correlated the clinical success of bone implants to their surface properties, i.e., surface topography and chemical composition [16]. Therefore, numerous studies have been focusing on the surface modifications of bone implants in order to improve their osseointegration. Optimal surface treatment of the implant could lead to faster and stronger bone formation around the implant, which may confer better stability during the healing process and thus allowing more rapid loading of the implant [16]. The surface topography relates to the degree of roughness of the surface and the orientation of the surface irregularities [17]. Regardless on the composition of the implant, the surface topography is considered as a critical component in achieving implant stability for sufficient osseointegration. For this reason, surface topography has been one of the main focuses of the scientific community working in the field of bone implants [16]. Surface topography has an influence on the adhesion, proliferation and differentiation of cells, their expression of local factors and on the biomechanical stability of the implant in the bone. The smooth or machined implant surfaces used in the past have been replaced by modified rough surfaces, which include topographic features in the millimeter to the nanometer range that are all believed to be relevant to the biological response of the host. In addition to surface topography, the quality of bone-implant interface has also been strongly associated with the surface chemistry, including surface chemical composition, crystallinity, free energy, charge, wettability and presence of impurities [18]. Surface chemistry strongly affects the adsorption of proteins, their conformation and consequently influences the cell and tissue response. Bone-bonding ability (bioactivity) is a result of material's specific surface chemistry. Numerous studies have focused on the modification of surface chemistry of high-performance ceramics, in order to prepare bioactive load bearing ceramics with improved stability in bone. An important advantage of implants with bioactive surfaces is that the biochemical attachment is more rapid compared to biomechanical fixation and it functions at a time when proper biomechanical bonding has not yet been developed. There are weeks of delay before bone starts growing into surface irregularities and bioactive surface can stabilize the implant before this event [17]. Various authors investigated the phenomenon of bioactivity and which materials can bond to living bone [19]. A common feature found at the interface between bioactive materials and the bone after in vivo tests was a thin hydroxyapatite layer. Kokubo's group made a significant contribution to the understanding of bioactivity. They proposed an in vitro experiment to reproduce the formation of a biological hydroxyapatite on the bioactive materials in vivo by immersing the material in the simulated body fluid (SBF) with the composition similar to the inorganic portion of the human blood plasma [19]. Despite the fact that experiments with SBF represent a big simplification of the real in vivo situation and that many authors expressed concerns regarding the method [20–21], it has been frequently used and became a widely accepted approach for testing the bioactivity of materials.

Studies on surface modifications of load-bearing bone implants have been mainly performed on metals [22], but much less work has been done on high-performance bioceramics. Surface modification techniques that have been applied to bioceramics can be divided in two parts: i) modifications of surface topography, and ii) modifications of surface chemistry. These two approaches of surface modification are commonly interrelated; for example, modifications of surface chemistry can alter the surface topography and vice versa. Hence, surface properties should be characterized in detail with appropriate and precise methods when studying the influence of various surface treatments on the biological response for correct interpretation of results.

1.4.1 Modifications of surface topography of bioceramics

Numerous studies have shown marked differences in the in vitro and in vivo responses to implants with different surface topographies, demonstrating that the ability of the implants to support bone formation can be enhanced by modifying the surface topography [23]. Surface topography can be divided into three levels according to the scale of the features: macro-, micro- and nano-sized. The macro level is meant here as topographical features being in the range of millimetres to tens of microns. This scale is directly related to implant geometry. The micro level determines the surface roughness in the range of 1–10 μm. This range of roughness maximizes the interlocking between mineralized bone and the surface of the implant. Nanometer range is considered below 100 nm. Surface profiles in the nanometer range play an important role in the adsorption of proteins, adhesion of cells and thus on the rate of implant osseointegration [24]. Numerous reports have shown that both the early fixation and long-term mechanical stability of the prosthesis is better in the case of rough surfaces compared to smooth surfaces. Rough surface enables bone ingrowth into small surface irregularities and enables biomechanical bonding. Thus osseointegration strongly depends on the strength of biomechanical bonding [17]. At a more fundamental level, surface topography affects protein adsorption and cell behaviour by inducing specific cell signals and consequently regulates the formation of extracellular matrix and bone apposition [23]. Animal trials with titanium implants have shown that a moderately rough surface with an average surface roughness (S_a) of about 1.5 μm and a developed surface area (S_{dr}) of about 50 % promotes better bone response compared to rougher or smoother surfaces [16]. The implants with higher roughness, i.e. more than 2 μm, have also shown good results, however, risks related to the higher roughness include increased incidence of peri-implantitis, increase in ionic leakage [17] and, in addition, excessive roughness can have the disadvantage of making the implant harder to remove if necessary, and may be detrimental for implant strength [23]. Texturing of the implant's surfaces at the nano-scale offers new possibilities for the manipulation of the biological response. It is believed that biological response to implant's surface could be improved by mimicking the nano-scale components of the extracellular matrix components of natural tissue. Various studies showed that nano-structured surfaces affect protein adsorption and conformation, improve cell attachment, decrease inflammation as well as accelerate wound healing and angiogenesis [25]. Furthermore, novel titanium implants that are supplied by world-leading manufacturers indeed exhibit a nano-roughness as a common property, which is absent in their commercial predecessors. Hence, a possible common mechanism behind the strong bone response to many new implants is a nano-roughness pattern. However, the optimal surface nano-topography for selective adsorption of proteins leading to the adhesion of osteoblasts and rapid bone apposition is still unknown [16].

Various methods have been developed in order to modify the topography of titanium implants, such as machining, sandblasting, titanium plasma spraying and chemical/electrochemical etching. Some of these surface modification techniques, in particular sandblasting and acid etching, have also been applied to high performance ceramics and clearly demonstrated that surface topography has a strong influence on the biological response to ceramics [26–34]. While abrasion and etching can easily be applied to metals, the comparatively high hardness and chemical stability of high performance ceramics renders this more difficult to achieve than in the case of metals. For this reason, alternative techniques are being developed for the surface modification of ceramics. One such innovative technique for preparation of rough and porous zirconia surface includes dipping of a pre-sintered zirconia implant in the zirconia slurry which includes a pore-former [35]. During subsequent sintering the pore-former is burned off and leaves a rough porous structure on the surface, while the core implant becomes fully dense. Using the above described procedure, Sennerby et al. [35] prepared zirconia implants with three different topographies and compared their osseointegration in the rabbit bone. The average roughness of implants with modified topography was $R_a = 1.24$ µm and $R_a = 0.93$ µm, while the untreated machined implants had $R_a = 0.75$ µm. Modified zirconia surfaces showed much stronger bone tissue response and 5-fold increase in resistance to removal torque compared to untreated machined surfaces after 6 weeks of healing in rabbit. In addition, bone integration of the modified implants was similar to commercial titanium implants. The results of the study suggested that surface modified zirconia implants can reach a firm stability in bone. Gahlert et al. [30] did an animal study aimed at evaluating the bone anchorage to machined ($R_a = 0.13$ µm) and sandblasted ($R_a = 0.56$ µm) zirconia implants in the pig model. After 4, 8, and 12 weeks of bone healing, removal torque testing was performed to evaluate the interfacial shear strength of each surface type. The results showed significantly higher removal torque values and quantity of bone apposition on rough zirconia compared with machined zirconia. This study confirmed the findings of Sennerby et al. [35] that rougher zirconia surface is preferential for bone anchorage. Recently, Hoffman et al. [31] compared bone healing and apposition around zirconia implants with different surface characteristics placed in rabbits. Zirconia implants with a) untreated, b) sandblasted, and c) laser treated surface were examined. After 6 and 12 weeks of healing, the trend of higher bone apposition on laser-modified surfaces was observed, however, the difference with other experimental groups was not statistically significant. Oliva et al. [36] reported a one-year-follow-up of zirconia implants in humans. They compared the osseointegration of implants with two different surface topographies: one group of implants had a surface roughness $R_a = 0.3$ μm while the second group was coated with a bioactive glass with the composition: Na_2O-K_2O-MgO-Al_2O_3-CaO-SiO_2-P_2O_5-F, and the surface roughness $R_a = 0.43$ μm. One year after implantation both groups of implants showed firm stability with no significant difference in the bone-to-implant contact. The overall success rate of implants was 98 %, which is comparable with the success rate reported for titanium implants. Nevertheless, this study focused only on differences in the surface topography. When comparing the two surfaces, difference in surface chemical composition should be taken into account since bioactive glass coatings could considerably affect the bone response solely on the basis of chemical composition. Park et al. [37] presented an innovative procedure for controlling the surface topography of zirconia implants using powder injection molding (PIM) technique. In the PIM process a suspension of ceramic particles and organic binders is used. The suspension is injected under low or high pressure into a mold which has a shape of the final product (negative), i.e. dental implant. Prior to sintering, the organic binders embedded in the molded parts must be removed via thermal pyrolysis or solvent detracting. It was shown that zirconia implant with controlled surface roughness can be prepared in the reproducible manner if the ceramic suspension is injected into the mold with a textured wall. Using such a procedure, two different ceramic implants with surface roughness $R_a = 0.5$ μm and 2 μm were prepared and tested, respectively. The implants were implanted into the rabbit bone and after a short period of healing time their osseointegration was investigated. While implants with roughness $R_a = 2$ μm showed much higher removal torque values compared to implants with smoother surfaces, there were no significant differences in the bone-to-implant contacts between the two implants. Study showed that PIM is an efficient technique for reproducible fabrication of implants with controllable surface topography. In addition, it is a cheap process and has a potential to be translated into a mass production. Laser treatments have also been applied to ceramics to modify the surface topography. For example, femtosecond laser treatment has been found as an efficient approach for microstructuring and nanostructuring of zirconia

[38–39]. Delgado-Ruiz et al. [38] presented for the first time that rapid femtosecond laser treatment can successfully modify the commercially available zirconia implants at micro- and nano-scale. Laser pulses could generate different surface patterns in a controlled manner, such as few micrometers big conical shaped holes and pyramidal grooves and nanometric polycrystal structures with the size of less than 100 nm. The R_a of dental implants could be enhanced from initial 1.58 µm of control implants to 2.43 µm for surfaces with holes, and up to 9.5 µm for surfaces with grooves. Moreover, laser ablation removed surface layers, which resulted in decreased concentration of contaminants, such as carbon and aluminium, and decreased the portion of the monoclinic zirconia phase. Both of these could significantly improve the performance of zirconia implants in vivo since it is known that surface impurities can affect biocompatibility and that monoclinic zirconia phase on the surface significantly decreases the mechanical properties and reliability of zirconia implants [40–41]. However, despite the encouraging results from the material point of view, there have not been any biological tests conducted so far to assess the influence of described surface topographical and chemical changes on the biological response. Another laser treatment that was found successful to roughen the surface of zirconia is CO_2 irradiation [42–43]. Surface roughness was increased linearly with increasing the laser power from the initial average roughness R_a = 0.295 µm of untreated samples to R_a = 0.305 µm (0.6 kW/cm^2), 0.333 µm (0.9 kW/cm^2), 0.717 µm (1.6 kW/cm^2), 1.882 µm (1.9 kW/cm^2) and 3.854 µm (2.5 kW/cm^2). Moreover, laser power also influenced on the surface microstructure of zirconia substrates. Furthermore, besides changing the surface topography, laser treatment also changed surface chemistry by increasing the number of –OH functional groups on the surface, which rendered the surface bioactive according to the SBF test. However, after 14 days of immersion only few apatite islands were observed on the surface which could indicate that laser treatment produced only certain areas with apatite-nucleating capacity. Several studies utilized in vitro cell culture tests and protein adhesion tests to evaluate the biological response at a more fundamental level and predict the clinical performance of materials. Although more reliable results can be expected from the in vivo investigations, in vitro tests clearly represent some benefits, such as faster and more convenient analysis, lower price, an ability to evaluate the biological response at a more fundamental level and being ethically less questionable than in vivo animal tests. Bachle et al. [29] studied how different zirconia surface topographies influence the response of Cal72 osteoblast-like cells. Zirconia substrates with three different surface treatments were used: machined surface

(R_a = 0.15 µm); sandblasted surface (R_a = 0.85 µm); sandblasted and HF acid-etched surface (R_a = 0.93 µm). Beside determination of the surface topography, other physico-chemical properties of the surface were not evaluated. The study revealed no significant difference in the behaviour of osteoblast-like cells on different surfaces. The initial adhesion and spreading of cells was good on all surfaces examined and cells showed similar vitality and proliferation rates on all surfaces. Even the non-treated machined substrates supported proliferation of cells. The authors concluded that cell attachment, morphology and proliferation were not affected by the topography of the substrate. Wang et al. [33] studied the response of osteoblasts to zirconia surfaces with different surface topographies, i.e. micro-rough surfaces with nanosized grains, micro-rough surfaces without nanosized grains and polished surfaces. SBF test of bioactivity showed that only the surfaces with nano-features had the apatite forming ability, suggesting that nano-features are essential for bioactive property. Similarly, the adhesion and proliferation rate of osteoblasts was significantly higher on those surfaces compared to micro-rough surface without nano-grains and polished surfaces. The authors concluded that combined macro- and nano-topography is favourable for implant osseointegration. In contrary to the results of Bachle et al. [29], this study showed difference in cell response, indicating that surface nano-features on zirconia have a significant impact on cell behaviour. Webster et al. [44] studied the protein adhesion and cell interactions with nanophase alumina ceramics. They prepared alumina substrates with 24, 45, and 167 nm sized grains. Ceramics with smaller grains and hence more grain boundaries exhibited higher roughness at the nanoscale and more hydrophilic character. Significantly higher amounts of serum proteins, collagen and vitronectin were adsorbed on nanophase alumina compared to conventional alumina. In addition, osteoblast adhesion was also statistically higher on alumina with smaller grains compared to coarser grained alumina. The results of higher vitronectin adsorption and higher osteoblast adhesion on nanophase ceramics supported earlier findings showing that vitronectin stimulates osteoblast adhesion. In contrast to osteoblasts, the fibroblasts and endothelial cell adhesion decreased with decreasing grain size. Ion beam assisted deposition (IBAD) technique was utilized for the preparation of transparent and nanocrystalline cubic and mixed phase zirconia films [45]. The coatings displayed ultrahydrophilic character and in vitro cell test showed that the growth and proliferation of bone marrow stromal cells on nanostructured zirconia coatings was enhanced compared with the conventional orthopaedic metallic and ceramic smooth surfaces. Moreover, it was also demonstrated that such coatings were superior even to bulk hydroxyapatite in terms of cell adhesion and growth. The same group also carried out computational analysis of the initial immobilization of one known structural fragment of the adhesive protein fibronectin and found out that the initial immobilization of the protein fragment on the nanostructured zirconia surface is achieved with much larger adsorption energy compared to the smooth surface. This difference is due to the strong attractive electrostatic interactions between the protein fragment and the nanostructured surface. In contrary, in the case of adsorption on the flat, uncharged surface this factor is negligible [46]. In another study [34], the response of SaOS-2 osteosarcoma cells on zirconia with two different surface topographies (sandblasted vs. sandblasted/acid-etched) and acid etched titanium surface was investigated. Both ceramics studied had surface roughness of about 1.1 µm. The behaviour of cells on both surfaces was very similar. While the adhesion rate was slightly higher on sandblasted surface, the differentiation rate was higher on sanblasted and acid-etched zirconia. Both surfaces showed improved osteoblast response compared to titanium.

1.4.2 Modifications of surface chemistry of bioceramics

Methods aimed at alteration of surface chemistry of bioceramics can be divided into three groups: chemical treatments, physical treatments and deposition of bioactive coatings.

1.4.2.1 Chemical treatments

Chemical treatments are aimed at applying functional groups on the surface of biomaterial and thus optimizing the surface chemistry. Studies on metal oxide gels and self-assembled monolayers (SAM) have shown that certain functional groups, such as OH, COOH, PO_4H_2, NH_2, have the apatite nucleation ability in SBF [47]. Chemical treatments, that have been so far applied to functionalize high performance ceramics include immersion in acidic and alkaline baths [48]. Hydroxylation of the surface was found as a very successful approach for the bioactivation of ceramics [42–43, 48–50]. During the hydroxylation treatments, additional OH groups are attached on the ceramic surface which increase the hydrophilicity, act as centers for apatite nucleation in SBF [48, 51] and promote cell attachment [42, 50, 52]. Uchida et al. [48] prepared bioinert nanosized ATZ composite with high strength and high fracture toughness and studied the possibilities of modifying the surface chemistry to induce apatite nucleation in SBF by soaking the materials in different concentrated and diluted alkaline and acidic solutions at 90 °C for four days, including H_3PO_4 (5 M and concentrated), H_2SO_4 (5 M and concentrated), HCl (concentrated) and NaOH (5 M and concentrated). All treatments applied were found successful and promoted apatite nucleation on the ATZ in SBF. The authors suggested that apatite nucleation occurred as a result of increased number of Al–OH and Zr–OH groups attached on the surface. In addition, the highest rate of apatite nucleation was observed on the substrates treated with 5 M H_3PO_4. This observation was explained with the hypothesis that the H_3PO_4 treatment resulted in the increased Zr/Al ratio on the surface, as detected with XPS and therefore in increased number of surface Zr-OH groups which are supposed to be more favourable for apatite nucleation than Al-OH, as already observed before in the study with metal-oxide gels [51]. Similar observation was made by Faga et al. [49] who studied the bioactive potential of chemically treated ATZ and ZTA composites. They adopted the procedure of Uchida et al. and applied various treatments with H_3PO_4 or NaOH with different concentrations at 80–100 °C for different times, in autoclave or under atmospheric pressure. The prepared samples were tested for bioactivity by immersing them in more supersaturated SBF (1.5X SBF) for four weeks. Only in the case of H_3PO_4 treatment of ATZ (80 wt.% zirconia) in autoclave for 4 hours, the ATZ specimens were able to induce apatite nucleation in concentrated SBF. XPS surface analysis of these samples did not detect any phosphate phase, the only observed difference was increased concentration of -OH groups. Another interesting observation was that apatite crystals grew more preferably on zirconia grains. This assumption agrees with the findings of Uchida et al. [48], giving support to the suggested existence of threshold percentage of zirconia in the alumina-zirconia composites for promoting apatite nucleation. Also worth mentioning here is that H_3PO_4 treatment did not cause any strength degradation due to low-temperature degradation of the ATZ composite. In another study [50], hydroxylation of alumina was achieved by soaking the substrate into 1 M NaOH solution at 100 °C for 24 hours, according to the following equation:

$$Al_2O_3 + 2NaOH + 3H_2O \rightarrow 2Na^+ + 2[Al(OH)_4]^- \qquad [1]$$

The as-treated alumina surfaces showed a pronounced effect on the activity of osteoblast-like cells. Cell proliferation, attachment and osteocalcin expression were significantly higher on the treated alumina compared to the non-treated one. Mechanical tests showed that aggressive treatments with NaOH had no deteriorating effect on the short- and long-term mechanical behaviour of the ceramic material. Heat treatment in NaOH solution was also found successful in the case of porous ZTA ceramics [52]. NaOH treatment resulted in increased proliferation of MG63 osteoblasts and alkaline phosphatase activity. Both studies showed that subjection of ceramics to the hot alkaline bath results in hydroxylation of the surface which elicits favourable cell response [50, 52]. Nevertheless, it is not known whether the as-treated surface has apatite nucleation ability in SBF. Also other functional groups have been conjugated to ceramics beside -OH groups by utilizing chemical treatments. Bertazzo et al. did studies on carboxylation of alpha- [53] and gamma-alumina surfaces [54–55]. Treatments included different carboxylic acids. When the alumina substrate was immersed in the dicarboxylic acid, carboxylato aluminoxane was formed on the surface [53–54]. Such treatment resulted in a very reactive surface which was able to induce nucleation of large elongated sharp-edged crystals in SBF already after 6 hours. In contrary, no crystal precipitation occurred on the non-treated specimens. The authors explained that bioactivity was achieved through the formation of free carboxyl groups on the surface of alumina which complex calcium ions from the SBF solution, thus forming nucleation sites on the surface of the sample. In addition, in vitro cell culture test showed that the viability of pre-osteoblasts was significantly higher on alumina substrates treated with carboxylic acid compared to the non-treated ones. Nevertheless, it is worth mentioning that the shape of the deposited large crystals on the treated alumina was very different from the nanocrystalline biological-like deposits that are usually observed on bioactive materials when immersed in SBF. Although the EDS analysis confirmed the presence of Ca and P elements on the treated alumina surface, the obtained Ca/P ratio of these crystals was much higher than in the case of biological-like CaP crystals that usually precipitate from the SBF and have a Ca/P ratio between 1.33–1.67. Unfortunately, the authors did not perform any analysis to get information about the phase composition of the deposits on alumina.

1.4.2.2 Physical treatments

Physical deposition methods, such as ion implantation, UV treatment, CO_2-irradiation and laser treatments have been applied to modify the surface chemistry of bioceramics in order to make it bioactive. CO_2 irradiation has been used as a method for the bioactivation of magnesium-partially stabilized zirconia (Mg-PSZ). CO_2 laser caused surface melting of Mg-PSZ and exposed Zr^+ and OH^- ions which created Zr-OH groups on the surface. As a consequence, surface wettability was improved. Laser treatment improved the bioactivity of Mg-PSZ and, in contrary to non-treated ceramics, apatite crystals formed on Mg-PSZ after 14 days of immersion in SBF. In addition, cell tests showed that osteoblasts had improved adhesion on the laser treated samples compared to untreated samples. Laser treatment also changed the topography of zirconia which could also have a major influence on the cell behaviour. Ion implantation, which has been studied in several works, resulted in the significant improvement of the biological response to alumina, zirconia and hydroxyapatite ceramics [56-59]. Zreiqat et al. [58-59] studied the implantation of magnesium ions in alumina ceramics by using metal vapour vacuum arc (MVVA) ion source. In vitro tests with human bone derived cells revealed that Mg incorporation in alumina ceramics significantly improved the initial adhesion and differentiation of cells by increasing the expression of bone related proteins, such as integrin receptors, focal adhesion kinase, collagen type I and intracellular signaling molecules [58-59]. In another study, Mg^{2+} implantation in ZrO_2 ceramics resulted in the apatite forming ability of zirconia after immersion in the SBF [56, 60]. Zhao et al. demonstrated that ion implantation can also be applied to graft $-NH_2$ groups on the surface of alumina. In further in vivo tests they compared the healing and osseointegration of NH_2^+ treated and bare, non-treated, alumina implants in the jaw bone of dogs [57]. Results have shown that NH_2 groups on the surface of alumina clearly accelerate the healing time and enhance the bone deposition around the implant, making the Al_2O_3 ceramic implants more biocompatible to surrounding tissue. Att and co-workers [61] examined the effect of ultra-violet (UV) light treatment of zirconia on the biological response of osteoblasts. Inspired by the previous studies, which demonstrated the ability of UV treatment to prepare superhydrophilic TiO_2 surface [62] and to significantly improve the osseointegration of titanium implants [63], the authors hypothesized that UV treatment will have a similar effect on zirconia and will promote cell's bioactivity. UV light treatment improved the wettability of zirconia surface from hydrophobic to hydrophilic and reduced the atomic percentage of surface carbon in a UV light dose-dependent manner. These photo-generated surface changes increased the capacity of zirconia for attachment, spread, proliferation and alkaline phosphates (ALP) activity of rat bone marrow-derived osteoblasts and enhanced their mineralization capacity.

1.4.2.3 Bioactive coatings on bioceramics

Bioactive materials, such as calcium phosphates (CaP) with compositional resemblance to bone mineral, as well as certain formulations of glasses or glass-ceramics, show excellent biological properties. After implantation in a bone tissue, they can elicit specific biological responses which result in the formation of chemical bonds between the tissue and the material. These bioactive materials can be applied as coatings onto the surface of stronger but bioinert ceramics and act as intermediary layer that enables better fixation of the implant in the bone [7]. Essential requirements for the bioactive coatings on load-bearing bone implants are the formation of a firm interface with a bone tissue and a sufficient mechanical stability to withstand the mechanical forces present during implantation in the bone. In addition, coatings should present controlled dissolution rate in body fluids and possibly act as a drug delivery system.

1.4.2.3.1 Calcium phosphate coatings

Calcium phosphate chemistry, biological properties and applications in medicine are described in section 1.4. The aim of this section of the Introduction chapter is to summarize different achievements in the area of CaP coatings on ceramics.

One of the techniques studied for the deposition of CaP coatings is the wet-chemical biomimetic method. More information about this method is given in the section 1.4.3.1.

Cortes et al.[64] studied the formation of a biomimetic hydroxyapatite on Mg-PSZ/Al_2O_3 composite in SBF developed by Kokubo et al. [65]. Their study revealed that apatite nuclei form on zirconia composite after 21 days of immersion, however, when the solution was not renewed, apatite coating did not form. In contrary, if the substrate was re-immersed into the fresh and more concentrated SBF, a 20 μm thick apatite coating precipitated on the Mg-PSZ/Al_2O_3 after 7 days of immersion. Rambo et al. [66] prepared highly porous Al_2O_3 scaffold from natural cellulosic sponges via pyrolysis and Al-vapour phase infiltration. Afterwards, they applied a two-step procedure and used two five times more concentrated SBF (5X-SBF) as the reaction solutions for deposition of a hydroxyapatite coating on Al_2O_3 porous scaffold. In the first step the Al_2O_3 samples were immersed in 5X-SBF for 24 hours in order to trigger precipitation of CaP coating. Such pre-coated porous bodies were then soaked for 72 hours in the second 5X-SBF solution, which had lower concentration of Mg^{2+} and HCO_3^- ions and consequently enabled faster precipitation of biomimetic hydroxyapatite coating. Klopcic et al. [67-68], who adopted a modified biomimetic procedure developed by Bigi et al. for titanium substrates [69], studied the deposition of CaP on alumina and zirconia ceramics. The procedure was effective to deposit thin hydroxyapatite [67] or octacalcium phosphate [68] coating on alumina and zirconia ceramics. The coatings were able to induce apatite nucleation in SBF in a short period of time. However, the prepared coatings had very poor mechanical strength and were easily removed from the substrate using the scotch-tape test. When the

OCP coatings were subjected to a heating at 1050 °C, the adhesion of the coating was improved, which was also accompanied by the transformation of the OCP phase to the HA. Despite several advantages of the biomimetic CaP coatings, a major drawback that is limiting their application in clinics remains poor mechanical strength.

Jiang et al. [70-71] prepared HA coating on porous alumina scaffold using thermal decomposition method. Firstly, they deposited a hydroxyapatite precursor layer on alumina by utilizing a precursor solution [70] or suspension [71] which was followed by a thermal treatment to remove organic parts and obtain thin and nanocrystalline layer of stoichiometric hydroxyapatite. Using such a procedure, they were able to obtain homogenous coating over the entire surface and also in the pores of the alumina scaffold. In addition, the coatings induced apatite nucleation in SBF and simple tape test indicated on the good adhesion of the coating to the alumina substrate. Sol-gel method was used to deposit flour-hydroxyapatite (FHA) coatings on zirconia [72]. The coating procedure included spin-coating of the FHA sol on zirconia and heating between 400 and 800 °C. The prepared FHA coatings had uniform and dense morphology and the coatings heated above 500 °C had very strong adhesion strength of around 70 MPa. In addition, proliferation of MG63 cells was similar to the plastic control. When the CaP coatings on substrates are exposed to high temperatures, this can lead to poor mechanical stability of the coating due to thermal stress caused by the difference of thermal expansions between the CaP coating and the substrate. Therefore, an idea of applying gradient hydroxyapatite-glass coating was introduced to circumvent this problem. The coating was prepared on α-Al_2O_3 ceramic substrate by a multi-layer slurry-dipping and sintering at 1100 °C [73]. The coating composition varied gradually, in which hydroxyapatite content increased and glass content decreased gradually from the interface to a surface layer. Prepared coatings showed good biological response in rats, had very good tensile strength and no cracking occurred at the substrate-coating interface or within the coating. However, the procedure for the preparation of the coating is rather time consuming since sintering of the substrate is needed after each slurry dipping. An interesting approach was suggested by Suzuki et al. [74] who deposited a Ti-HA composite coating onto a zirconia femoral component of the cementless type for total knee arthroplasty. The composite coating was prepared by firstly arc spraying 500 μm thick and macro porous titanium layer on zirconia onto which a 50 μm HA layer was then flame sprayed. In vivo tests, performed on beagle dogs, showed improved osseointegration of the coated zirconia implants compared to non-coated ones. Improved osseointegration supposed to be achieved by macro-porous structure of Ti which enabled mechanical interlocking of the implant in the bone and osteoconductive behaviour of HA which enhanced the bone ingrowth into the pores and grooves of the implant. Rochietta et al. [75] evaluated whether CaP coatings on zirconia can improve osseointegration of topographically altered zirconia implants when implanted in rabbits. They applied two different CaP coatings. One type was composed of 20 nm thick layer of nanostructured HA crystals, which were prepared by dipping the zirconia implants into a solution which contained HA nanoparticles, followed by drying and heating at 700 °C. The second type was composed of 150 nm thick and dense CaP coating which was obtained by sputtering. To assess the osseointegration of different surfaces, they measured removal torque and bone-to-implant contacts in rabbit femur and tibia. Results showed that CaP coatings did not significantly improve the final outcome in terms of strength and the speed of osteoconductivity. In a similar study, Lee et al. [76] compared the osseointegration of micro-structured zirconia implants with and without CaP coatings and commercially available titanium implants TiUnite^{TM} in a rabbit trabecular bone model. Micro-structured surfaces on zirconia were prepared according to the already described procedure [35], which included spraying of a slurry including zirconia powder and a pore-former onto a pre-sintered zirconia ceramic implant. Afterwards, the slurry-coated implant is sintered to full density and during sintering, the pore-former is burnt away, leaving a porous coating on the core implant. In addition, two different kinds of CaP coatings were applied onto a ceramic implant (coatings A and C), both composed of a nanocrystalline hydroxyapatite particles. In fact, coating C was prepared in the same manner as in the study of Rocchietta et al. [75]. After 3 weeks of healing, the CaP-coated ceramic implants showed statistically lower osseointegration compared to titanium implants. There were no statistically significant differences in osseointegration following a 6-week healing interval. Study showed that thin nanocrystalline CaP coatings on zirconia implants do not enhance the bioactivity of zirconia implants.

Available results of the in vivo trials do not indicate the superior osseointegration of CaP-coated ceramic implants compared to the non-coated ones. Nevertheless, due to the limited number of in vivo studies performed and types of CaP coatings tested, it is not possible to draw any conclusions about the usefulness of CaP coatings on high performance ceramics. In addition, since positive effects of CaP biomaterials on in vivo bone formation and healing have already been well-reported, CaP coatings remain a promising approach for bioactivation of inert bioceramics.

1.4.2.3.2 Bioactive glass and glass-ceramic coatings

Bioactive glasses and glass ceramics have been extensively studied since the early 1970's when Hench et al. [7] discovered that some glasses in the system SiO_2-CaO-Na_2O-P_2O_5 form direct contact with bones and soft tissues without any rejections of the body. They proposed a twelve-step model to describe interfacial reactions between bioactive glasses and bone that lead to the formation of bonds and a tight contact. Their findings led to development of second generation of biomaterials [7]. Later, various different bioactive glass and glass-ceramic formulations have been developed and studied in order to tune their bioactivity and adjust their properties for specific applications. Nevertheless, nowadays commercially available bioactive glasses are still based on mixtures from the SiO_2–CaO–Na_2O–P_2O_5 system. While in the past, bioactive glasses have been mainly produced by means of standard melting techniques, recently great attention has been focused on glasses, obtained by sol-gel methods. Sol-gel procedure makes it possible to produce glasses with compositions unobtainable via conventional melting and which are bioactive in a wider range of compositions. In addition, sol–gel glasses can be produced with a strictly controlled porosity, which makes them very promising for specific biomedical applications [77]. Bioactive glasses and glass–ceramics have been clinically employed mainly in non-load-bearing applications, such as middle ear implants, endosseous ridge maintenance implants, as particulates for bone regeneration and as active agents in tooth pastes for reduction of tooth sensitivity [78]. Due to their favourable biological properties, they also show a great potential to act as coatings on inert load-bearing ceramic implants and improve their osseointegration. However, despite their potentialities, bioactive glass coatings are not used in clinics. The most studied techniques for fabrication of glass coatings are enamelling and thermal spraying [7]. Beside them other techniques are also being under investigation, such as rapid-immersion coating [7], electrophoretic [79] and sol-gel [80] deposition, grit blasting [81], laser cladding [82], pulsed laser deposition [83] and particle vacuum infiltration [84]. However, only few of them, such as enameling [7, 85-92] and dip-coating [72, 93] route have been applied for coating ceramic substrates with bioactive glass and glass-ceramics. Enameling is a traditional technique for production of glass coatings. This process is relatively simple and cheap and enables good control over the thickness of coatings. During the enameling procedure, a thin piece of glass or a suspension containing the glass powder is deposited onto the substrate. Subsequently, the glass is glazed by a proper heat treatment. The temperature of the glazing process must be carefully set in order to avoid the crystallization of glass and cracking of the coating [77]. Most of the bioactive glasses have a thermal expansion coefficient much higher than that of high-performance ceramics, such as alumina or zirconia. For this reason, a considerable residual tensile stress is induced in the glass coating upon cooling, resulting in a crack formation and insufficient adhesion at the interface. This problem can be avoided by increasing the content of silica in the glass and reducing the thermal expansion coefficient. However, this can lead to two drawbacks. Firstly, a window of glass composition is markedly reduced. It is known that glass with a too high concentration of silica has a reduced bioactive capacity. Secondly, increased silica content requires higher heating temperatures which can result in ion exchange between the glass and the ceramic substrate and consequently this can lead to undesirable changes in the glass composition which can adversely affect its bioactivity. For example, in the case of bioactive glass coating on alumina ceramic, only a small amount of alumina (1.5 wt.%) in a glass can result in a bioinert character of the glass [90]. In addition, high processing temperature can result in the formation of chemical by-products at the ceramic-glass interface which may reduce the coating adhesion [77]. Enamelling was used to coat zirconia and alumina with bioactive phosphosilicate glass and glass ceramics AP40 and RKKP with composition in the system SiO_2–β-$Ca_3(PO_4)_2$–CaO–Na_2O–K_2O–MgO–CaF_2 [85, 88-90]. In order to prevent coating cracking due to the thermal coefficient mismatch between the glass coating and the ceramic substrate, additional zirconia-glass composite layer was introduced at the interface [89-90]. By finding the optimal heating regime, they could prepare homogenous and crack-free coatings with good adhesion and without residual porosity. *In vitro* and *in vivo* biological tests on AP40 and RKKP coatings revealed that coatings induced apatite nucleation in SBF, increased serum protein adsorption, enhanced adhesion, spreading and growth of fibroblasts and osteoblast-like cells [87, 94], improved the metabolic activity of both healthy and osteopenic primary osteoblasts and induced higher bone apposition in rats compared to non-coated ceramics. Rahaman et al. [86] used enameling approach to coat Mg-stabilized zirconia (Mg-PSZ) with silicate-based glass, designated as 13–93 and 6P68, and borate-based glasses, designed as H12, which have similar thermal expansion coefficient as Mg-PSZ substrate. Thus, they could obtain crack-free glass coatings without the need of applying additional intervening layer on the substrate. The 6P68 glass provided the highest adhesive strength (40 ± 2 MPa) but the in vitro test showed that it had very limited bioactivity, whereas the H12 glass had lower adhesive strength (18 ± 2 MPa) but the highest bioactivity. In order to prepare the coating with optimum adhesion strength and bioactive properties, they successfully developed a functionally graded coating, consisting of 6P68 interfacial layer and an H12 surface layer. Kim et al. [72] deposited composite coatings of a $CaO–Na_2O–P_2O_5$ glass and HA particles on zirconia disks. Their coating procedure included dip coating of substrate in the HA-glass slurry, drying and heat treatment. They investigated the effects of glass compositions, mixing ratios of glass to HA, and heat treatment temperatures (800 °C, 900 °C, 1000 °C) on the coating properties. Coatings with the high amount of glass phase (50 wt.%) reached the highest values of tensile strength of 40 MPa, which was 80 % higher than the adhesion of pure HA coatings (22 MPa). The osteoblast-like cells grew and spread actively on the composite coatings. The proliferation numbers and alkaline phosphate (ALP) activities of the cells on the composite coatings were improved by 30 %–40 % when compared to bare zirconia substrates. Dip coating was also found successful to coat alumina disks with sol–gel derived 58S bioglass, with the composition of 58 mol% SiO_2–38 mol% CaO–4 mol% P_2O_5 [93]. Alumina specimen was dipped into a 50 wt. % 58S bioglass suspension for 5 min. After drying and firing at 1200 °C for 1 h, a bioglass coating with a thickness of 200–300 μm was formed on the alumina specimen. Although the thermal expansion coefficient of bioglass was lower compared to alumina substrate ($0.73 \cdot 10^{-6}\ °C^{-1}$ vs. $9.47 \cdot 10^{-6}\ °C^{-1}$), the resultant thermal stresses could be relaxed due to softening of the glass and the obtained bioglass coating was adherent and crack-free. Concerning the biological tests on glass and glass-ceramic coatings on bioceramics, there have not been many in vitro and in vivo tests performed. Beside the above mentioned in vitro [87-88] and in vivo [95] tests, there have also been two case-reports on the in vivo performance of apatite-mullite glass-ceramics coated zirconia implant compared to untreated and acid-etched commercial zirconia implants in humans [36, 96]. The prepared surfaces had different surface roughness: uncoated zirconia (R_a = 0.62 μm), apatite-mullite glass-ceramics coating (R_a = 0.92 μm), acid etched surface (R_a = 1.16 μm). The highest implant success rate was observed for acid-etched implants (97.5 %) while there have not been any statistical differences in the success rate of glass-ceramics-coated (93.6 %) and uncoated (92.8 %) zirconia implants. The authors proposed that higher surface roughness of acid-etched implants was the main reason for their superior success.

1.4.2.3.3 Other approaches for modification of surface chemistry of bioceramics

Schickle et al. [97] reported on an innovative method for introduction of different functional groups on the alumina ceramics using tailored self-assembled monolayer (SAM) technique. The method included three steps. Firstly, silane groups were attached on the surface by using PVD or spray pyrolysis. These reacted with octenyltrichlorosilane (OTS) SAM with $CH=CH_2$ functional groups that were introduced by immersing the samples in 5 % ethanol solution of OTS. In the last step, –OH or –COOH groups were coupled on the –CH=CH2 groups by applying further chemical treatment. Unfortunately, no biological tests have been conducted to evaluate the prepared surfaces. Vargas et al. [98] fabricated thin silica coatings with micropatterned pillars on zirconia. Their fabrication strategy combined sol-gel synthesis of silica coatings and subsequent patterning of the coatings using soft lithography. The Alamar blue assay showed that the viability of MG63 osteoblast-like cells was higher on zirconia with flat or micropatterned silica coatings compared to bare zirconia substrates. Higher viability of cells was explained with higher silicon content since the topography of silica had no influence on the biological response. Leivvo et al. produced different $3Al_2O_3$–$2SiO_2$ coatings on α-alumina substrates using sol-gel synthesis. Prepared sol-gel coatings were either amorphous or contained nanosized mullite crystals. In addition, coatings of thermally sprayed aluminosilicate and diphasic γ-alumina–silica nanosized colloids were prepared. Despite the differences in physical and chemical structures among individual alumina-silicate coatings, cell culture testing by rat osteoblasts showed good biocompatibility to all tested coatings. Recently, Liu et al. [99] reported on a study, which examined the possibility of improving the biocompatibility of zirconia by coating it with 3,4-dihydroxy-L-phenylalanine (L-DOPA) film. Previous studies showed that L-DOPA is an important molecule secreted by marine mussels for the formation of adhesive pads. The bio-inspired L-DOPA film altered the chemical properties of the zirconia surface considerably without affecting its topography. Moreover, the L-DOPA coating also outperformed uncoated zirconia in osteoblast responses, including cell adhesion, cytoskeleton development, and cell number increase.

1.5. Calcium phosphates

Calcium phosphates (CaP) represent an important group in the field of bioceramics and biomaterials research and they are used for a variety of different applications in medicine, including all areas of the skeleton repair and replacement. CaP comprise the largest group of biological minerals in vertebrate animals. They also have many uses in industry, medicine and everyday life. CaP are salts of the tribasic orthophosphoric acid, which include $H_2PO_4^-$, HPO_4^{2-} or PO_4^{3-} ionic species. The CaP containing HPO_4^{2-} and PO_4^{3-} generally constitute the biologically relevant calcium phosphates. The exceptions in the group of biologically important CaP are calcium pyrophosphates (CPP), which are salts of calcium and polyphosphates. The CaP salts constitute a wide group of compounds [100]. Table 3 summarizes the chemical name, the formula, calcium to phosphorus ratio (Ca/P) and the abbreviation of some CaP compounds.

Table 3. Chemical names, compositions, Ca/P ratios and abbreviations of some CaP compounds.

Name	*Formula*	*Ca/P ratio*	*Abbreviation*
Monocalcium phosphate	$Ca(H_2PO_4)_2$	0.5	MCP
Dicalcium phosphate dehydrate (brushite)	$CaHPO_4 \cdot 2H_2O$	1	
Dicalcium phosphate anhydrous (monetite)	$CaHPO_4$	1	DCPA
Calcium pyrophosphate	$Ca_2P_2O_7$	1	CPP
Octacalcium phosphate	$Ca_8H_2(PO_4)_6 \cdot H_2O$	1.33	OCP
β-tricalcium phosphate	$Ca_3(PO_4)_2$	1.5	β-TCP
Calcium hydroxyapatite	$Ca_{10}(PO_4)_6OH_2$	1.67	HA
Tetracalcium phosphate	$CaO \cdot Ca_3(PO_4)_2$	2.0	TTCP

CaP salts differ in their composition and crystal structures, leading to specific physico-chemical properties. Most of calcium phosphates are sparingly soluble in water, and some are very insoluble, but all dissolve in acids.

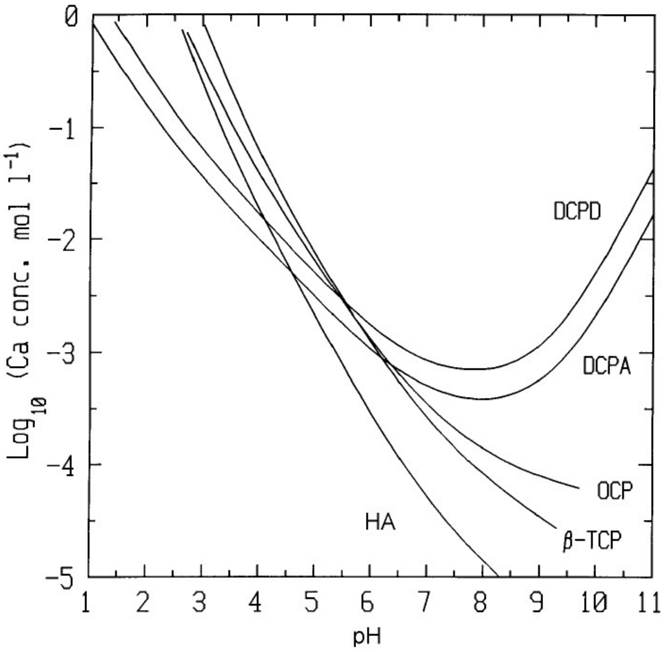

Figure 3. Solubility isotherms of some CaP compounds at 37 ºC and 1 atm [100].

The diagram in the Figure 3 indicates the thermodynamical stability at 37 ºC of various CaP phases. Besides thermodynamic stability, an important factor to consider is the kinetics of formation, which can dictate the formation of a thermodynamically less stable CaP phase. The solubility of calcium phosphates decreases with increasing temperature and pH [100]. The diagram displayed in Figure 3 shows that HA is the most thermodynamically stable phase at physiological pH.

1.5.1 Calcium phosphates of biological importance

1.5.1.1 Calcium hydroxyapatite

Calcium hydroxyapatite (HA) belongs to the general and wide apatitic group, represented by the formula: $Me_{10}(XO_4)_6Y_2$, where Me is a divalent metal (Ca, Sr, Ba, Pb…), XO_4 is a trivalent anion (PO_4, AsO_4, VO_4…), and Y is a monovalent anion (F, Cl, Br, I, OH…). Stoichiometric HA is represented by the chemical formula $Ca_{10}(PO_4)_6OH_2$ and has Ca/P ratio of 1.67. The HA crystal structure has a hexagonal lattice and has been described in the space group $P6_3/m$. HA crystal structure has a strong ability to form solid solutions, and to accept numerous substitutions. In nature, no pure form of HA can be found: substitutions for Ca^{2+} (Sr^{2+}, Ba^{2+}, Mg^{2+}, K^+, Na^{2+},$Fe3^{2+}$), $PO4^{3-}$ ($AsO4^{3-}$, $CO3^{2-}$, $VO4^{3-}$), and OH^- (F^-,$CO3^{2-}$, Cl^-, Br^-) all occur [101]. The ionic substitutions affect the lattice parameters and consequently influence the physico-chemical properties of crystallites, e.g., crystal size, surface area and dissolution. Indeed, stoichiometric HA does not occur in biological systems. Biological HA that forms a human skeleton is nonstoichiometric, calcium deficient HA with carbonate substitution (wt. % vary between 3 %–8 %) and trace substitutions with sodium, chlorine, potassium, and magnesium. Calcium deficient hydroxyapatite (CDHA) has a Ca/P ratio lower than 1.67, usually between 1.5–1.61, although there have been reports of CDHA with Ca/P ratio around 1.33 [100]. In relation to stoichiometric HA they are characterised by a) incorporation of HPO_4^{2-} ions in the crystal lattice; b) larger dimensions of the crystal lattice due to HPO_4^{2-} incorporation; c) higher dissolution; d) formation of calcium pyrophosphate and β-tricalcium phosphate upon ignition above 300 °C and 700 °C, respectively.

1.5.1.2 Octacalcium phosphate

Octacalcium phosphate (OCP, $Ca_8H_2(PO_4)_6 \cdot 5H_2O$) crystals are triclinic, space group P1. They consist of alternating "apatite layers", where the arrangement of calcium and phosphate groups is similar to that of the HA, and the "hydrated layers", which correspond to the structure of dicalcium phosphate dihydrate (DCPD or brushite, $Ca(HPO_4) \cdot 2H_2O$) with two additional water molecules. These two layers are linked to each other's by Van der Walls and hydrogen bonds. As a result of such layered crystal structure, OCP crystals preferentially grow in (100) direction and form thin lamellas. OCP often occurs as a transient intermediate during the wet-chemical precipitation of the thermodynamically more stable HA. Moreover, OCP is believed to be a precursor of biological HA in the process of mineralization and formation of hard tissues in vertebrate animals [8].

1.5.1.3 β-tricalcium phosphate

β-tricalcium phosphate (β-TCP, $Ca_3(PO_4)_2$) has a rhombohedral crystal structure with a R3c space group. Pure β-TCP is not found in biological systems, but Mg-substituted β-TCP is found in nature and occurs in some pathological calcifications [100]. β-TCP cannot be precipitated from aqueous solutions. It can be obtained by thermal treatment of amorphous CaP, OCP or CDHA at temperatures above 700 °C [8, 102]. As seen from Figure 3, it is more soluble compared to HA at physiological pH. The β-TCP phase is thermally stable at temperatures below 1125 °C. Above 1125 °C, β-TCP transforms into α-TCP. α-TCP has a monoclinic crystal structure. It is known as high-temperature stable form. Its stability region ranges from 1125 °C to 1430 °C. Upon cooling, it usually transforms back to β-TCP [100].

1.5.1.4 Calcium pyrophosphate

Calcium pyrophosphates (CPP, $Ca_2P_2O_7$) exist in amorphous form and in three crystalline structures, i. e., α, β and γ. The existence of CPP crystal structures depends on the temperature of firing [103]:

$$\gamma\text{-}Ca_2P_2O_7 \xrightarrow{750\,°C} \beta\text{-}Ca_2P_2O_7 \xrightarrow{1171\,°C} \alpha\text{-}Ca_2P_2O_7$$

CPP are formed upon ignition of hydrogen orthophosphates, such as DCPA, DCPD, CDHA and OCP. CPP are salts of Ca^{2+} and condensed phosphates, which are formed during a condensation reaction between two orthophosphates. This reaction forms a P-O-P linkage, the characteristic bonding motif of condensed phosphates, and expels water, as shown in Figure 4 [104].

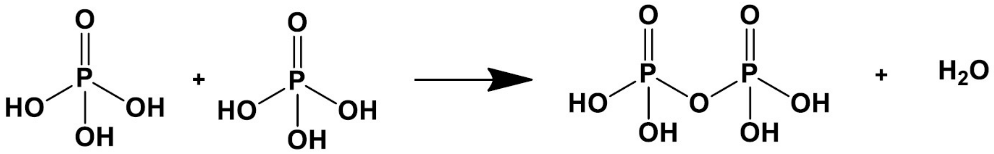

Figure 4. Condensation reaction between two orthophosphates forming a pyrophosphate.

Calcium pyrophosphates are very important molecules in biological systems. CPP have been identified as being the cause of pseudogout disease, when they build up in large amounts in the joints and certain internal organs such as the spleen [105]. Moreover, pyrophosphate molecules play a key role in ensuring the homeostasis during bone mineralization in humans by adsorbing to HA minerals and preventing their crystal growth. The content of available pyrophosphate is enzymatically regulated in humans [106-107]. However, it has to be stressed that although pyrophosphate and CPP play a very important role in biological systems, there are only few reports about the characterization of biological CPP and on the synthesis and characterization of synthetic CPP, especially about the amorphous pyrophosphates [104-105].

1.5.1.5 Amorphous calcium phosphate

Amorphous calcium phosphates (ACP) phase is one of the most frequently occurring forms of CaP minerals in biological organisms and are considered a precursor phase of bone mineral in vertebrates [108]. ACP is obtained only by wet chemical precipitation at conditions of solution's high supersaturation and at low temperatures [8]. ACPs are characterized by the broad bumps in the X-Ray diffractogram, and by monocomponent

PO_4 bands in the infrared spectrum. The basic structure unit of amorphous calcium phosphates, also known as the Posner's cluster, is a cluster of ions comprising $Ca_9(PO_4)_6$ with an average diameter of 0.95 nm [108].

1.5.2 Thermally induced transformations of calcium phosphates

CaP salts do not behave equally under thermal treatments. β-TCP and stoichiometric HA are thermally stable phases. In the case of stoichiometric HA, no secondary phases form up to about 1350–1450 °C in ambient air. Only partial dehydration of HA into oxyhydroxyapatite may occur according to a reversible reaction [109]:

$$Ca_{10}(PO_4)_6(OH)_2 \rightarrow Ca_{10}(PO_4)_6(OH)_{2-2y}O_y + yH_2O \text{ (gas)} \qquad [2]$$

As described in 1.5.1.3 section, β-TCP is stable up to 1125 °C when it transforms to α-TCP. In contrast, all water-containing phases (OCP, ACP, DCPD) and compounds that contain HPO_4 groups in their lattice (CDHA, OCP, ACP, DCPD, DCPA) are thermally unstable and structural changes occur in their crystal structures at low temperatures. The water-containing crystals in OCP and DCPD get partly dehydrated at ≈180 °C. HPO_4^{2-} groups condensate to pyrophosphate groups ($P_20_7^{4-}$) in the range 350–720 ºC (Equation 3) [100].

$$2HPO_4^{2-} \rightarrow P_2O_7^{4-} + H_2O \qquad [3]$$

The amount of $P_20_7^{4-}$ formed depends on the conditions of thermal treatments and the amount HPO_4^{2-} groups in the sample, respectively [110–111]. Between 700 and 900 ºC the reaction described in Equation 4 occurs resulting in the formation of the β-TCP [112–113].

$$P_2O_7^{2-} + 2OH^- \rightarrow 2PO_4^{3-} + H_20 \qquad [4]$$

Beside the dehydration of the crystal and reactions described above, OCP presents two additional transformations during heating. It has been observed that upon heating at ≈200 °C DCPA is formed in a small amount. In addition, the crystal structure can distort, leading to the formation of the so-called “collapsed OCP” structure, which is characterised by the contraction in the lattice cell parameters, due to the loss of water molecules from the crystal structure [100, 114].

1.5.3 Calcium phosphate coatings

CaP bioceramics are widely studied for orthopaedic and dental applications due to their favourable biological properties. Generally, CaP materials interact with surrounding bone, resulting in the formation of chemical bonds with the bone tissue and forming a strong interface with it. The first successful clinical application of CaP for healing bone defect was reported by Albee et al. in 1920 [13]. Ever since, several in vivo studies with encouraging results led to the commercialization of synthetic CaP materials as bone implants. At the present time, numerous commercial CaP products are available, in various physical forms (granules, dense or porous blocks, pastes, cements, coatings on orthopaedic and dental implants) for different applications (bone fillers, scaffolds, ear implants, abrasives in toothpastes, etc.) from biological origin (coral HA, bovine HA) or synthetic [115].

CaP bioceramics are too brittle for use as bulk material under loaded condition. Therefore, CaP are frequently applied as coatings on the surface of strong implants, in order to combine the mechanical strength of the core implant with the excellent biological properties of CaP [116].

Until now, numerous technologies have been developed for the production of CaP coatings with different phase compositions and physico-chemical properties. Among the most studied techniques are plasma spraying, ion beam assisted deposition, pulsed laser physical vapour deposition, magnetron sputtering, electrospraying, dip coating, hot-isostatic pressing, sol-gel, biomimetic methods etc. Currently, physical deposition with plasma spraying is the most widespread method for the production of CaP coatings on bone implants and has been widely applied in clinics since the 1980’s. However, this technique exhibits several inherent drawbacks, such as high price, poor control over the coating's composition, coating delaminations and the fact that it is a line-of-sight technique. These drawbacks stimulate the further development of CaP coating technologies.

Generally, CaP coatings must adhere satisfactorily to the underlying substrate in order to survive the forces present during the implantation and maintain their functionality at the site of the surgical installation. Moreover, coatings should allow rapid osteogenesis and sometimes exhibit complete resorption in the host tissues so that they may be eventually entirely replaced by the bone tissue. In addition, the negative publications about thick plasma-sprayed coatings have resulted in the trend of developing thin CaP coatings [117-

118].

1.5.3.1 Biomimetic method for deposition of calcium phosphate coatings

Throughout the history of mankind the possibility of integrating the ideas from nature to the materials science have been investigated due to the fact that unique structures form in nature in terms of complexity, organization, assembly, and functionality [119-122]. The concept of preparing biomimetic CaP coatings is to copy the process of mineralization of bones, respectively. Advantages of the method are simplicity, low working temperatures and controllable synthesis of homogenous coatings in term of thickness, morphology and phases, also on the substrates with complex shapes. Besides, coatings can be applied to different substrates, such as metals, polymers and ceramics [123]. Moreover, low temperatures enable incorporation of biological molecules in the coatings, which makes them also a potential drug delivery system [10, 123-124].

The inventors of the simulated body fluid (SBF) were the first who studied the possibility of depositing CaP coatings on medical implants by applying a biomimetic approach and developed a method for coating different organic, inorganic and metallic materials [123]. Their method was essentially the modified SBF test and involved immersion of the substrate in the SBF (Table 4) for longer periods of time. The heterogeneous nucleation of HA crystals on the surface of inert substrates was induced either by chemical pretreatments of substrates or by using more supersaturated reaction solution e.g. 1.5 times more concentrated SBF [125-126]. After 7–14 days of soaking in SBF, a 1–10 μm thick HA coating was deposited on a substrate. The morphology and composition of the as-deposited HA crystals in the coating was similar to the HA crystals that formed on bioactive implants when implanted in vivo, i.e., it was composed of nanocrystalline carbonated-HA crystals with traces of Mg ions incorporated in the crystal structure. Due to these similarities, HA deposited from SBF is often called bone-like apatite.

Table 4. Concentration of ions in blood plasma and in SBF [123].

Ion	**Concentration of ions (mM)**	
	Blood plasma	**SBF**
Na^+	142.0	142.0
K^+	5.0	5.0
Mg^{2+}	1.5	1.5
Ca^{2+}	2.5	2.5
Cl^-	103.0	148.8
HCO_3^-	27.0	4.2
HPO_4^{2-}	1.0	1.0
SO_4^{2-}	0.5	0.5
Buffer type	$HCO_3^-/H_2CO_3^-$ $HPO_4^{2-}/H_2PO_4^-$ Haemoglobin system	TRIS/HCl
pH	7.4	7.4

However, original biomimetic coating method suffered from several drawbacks related to the relatively slow process, poor reproducibility, complex preparation, bacterial contamination of the reaction solutions, etc. [117, 127]. In order to circumvent these problems, various modified biomimetic procedures and reaction solutions have been proposed [69, 128-129]. Parameters that affect the properties of CaP coatings, such as phases present, morphology, thickness and adhesion of coating are composition of solution, concentration of salts present in the solution, volume of solution, agitation, renovation, temperature and time of the synthesis. Since time of synthesis is an important parameter to consider when thinking about applicability of the method, many studies focused on the synthesis of CaP coatings in as short time as possible, while preserving satisfactory properties of the coatings. Adhesion strength between biomimetic CaP coating and the substrate is relatively low when compared to CaP coatings produced by other coating technologies. Different tensile strengths of the biomimetic coatings on substrates were reported, ranging from 3 MPa to 30 MPa [130-133]. Figure 5 shows SEM images of CaP coatings prepared by different biomimetic methods.

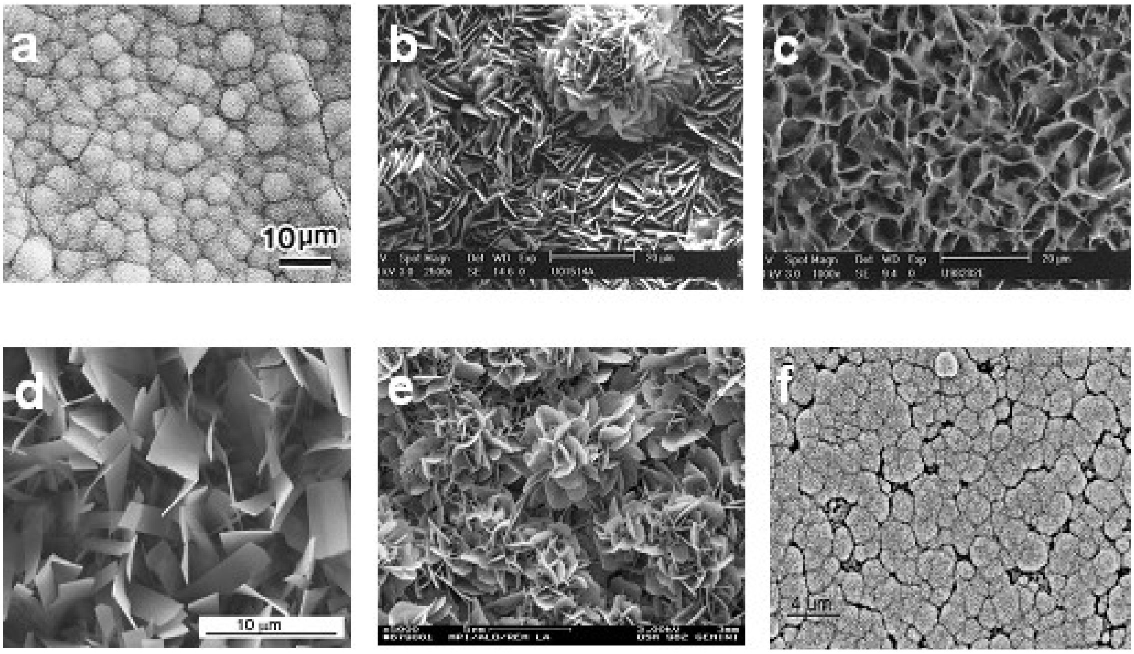

Figure 5. SEM images of calcium phosphate coatings prepared by different biomimetic methods.

Several attempts authors were made to determine which functional groups can initiate the nucleation of CaP on the substrates from the SBF solution. Kokubo's group found out that Si-OH, Ti─OH, Zr─OH, Ta─OH, Nb─OH can promote HA nucleation in SBF. In contrast, Al─OH groups are not effective. Furthermore, they showed that spatial arrangement of groups plays an important role, for example anatase form of titania is preferential in promoting HA nucleation compared to rutile [134]. Tanahashi et al. [47] demonstrated that negatively charged surfaces favour the CaP nucleation on the substrate in the SBF. They found that ─COOH and $-H_2PO_4$ groups effectively enhanced CaP nucleation, while $-CONH_2$, ─OH, $-NH_2$ have weaker nucleating ability. Moreover, they showed that methyl $-CH_3$ group cannot initiate CaP formation in the SBF solution. Among these functional groups, it was also shown that $-SO_3H$ group serves as the nucleation group [135]. Toworfe et al.[136] studied the nucleation mechanism of -COOH, $-NH_2$ and -OH functional groups on silicon wafers and confirmed that they possess apatite nucleation ability. These results suggest that functional groups with negative charge at the pH of blood plasma (7,4) can potentially promote CaP nucleation in SBF and also in vivo. Himeno et al. [137-138] confirmed these results with electrophoretic study. They have shown that surface potential by functional sites is initially negative, indicating that initialization of CaP nucleation involves electrostatic interactions between Ca^{2+} ions and functional groups.

1.5.3.2 Chemistry of calcium phosphate reaction solutions

Biomimetic synthesis involves the immersion of the implant in the simulated body fluid which results in the precipitation of the CaP coating on the implant. In the Figure 6, a general diagram which describes the nucleation of salts and the formation of a coating on a substrate in the supersaturated solution, is shown. From the diagram, it can be observed that CaP crystals precipitate when conditions in the solution are changed from a pH, concentration, and temperature regime in which precursors are soluble to a regime in which solutions are supersaturated, inducing crystal nucleation and growth (Figure 6). Nucleation and growth can occur spontaneously (homogeneous nucleation), it can be induced by seeds of structure similar to that of the salt (secondary nucleation), or by a foreign substrate (heterogeneous nucleation) [139]. Successful biomimetic synthesis occurs when heterogeneous or secondary nucleation is promoted and homogeneous nucleation is suppressed. Therefore, a key element that leads to successful biomimetic synthesis of CaP coatings is an understanding of the factors that control crystal nucleation and growth in aqueous solutions.

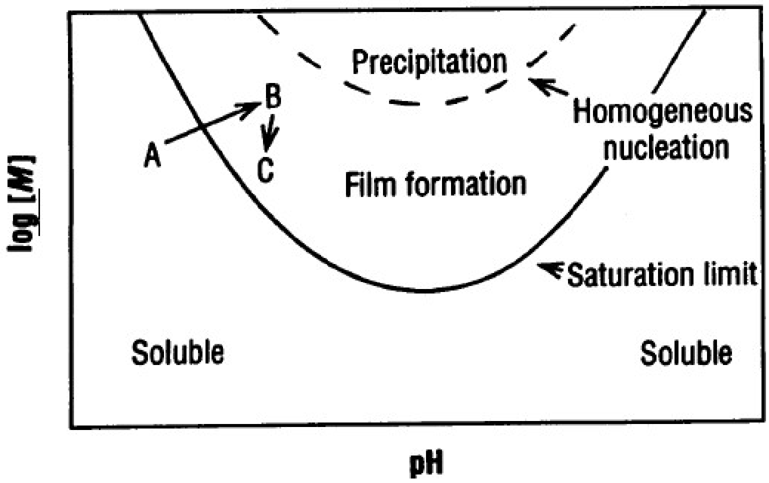

Figure 6. Idealized solubility diagram for coating precursor species dissolved in water. Solubility generally depends on species concentrations, [M], and pH. Coating formation occurs when solution conditions change from (A) (a regime in which precursors are soluble) to (B) (a condition of supersaturation). Proper supersaturation promotes coating growth on a substrate without precipitation in the solution. During the CaP coating deposition from solution, the consumption of soluble precursors in the solution changes the degree of supersaturation (moving to C). Normally, the regime in which homogeneous nucleation and precipitation occur is to be avoided for optimum coating growth [140].

Solubility generally depends on species concentrations, [M], and pH. Coating formation occurs when solution conditions change from (A) (a regime in which precursors are soluble) to (B) (a condition of supersaturation). Proper supersaturation promotes coating growth on a substrate without precipitation in the solution. During the CaP coating deposition from solution, the consumption of soluble precursors in the solution changes the degree of supersaturation (moving to C). Normally, the regime in which homogeneous nucleation and precipitation occur is to be avoided for optimum coating growth [140].

According to classical theories for homogeneous crystallization [139], the free energy for formation of stable nuclei (ΔG) depends on the degree of supersaturation (S), the temperature (T), the net solution-particle interfacial energy (γ), and the particle surface area (A):

$$\Delta G = -RT \text{ In } S + \gamma A \qquad [5]$$

where R is the ideal gas constant.

Supersaturation level, the interfacial energy, and the temperature also influence the rate of nucleation, induction time for nucleation and the final number of nuclei.

Similar expressions apply to heterogeneous nucleation and film formation at an interface, except that the surface free energy is described by three terms:

$$\Delta G = -RT \text{ In } S + \gamma_{cl}A_{cl} + (\gamma_{cs} - \gamma_{sl})A_{cs} \qquad [6]$$

where c, s and l subscripts refer to interfaces involving the crystalline particle, the substrate, and the liquid phases. If interactions between the growing nucleus and a substrate surface represent a lower net interfacial energy, than the particle-solution interfacial energy, heterogeneous nucleation is favoured over homogeneous nucleation. Regarding the metastable CaP solutions, the degree of saturation, temperature and the pH influence the nucleated CaP phase. The secondary nucleation markedly depends on the nature of the calcium phosphate seeds, on the degree of supersaturation, on calcium to phosphorus ratio, on the pH of the solution, and on the temperature [141-148]. The closer the relationship is between the lattices of the seed and the nuclei, the more favoured the nucleation is [142]. In the case of heterogeneous nucleation, calcium phosphate nucleation kinetics is relatively slower than secondary nucleation [142-143]. The supersaturation degree required to induce heterogeneous CaP nucleation is higher than the one that can induce secondary nucleation [149]. Moreover, the physicochemistry of the heterogeneous surface can drastically affect the calcium phosphate nucleation ability [47]. The nucleation of CaP salts, either from supersaturated CaP solutions with simple composition or from simulated body fluids, is a complex event. With respect to simple supersaturated CaP solutions, the first calcium phosphate that precipitates from neutral and alkaline calcium phosphate solutions is usually amorphous (ACP). It is highly unstable and readily transforms to crystalline OCP or the HA phase. The synthesis conditions, such as solution's temperature, pH, reactant concentration and the impurities present markedly influence the ACP transformation. In numerous studies, OCP was detected as the first crystalline phase. Precipitation of OCP is kinetically more favourable compared to HA precipitation. During aging in the solution, OCP transforms to thermodynamically more stable HA. This conversion is most probably an in situ process whereby the OCP undergoes a solid state rearrangement, with concomitant water loss, into an anhydrous HA structure. Again, conditions in the solution have a great effect on this event. In some cases, OCP was not detected as the intermediate phase during the precipitation of HA. The transformation of OCP to HA is slowest at neutral pH but steadily increases as the pH rises until at pH above 9.25 the lifetime of OCP is too brief to obtain experimental evidence for its existence as an intermediate phase [150].

2 Aims and hypothesis

Calcium phosphate (CaP) coatings on zirconia bone implants have a great potential to improve the osseointegration of ceramic dental implants, owing to their high biocompatibility and bone-bonding ability. The wet-chemical biomimetic deposition method, which utilizes the immersion of the implant in the simulated body fluid (SBF) with a composition similar to human blood plasma, has attracted considerable attention from researchers due to it having several benefits, such as a low price, the ability to control the composition of the coatings, the possibility to deposit bone-like CaP crystals on the surface of implants, etc. However, there are drawbacks related to the biomimetic deposition method, such as its lengthy synthesis, poor reproducibility, complex preparation of the SBF solution and, in particular, low adhesion of the deposited CaP coatings to the substrate. The current thesis is aimed at circumventing these problems related to the classic biomimetic deposition method.

In the first part of my work I focused on the development of an alternative biomimetic procedure for the deposition of CaP coatings on zirconia ceramics. The aim of this part of the research was to establish an alternative biomimetic procedure, which would allow the rapid, simple and reproducible deposition of CaP coatings on zirconia. The main reason for the drawbacks of the classic biomimetic synthesis lies in the composition of the SBF solution, which has a low level of supersaturation and therefore the coating deposition rate is low. Moreover, the SBF solution is a metastable solution containing calcium and phosphate ions that are already supersaturated with respect to the CaP salts, and so one has to be very careful during the preparation of the solution so as not to induce the homogeneous precipitation of the CaP in the solution prior to the start of the synthesis. Based on the literature data and preliminary experiments I hypothesized that that the synthesis can be significantly accelerated and simplified by the application of a highly supersaturated CaP reaction solution. Such a solution can be prepared by mixing together concentrated $CaCl_2$ and Na_3PO_4 solutions just prior to the synthesis. In this way, the deposition rate can be significantly accelerated and the homogenous precipitation of CaP salts in the reaction solution prior to the start of the synthesis can be avoided. Moreover, the aim was to characterize the composition of the deposited biomimetic CaP coatings on zirconia and to investigate the mechanisms of CaP crystal nucleation and growth on the substrate. Furthermore, the aim was to study the physico-chemical properties of the deposited biomimetic CaP coatings, such as their topography, dissolution rate in a physiological solution, bioactivity and adhesion to the substrate.

The second part of the thesis was dedicated to a post-deposition thermal treatment of biomimetic CaP coatings on zirconia. The aim of the thermal treatment was to improve the adhesion of the CaP coatings to the zirconia ceramics. It was hypothesized that stronger chemical bonds will be established between the CaP coating and the zirconia substrate upon heating. Moreover, it was also assumed that heating will result in phase transformations of the CaP coating. Therefore, my aim was to characterize the composition of the CaP coatings obtained after heating the biomimetic CaP coating between 600 °C and 1200 °C and to study the influence of the heating temperature on the topography, bioactivity and dissolution rate of the obtained CaP coatings.

3 Materials and Methods

3.1 Materials

In the experiments, zirconia discs and implants (type S10, Thomas Recording GmbH, Germany) were used as the substrates (Figure 7). The discs were prepared by the dry pressing of granulated powder (TZ-3Y-BE, Tosoh, Japan) and sintering at 1400 °C for 4 h. The diameter of the sintered zirconia disks was 15.5 mm and the thickness was 1.5 mm. After grinding and polishing, the substrates were cleaned with soap and sonicated for 10 min in acetone, absolute ethanol and deionized water. The clean substrates were used for the synthesis of the CaP coatings.

Figure 7. Photograph of the zirconia substrates used in the experiments.

3.2 Preparation of the calcium phosphate reaction solutions

In our experiments, two different calcium phosphate (CaP) solutions were used: CPS1 and CPS2. Their compositions are given in Table 5. Both solutions were prepared in the same manner by mixing equal volumes of calcium and phosphate stock solutions just before the synthesis. The procedure for preparing the solutions was adapted from Bigi et al.[69]. A calcium stock solution was prepared by dissolving $CaCl_2$ (Sigma Aldrich) in ultrapure water (resistivity 18.2 MΩ·cm at 25 °C). A phosphate solution was prepared by dissolving $Na_3PO_4\cdot 12H_2O$ (MERCK) in ultrapure water. For the preparation of CPS1, both solutions were buffered at 7.4 with Tris/HCl, while for the preparation of CPS2, the solutions were buffered at 7.0 with Tris/HCl.

Table 5. Ionic composition of CPS1 and CPS2 in mM.

	Na^+	Ca^{2+}	Cl^-	PO_4^{3-}	*pH*	*buffer*
CPS1	7.5	2.5	5.0	2.5	7.4	HCl/TRIS
CPS2	7.5	2.5	5.0	2.5	7.0	HCl/TRIS

3.3 Biomimetic synthesis of the calcium phosphate coatings on the zirconia ceramics

The biomimetic synthesis method consisted of two steps. In the first step, each zirconia substrate was soaked vertically in a plastic beaker filled with 30 ml of CPS1 solution. The beaker was sealed and stored in a water bath at 37 °C for 1 hour. In the second step, the substrate was transferred from CPS1 into the beaker filled with CPS2, sealed and stored in a water bath at 37 °C for different time periods, ranging from 45 minutes to 430 hours. The variation in pH of the CPS1 and CPS2 solutions during the coating deposition was recorded with a glass electrode (713 pH Meter, Metrohm, Switzerland). At the end of the synthesis, the coated substrates were removed from the reaction solution and dried under ambient conditions.

3.4 Post-deposition processing of the biomimetic calcium phosphate coating

In order to alter the physico-chemical properties of the CaP coatings the deposited biomimetic CaP coatings on zirconia substrates were further processed by means of various thermal and mechanical treatments. These involved heat treatments at various temperatures in a furnace (Nabertherm, Germany) and sonication in a water bath (Iskra Pio, Slovenia). The biomimetic CaP coating, which was prepared by immersing a zirconia disc in the CPS2 solution for 11 hours, was used as a basis for the further processing. Altogether five (a-e) different post-deposition processing procedures of the biomimetic CaP coating were studied:

a) heat treatment at 600 ºC (1 h, rate: 300 ºC/h) (abbreviation: HA-600);
b) heat treatment at 800 ºC (1 h, rate: 300 ºC/h) and short (≈1 minute) sonication in a water bath (abbreviation: βTCP-800);
c) heat treatment at 900 ºC (1 h, rate: 600 ºC/h) and short (≈1 minute) sonication in a water bath (abbreviation: βTCP-900).
d) heat treatment at 1100 ºC (1 h, rate: 300 ºC/h) and short (≈1 minute) sonication in a water bath (abbreviation: βTCP-1100).
e) heat treatment at 1200 ºC (1 h, rate: 300 ºC/h) and short (≈1 minute) sonication in a water bath (abbreviation: βTCP-1200).

3.5 Characterization of the calcium phosphate coatings

3.5.1 Composition

The morphology of the deposited coatings was examined using a scanning electron microscope (SEM; Jeol 5800 and Jeol JSM-7600F, Japan). For the determination of the structure of the coatings, the following methods were applied: Fourier-transform infra-red spectroscopy (FTIR; Perkin Elmer System 2000, United States), X-ray diffraction spectroscopy (XRD; Model X'Pert PRO, PANalytical, Holland) and transmission electron microscopy (TEM; JEM-2010F, JEOL, Japan).

The FTIR spectroscopy was performed in transmission mode, attenuated total reflectance (ATR) mode or in a near-grazing incidence angle (NGIA) mode. For performing transmission FTIR spectroscopy, transparent KBr pellets were prepared by mixing 200 mg of KBr and 1 mg of CaP coating. The FTIR NGIA spectroscopy was used to characterize the thin CaP layers. For the analysis of thin films on substrates using FTIR NGIA spectroscopy, the substrate must be reflective. Because zirconia is a non-reflective material, a reflective fluoro-doped tin oxide (FTO) glass was used as a substrate to study the formation of the CaP layers.

For the XRD analysis (Panalytical X'Pert PRO MDP, Holland) the monochromatic source was a Cu generator (45 kV, 40 mA) and an open detector X/CELERATOR was used. The XRD measurements were performed in the 2θ range from 4° to 55° at a 600 s/step scanning speed. For the XRD analysis of a thin CaP layer that formed on zirconia substrates in the first step of the biomimetic synthesis, the measurement conditions were additionally adapted in order to obtain more signal from the coating. The glancing angle of the X-rays was 1°, the step size was 0.03° and the total measurement time was 11 hours.

3.5.2 Topography and thickness of the calcium phosphate coatings

The thickness of the CaP coatings was determined with a mechanical stylus profilometer (Taylor Hobson Talysurf – Form Talysurf series 2, United States).

The topography of the coatings was analyzed using atomic force microscopy (AFM, Nanoscope IIIa, Digital Instruments) and by stereometrical analysis.

For the AFM analysis of the biomimetic CaP and HA-600 coatings, which were composed of brittle lamellar crystals, measurements were performed using the tapping mode, with a very low scan rate of 0.1 Hz in order not to damage the crystals during the scanning of the surface with a cantilever. The β-TCP coatings were measured with the contact mode. Different cantilevers were used for the tapping (OMCL-AC160TS, f ~ 250 kHz, Olympus) and contact modes (MSNL, Veeco, k = 0.01 N/m). AFM imaging software was used to determine the arithmetic average of the absolute surface values (R_a) (Equation 7) and the developed surface area ratio (S_{dr}). S_{dr} is expressed as the percentage of additional surface area contributed by the texture as compared to an ideal plane with the size of the measurement region (Equation 8).

$$R_a = \frac{1}{n}\sum_{i=1}^{n}|y_i| \qquad [7]$$

$$S_{dr} = \frac{\Delta S}{S} \cdot 100\% \qquad [8]$$

where ΔS is an additional surface area contributed by the texture and S is the surface area of the ideal plane.

Stereology is a multidisciplinary science aimed at estimating, from a proper sampling design, the geometrical parameters of a spatial structure, such as the length, curvature, particle density, volume, surface area, surface roughness, etc. [156]. In my doctoral work, I estimated the developed surface area ratio (S_{dr}) of the biomimetic CaP coating based on six SEM images of the coating. The S_{dr} value was calculated according to Equation 9.

$$S_{dr} = \frac{\Delta S}{S} \cdot 100\% = \frac{2\sum_{i=1}^{N} w_i^2}{S} \cdot 100\% \qquad [9]$$

where ΔS is the surface area of the lamellas, S is the surface area of the zirconia substrate, N is the number of lamellae counted across the analyzed area, w is the width of a lamella. In order to simplify the stereometrical determination of S_{dr}, I approximated that the lamellar plates have the shape of squares with a thickness d = 50 nm and the edge w. In Equation 9, the symbol w_i was used because the lamellae have different widths. We neglected the contribution of the side faces of the lamellae because the thickness is small. The factor 2 in Equation 9 appears because each lamella has two square faces.

3.5.3 Adhesion of calcium phosphate coatings on zirconia substrates

The adhesion of the prepared CaP coatings on zirconia was evaluated using a tape test, scratch test, a tensile bond strength test and by assessing the coating damage after the implantation and explantation of the coated zirconia screws from the artificial bone.

3.5.3.1 Tape test

A standardized, cross-cut, tape test (ASTM D-3359) was used to assess the adhesion of the biomimetic CaP coating on a zirconia substrate. First, a lattice pattern was made in the coating using a razor blade. Then, a pressure-sensitive tape (Elcometer 99 tape, Elcometer Ltd, UK) was applied over the lattice and removed after 90 s of application. After the tape test, the coated substrates were examined using SEM. The coating retention was qualitatively evaluated and assessed on a 0 to 5 scale by a comparison with the standard chart given in the ASTM standard. In addition, the amount of coating retention was quantified by weighing the coated ceramic substrates on a microbalance (Mettler Toledo, UMT-2 ultramicrobalance, Switzerland) before and after the tape test. Measurements were performed on three samples and the retention value was determined by averaging the data.

3.5.3.2 Scratch test

The scratch test was applied to evaluate the adhesion of the biomimetic CaP and the βTCP-900 coating. The scratch test was performed according to the standard ASTM C1624–05 [152]. In this test, an automatic scratch tester (CSEM Revetest®, CSM Instruments, Switzerland) with a spherical Rockwell C diamond stylus of 200 µm radius was used. For testing the biomimetic CaP coatings on a zirconia disc a progressive load from 0 N to 20 N was applied with a loading rate of 20 N/min and the length of the scratches being 10 mm. For testing the βTCP-900 coatings on a zirconia disc, a progressive load from 0 N to 120 N was applied with a loading rate of 200 N/min and the length of the scratches was 10 mm. Three scratches were generated on two samples for each coating group and subsequently analyzed with optical microscopy (Zeiss, Germany) and SEM. The point of the adhesion failure of the coating from the substrate in the scratch groove was determined as the critical load (L_c). The L_c values for each coating group were averaged and the standard deviation was taken as an error. Different testing conditions were used for the βTCP-900 and biomimetic CaP coatings because of the difference in their scratch resistance.

3.5.3.3 Tensile bond strength test

The tensile bond strength test was performed using a universal mechanical testing system (Galdabini, Italy). In this test, an iron or aluminium rod was attached onto the CaP-coated zirconia discs using the HTK ULTRA BOND® (HTK, Germany) adhesive. A full cure of the adhesive was obtained with an exposure of the samples to 170 °C for 2 hours. In the testing, the rod was pulled at a cross-head speed of 0.5 mm/min until the coating failure. The failure mode was evaluated by examining the surface of a zirconia disc and of a metal rod with the SEM. The tensile bond strength was calculated according to Equation 10.

$$tensile\ strength = \frac{F}{S}\ \left[\frac{N}{mm^2} = MPa\right] \qquad [10]$$

where F is the measured force at which the facture occurred and S is the area of the metal rod, which faced the coating during testing.

The measurements were performed on five different samples for each test group and the standard deviation of these data was taken as the uncertainty.

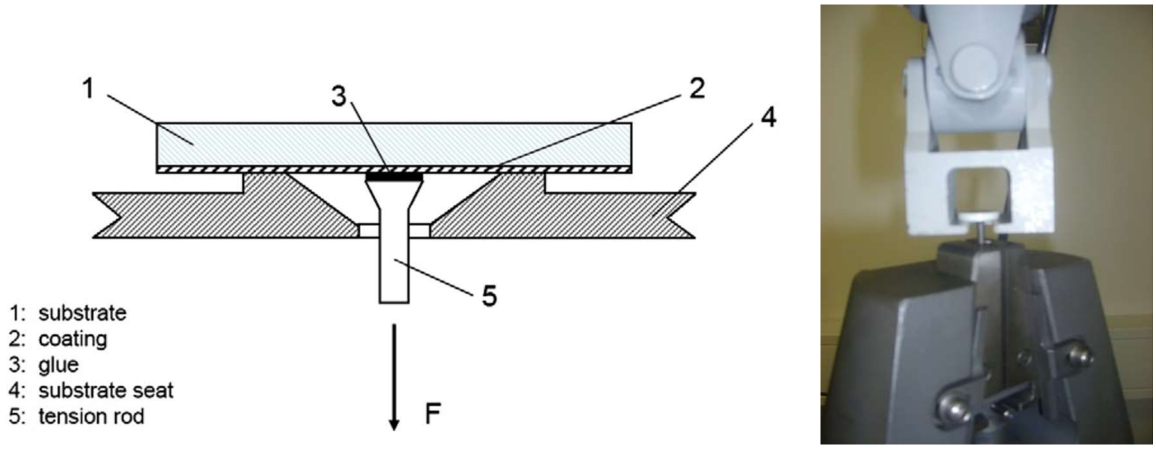

Figure 8. A schematic drawing (left) and a photo (right) of the tensile test apparatus and arrangement.

3.5.3.4 Implantation in the artificial bone

The implant socket was prepared in the artificial bone (Pacific Research Laboratories, USA), which is a rigid polyurethane foam (density: 0.48 g/cm^3), and cleared of debris. The diameter of the socket was 2.7 mm. Zirconia implants were coated with a biomimetic CaP coating, HA-600 coating, βTCP-800 and βTCP-900 coatings. The coated zirconia implants were screwed and unscrewed from the artificial bone under reproducible conditions. After their removal, the implants were carefully cleaned with distilled water and dried. SEM analysis was applied to qualitatively evaluate the damage to the coatings. In the case of the biomimetic CaP and βTCP-900 coatings the coated implants (n=4 per coating group) were weighed on a microbalance (XP6U, Mettler Toledo, Switzerland) before and after insertion into the artificial bone to detect any possible changes in the mass of the coatings.

3.5.3.4.1 Implantation of the β-TCP coated titanium implant in the pig's cadaver bone

The βTCP-800 coating was deposited on the commercial titanium implant (Ankylos^{TM}, Dentsply Friadent, Germany) according to the procedure described under 3.4. b). A pig cadaver model was used to evaluate the mechanical performance of the βTCP-800 coating. The jaw-bone of an adult pig was removed within 12 h of slaughtering at a local abattoir. A surgeon implanted a titanium implant coated with βTCP-800 into the jaw-bone according to a standard procedure for Ankylos^{TM} implants and afterwards it was immediately explanted by means of unscrewing. The implant was cleaned with ultrasound treatment in acetone. After drying, it was analyzed with SEM for possible damage to the coating.

3.5.4 Dissolution of calcium phosphate coatings in a physiological solution

The coated ceramic discs were immersed in a plastic vial with 4.5 ml of physiological solution, which was a phosphate buffer saline (PBS) with a pH = 7.2 at 37 °C (Table 6). The experiment was conducted in triplicate. After certain periods of time (2, 4, 6.5, 9, 11, 13, 19, 24 hours) the ceramic discs were transferred from the PBS solution to a plastic vial with the same volume of fresh PBS solution and the amount of Ca^{2+} released in the PBS solutions was quantitatively determined by the utilization of flame atomic absorption spectrometry (AAS). The cumulative amount of calcium released (A_i) in the PBS solutions at the immersion intervals was calculated according to Equation 11 and was expressed as the mass of calcium per surface area of the zirconia substrate (ng/mm^2). The standard deviation was also calculated.

$$A_i = \frac{m_i\,(Ca^{2+})}{S} = \frac{\sum_{j=1}^{i} \Delta m_j\,(Ca^{2+})}{S} \qquad [11]$$

where i is the number of immersion intervals (i=1-8), $m_i(Ca^{2+})$ is the cumulative mass of Ca^{2+} released in PBS, and $\Delta m_j(Ca^{2+})$ is the mass of Ca^{2+} released into the PBS during a specific immersion interval j.

Table 6. Composition of the PBS solution.

Salt	*NaCl*	*KCl*	$Na_2HPO_4 \cdot 2H_2O$	KH_2PO_4	*pH*
Concentration (g/l)	8.01	0.2	1.78	0.27	7.2

3.5.5 *In vitro* test of bioactivity

The simulated body fluid (SBF) test was used for a preliminary evaluation of the material's bioactivity [19]. The test was performed by immersing the materials in the SBF with the composition given in Table 7. The solution was prepared by dissolving high-purity reagents in MQ water and it was buffered at 7.4 with TRIS/HCl. Subsequently, the prepared SBF was filtered through a 0.2-µm filter into a sterile flask (Nalgene, USA). NaN_3 was added to the solution in order to inhibit the growth of the bacteria in the solution [127]. CaP-coated zirconia discs were immersed in 30 ml of SBF at 37 °C. The samples were removed from the SBF after different periods of time (4 days to 2 months), washed with deionized water and dried at room temperature. Afterwards, the soaked samples were characterized by SEM and XRD, in order to examine any surface modifications.

Table 7. Ionic composition of the SBF in mM.

	Na^+	Ca^{2+}	Cl^-	*Pi*	Mg^{2+}	HCO_3^-	K^+	SO_4^{2-}	N_3^-	*pH*	*buffer*
SBF	144.5	2.5	147.8	1	1.5	4.2	5	0.5	2.5	7.4	HCl/TRIS

4 Results

4.1 Biomimetic synthesis of calcium phosphate coatings on zirconia ceramics

The main aim of this part of the thesis was the development of a biomimetic synthesis procedure that would be simple, reproducible and that would allow a high deposition rate of the CaP coatings on sintered zirconia substrates. Moreover, one of the goals was to study the mechanisms of coating deposition and to characterize the physico-chemical properties of the deposited CaP coatings, such as their dissolution in a physiological solution and adhesion to the substrate.

The biomimetic synthesis of a CaP coating on zirconia substrates involved two steps using two different CaP solutions. In the first step the zirconia discs were immersed into the CPS1 solution (pH = 7.4) and after one hour of soaking they were transferred to the CPS2 solution (pH = 7.0) for various periods of time. The purpose of the first step of the synthesis was to deposit a seeding layer on the surface of zirconia that would allow the rapid growth of the CaP coating in the CPS2 solution in the second step of the synthesis.

4.1.1 First step of the synthesis

During the immersion of the zirconia substrates in the CPS1 solution the pH of the solution was monitored. A slight decrease in pH was observed with immersion time, indicating the precipitation of a CaP phase [153]. Figure 9 shows the pH of the CPS1 solution in dependence with the immersion time. Although the pH change is relatively small, three distinct stages, i.e., I, II, and III, can be clearly distinguished from the curve.
FTIR NGIA spectroscopy was applied to study the structure of CaP deposits at each stage. An FTO glass was used as a substrate instead of a non-reflective zirconia. The fact that the pH profile of the CPS1 was the same when zirconia or FTO substrates were immersed in the solution suggests that in both cases the mechanisms of CaP nucleation and growth are the same. The FTIR NGIA spectra of the CaP deposits formed on the FTO

substrates at each stage are gathered in Figure 10.

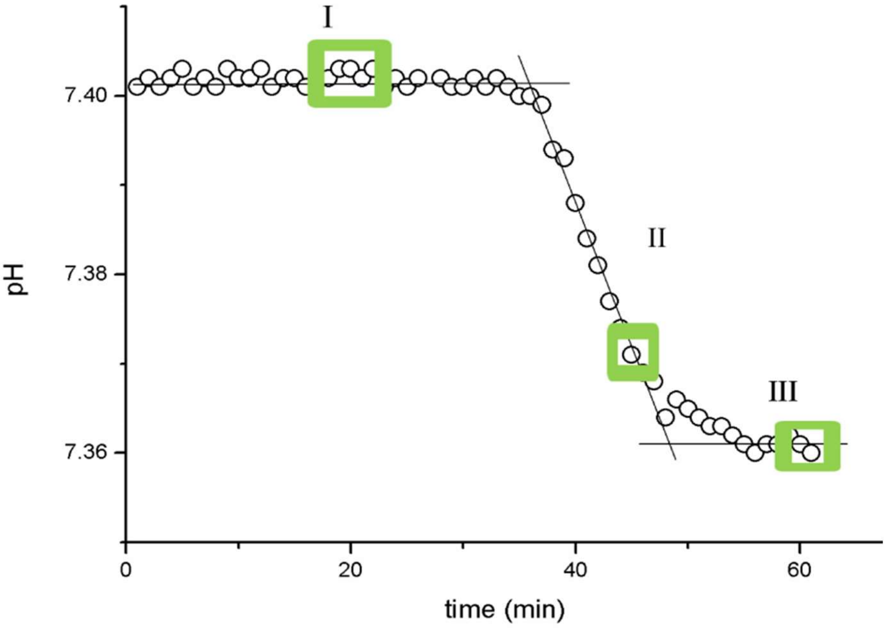

Figure 9. Variation of the pH with the immersion time of the zirconia substrates in CPS1. I, II and III denote the three regimes that take place during the immersion. The green squares mark the times at which the samples were taken out from the CPS1 solution for the FTIR NGIA analysis.

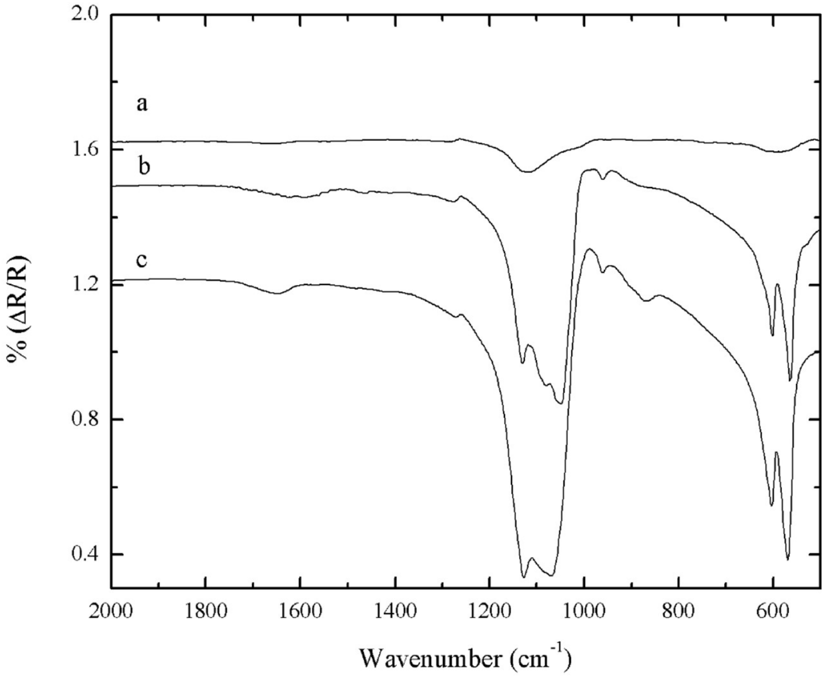

Figure 10. FTIR NGIA spectra of the CaP layers formed on an FTO substrate in CPS1 solution and the structure evolution versus soaking time: (a) 20 min, (b) 45 min, (c) 60 min.

Curve a in the FTIR NGIA spectrum (Figure 10) shows a spectrum of deposits formed after 20 min of immersion in the CPS1. The intensity of the peaks on the spectrum is relatively low due to the small amount of deposits on the substrate. Broad and featureless ν_4 and ν_3 phosphate absorbance bands can be observed at 600, 1020 and 1120 cm^{-1}, respectively, which are typical for an amorphous CaP structure. The weak signal at 1280 cm^{-1} belongs to the FTO substrate. An SEM micrograph of the deposits that formed on the zirconia after 20 min of immersion is shown in Figure 11. As can be observed on the SEM image, the amorphous CaP deposits did not fully cover the zirconia substrate and it could be seen beneath the deposits.

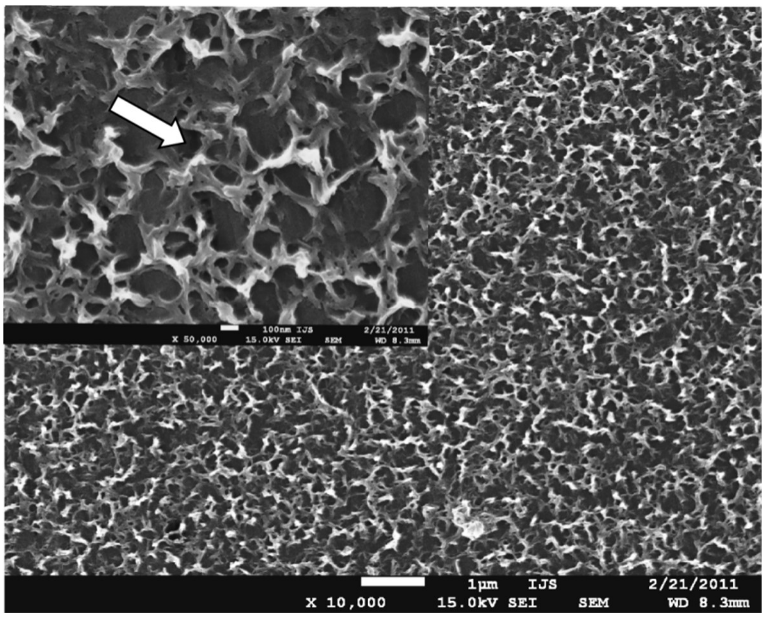

Figure 11. SEM image of the amorphous CaP layer formed on zirconia after 20 min of soaking in CPS1. The CaP layer did not fully cover the zirconia substrate. The white arrow shows a superficial scratch that remained on the zirconia substrate after polishing.

After approximately 40 min of immersion the pH starts to decrease sharply until pH ≈ 7.36 is reached after 50 min of immersion (stage II). The FTIR spectrum of the deposits after 45 min of soaking exhibited a pattern that indicates the deposition of a crystalline phase (Figure 10 (curve b)). The broad ν_3 and ν_4 absorbance bands at 600 and 1120 cm^{-1} of the amorphous structure split into two distinct peaks at 565 and 605 cm^{-1}, three peaks at 1050, 1080 and 1130 cm^{-1} and a shoulder at 1190 cm^{-1}. A weak signal was observed at 960 cm^{-1}, which corresponds to the ν_1 P-O stretch of the PO_4 group. Moreover, a very weak and broad band appeared at 870 cm^{-1}, which is specific to the P-OH stretch of the HPO_4^{2-} [154]. The weak vibration at 1280 cm^{-1} is an artefact and is specific to the FTO substrate. All these absorption bands in the spectrum can be attributed to the OCP crystal structure and indicate the precipitation of OCP in stage II. After about 50 min of immersion, the pH reached its constant value at 7.36 (stage III), suggesting that the precipitation process stopped. The SEM and AFM images of deposits after 60 min of immersion in CPS1 are shown in Figure 12 and Figure 13, respectively. As can be observed from the SEM image the CaP layer fully covered the substrate and its surface could not be seen. The CaP layer was porous and had a nanostructured morphology. An AFM analysis showed that the thickness of the layer was around 200 nm (Figure 13).

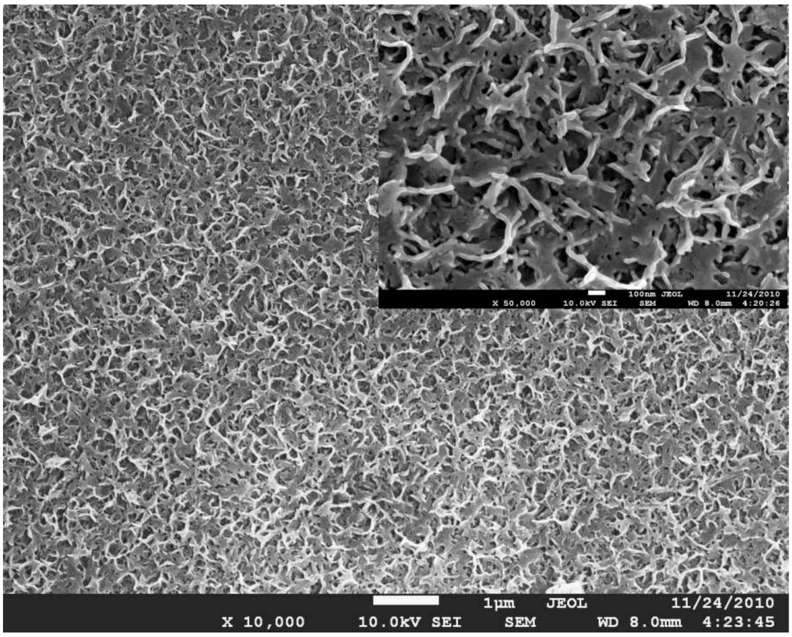

Figure 12. SEM image of the CaP layer on zirconia after 1 h of immersion in CPS1.

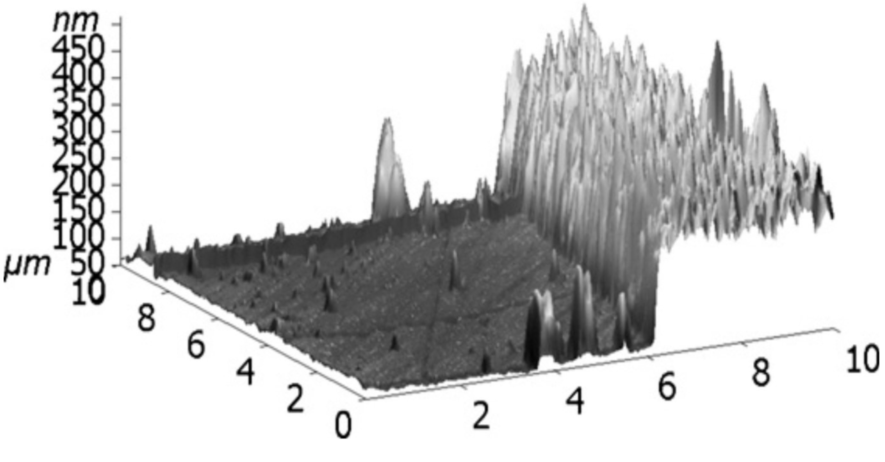

Figure 13. AFM image of a CaP layer on a zirconia substrate after immersion in CPS1.

The structure of the CaP layer after 60 min of immersion was analyzed with NGIA FTIR spectroscopy and thin-film XRD diffractometry (TF-XRD). The FTIR NGIA spectrum of deposits after 60 min of immersion (Figure 10 (curve c)) showed peaks specific to the orthophosphatic ν_3 P-O stretch absorption at 1070 and 1130 cm^{-1} with a shoulder at 1088 cm^{-1}. A doublet specific to the ν_4 P-OH deformation of the HPO_4^{2-} group was observed at 560 and 600 cm^{-1}. The peak at 960 cm^{-1} arose from the symmetric ν_1 P-O stretch mode and a weak and wide band that appeared at 875 cm^{-1} can be assigned entirely to the P–OH stretch of the HPO_4^{2-} [100, 154]. The FTIR pattern could correspond to the OCP or calcium deficient hydroxyapatite (CDHA) crystal structure. The presence of peaks that are typical for HPO_4^{2-} groups indicates that the layer is not composed of stoichiometric hydroxyapatite but rather of calcium deficient hydroxyapatite (CDHA). On the TF-XRD diffractogram of the CaP layer only three peaks that belong to the CaP coating appeared at 2θ angles of 25.9º, 28.2º and 32° besides the zirconia peaks (Figure 14). They could correspond to either hydroxyapatite (HA) or to the octacalcium phosphate (OCP) crystal structure. However, at 2θ = 4.7º, which is the position where the typical and most intensive signal of the OCP crystal structure appears, there was no signal, indicating that the detected peaks correspond to the CDHA crystal structure.

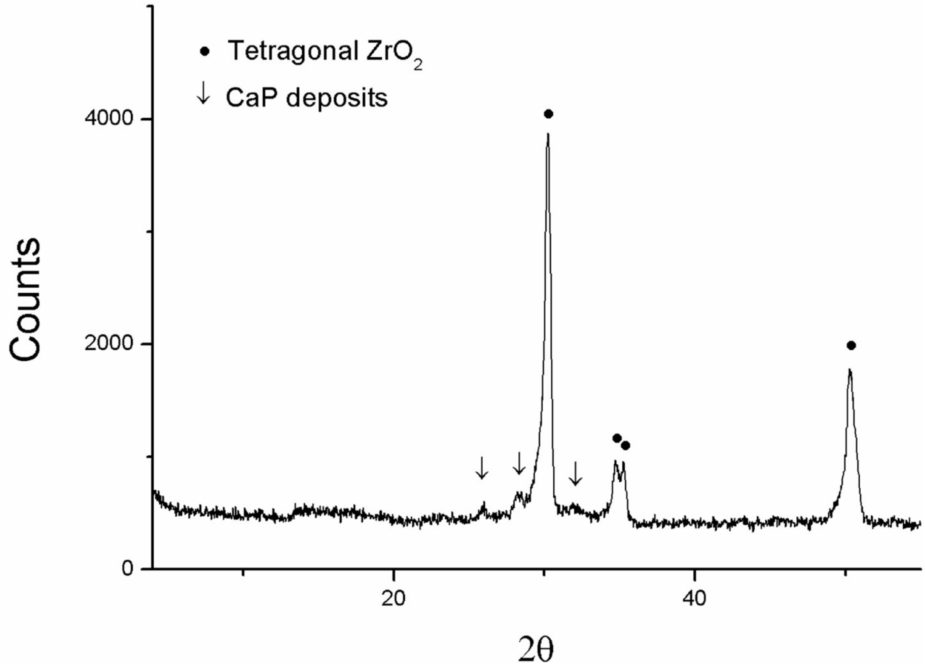

Figure 14. TF-XRD diffractogram of the zirconia disc after 60 minutes of immersion in CPS1.

4.1.2 The second step of the synthesis

In the second step of the synthesis, the zirconia discs covered with a thin CDHA seeding layer were immersed in the CPS2 solution, which had a lower degree of supersaturation compared to CPS1. No homogenous precipitation of CaP salts occurred in the CPS2 as the solution remained clear throughout the experiment. The pH value and the concentration of Ca^{2+} ions in the CPS2 decreased with the propagating reaction, as shown in Figure 15.

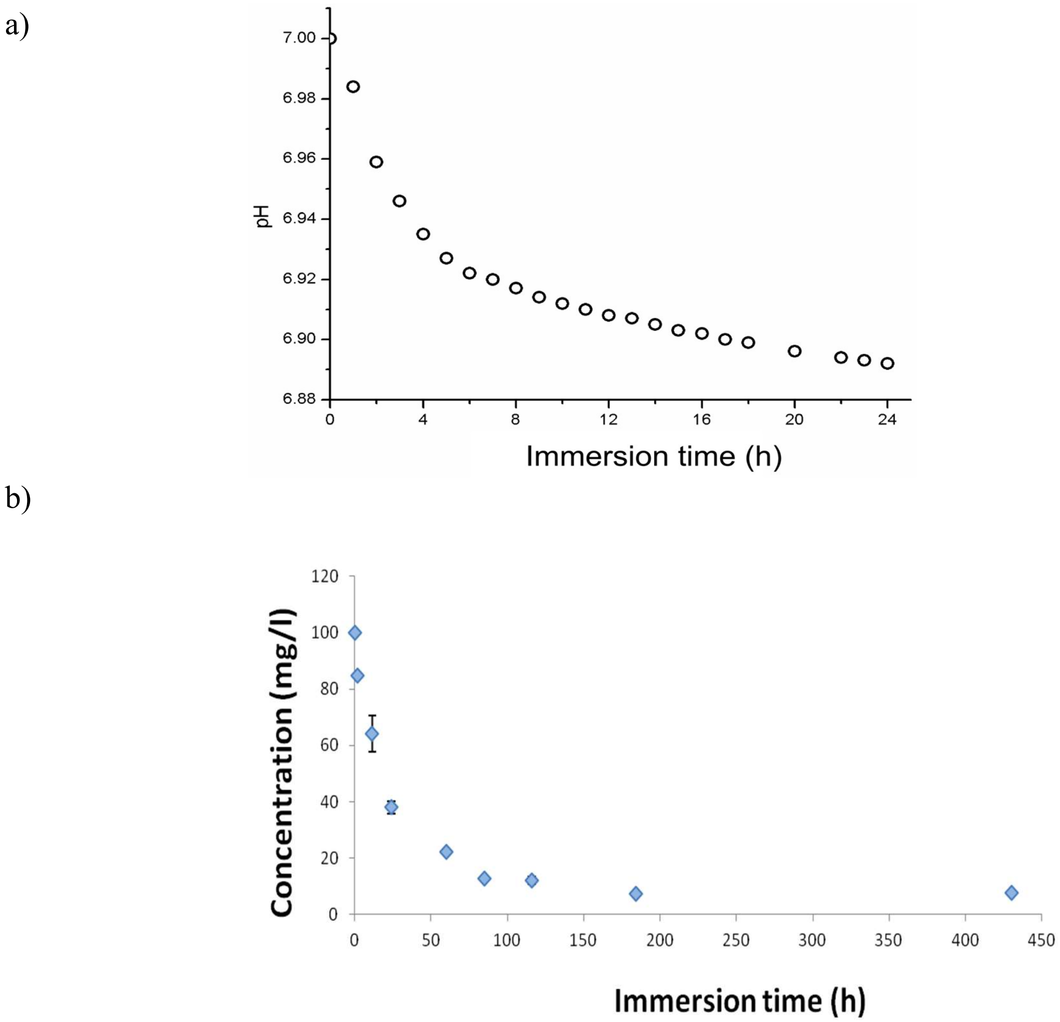

Figure 15. Influence of immersion time of the zirconia substrates in CPS2 on the pH (a) and the concentration of Ca^{2+} ions (b) in the CPS2 solution.

As illustrated in Figure 16, a 5-µm-thick biomimetic CaP coating formed on the ceramic surface after 3 hours of immersion in CPS2. From the profile images it can be seen that the coating was not morphologically uniform. The lower part of the coating was dense and the upper part was porous and composed of intersecting lamellas. With increasing the immersion time the lamellar crystals increased in size and the coating became thicker. Figure 17 shows the influence of immersion time on the thickness of the prepared CaP coating.

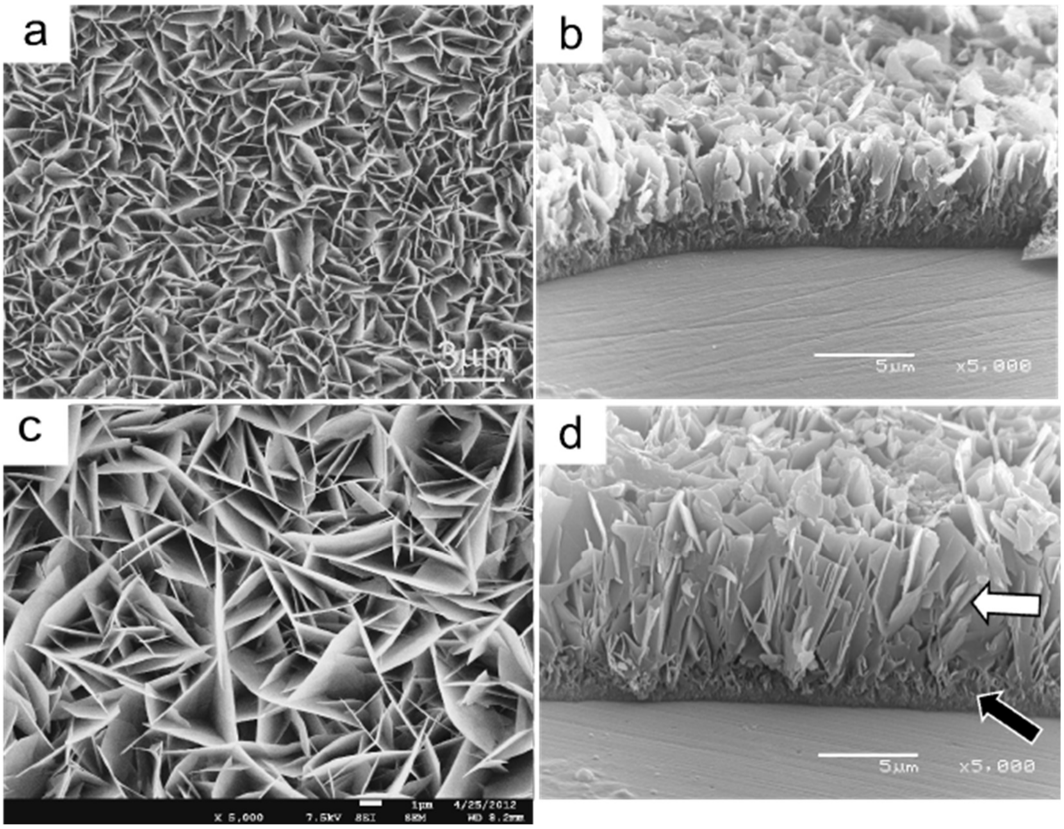

Figure 16. SEM images of the biomimetic CaP coating after 3 h (a and b) and 11 h (c and d) of immersion in CPS2. (d) The white arrow depicts the upper part of the coating with a lamellar morphology, and the black arrow shows the lower part of the coating, which was more dense.

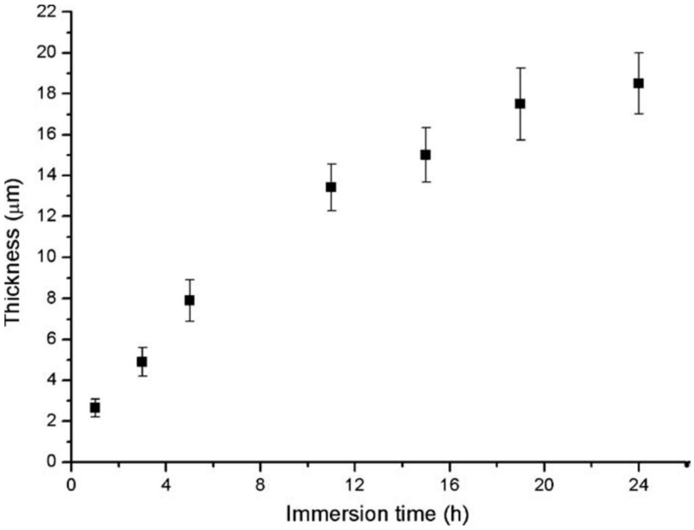

Figure 17. Influence of soaking time in CPS2 on the thickness of the biomimetic CaP coating.

For the XRD analysis the biomimetic CaP was peeled-off from the substrate. The XRD diffractogram (Figure 18) of the coating showed diffraction lines characteristic of triclinic OCP crystals (JCPDS 26-1056). Similarly, the FTIR spectrum corresponded to the OCP structure (Figure 19). Strong bands appeared between 1020 cm^{-1} and 1120 cm^{-1}, originating from the orthophosphatic υ3 P-O stretch absorption, and at 560 and 600 cm^{-1}, there was a doublet originating from the υ4 P-O deformation. The weak bands at 530, 870, 913 and 1192 cm^{-1} were ascribed to the HPO_4^{2-} and a small peak at 960 cm^{-1} to the PO_4^{3-} group. The weak signal at 630 cm^{-1} is specific to the vibration of the $H_2O(4)$ molecule, which is located in the junction of the hydrated and apatitic layers in the OCP. The H_2O bending signal was found at 1640 cm^{-1}. An Electron-diffraction (ED) analysis revealed that the individual lamellae are OCP monocrystals (Figure 20).

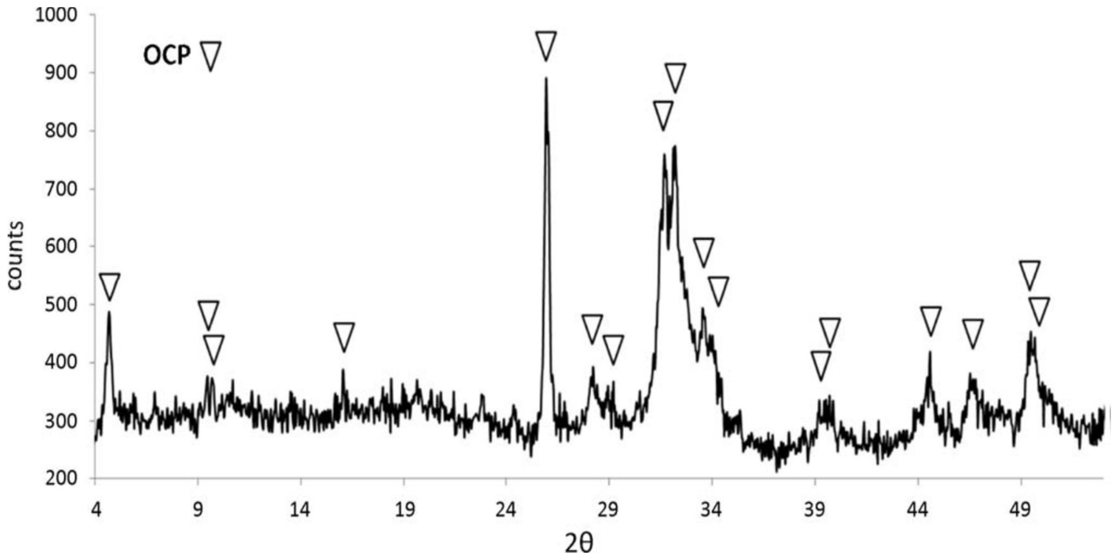

Figure 18. XRD diffractogram of the peeled-off coating after 3 h of soaking in CPS2.

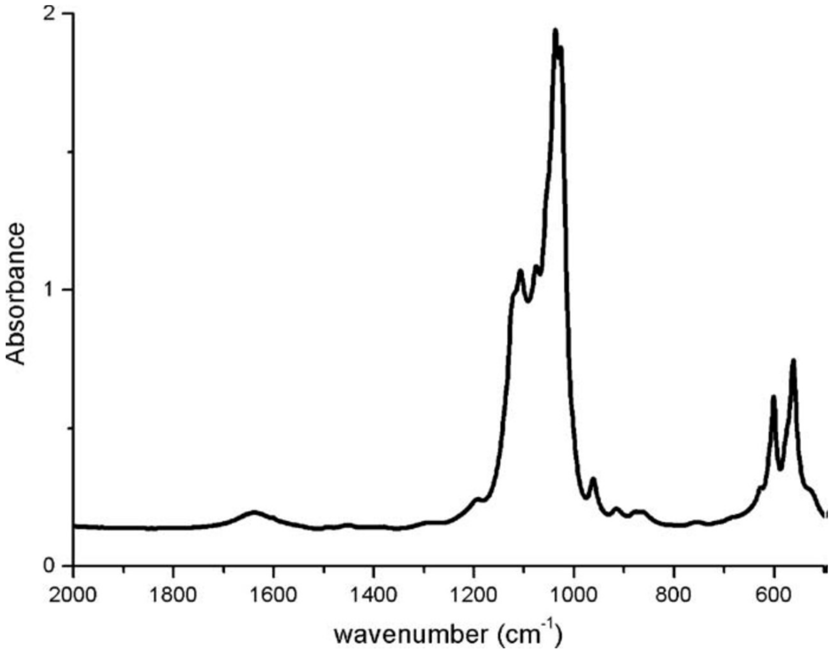

Figure 19. FTIR spectrum of the coating after 3h of immersion in CPS2.

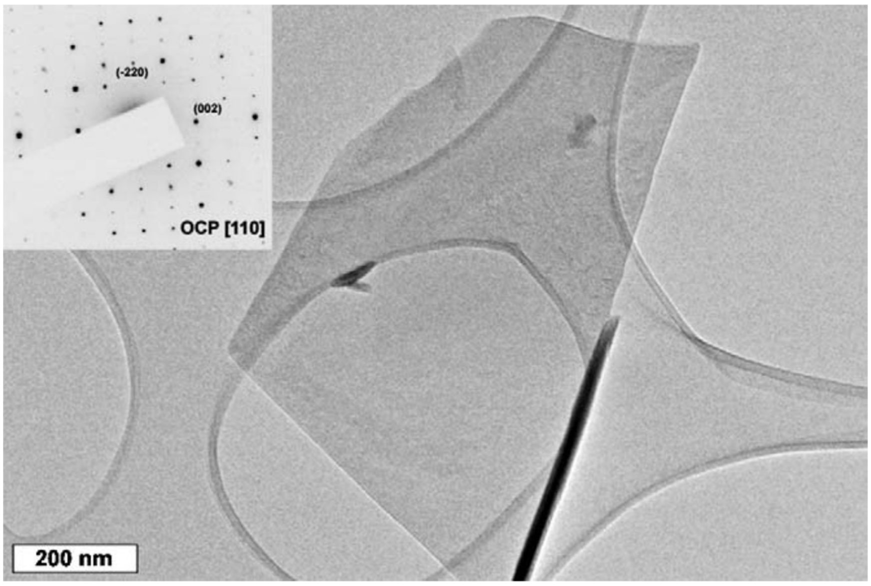

Figure 20. TEM bright-field image of an individual lamella scratched from the zirconia surface after the second step of the synthesis. Its SAED pattern is inserted in the top-left corner. The experimental SAED pattern is in agreement with the calculated electron diffraction of the OCP crystal structure in the [110] direction.

In order to get more information about the structure of the lower and denser part of the biomimetic CaP coating, the substrates were immersed in CPS2 for only 1.5 hour to allow the formation of only the denser coating on the zirconia (Figure 21). The XRD pattern of the coating corresponded to the poorly crystalline HA structure (Figure 22).

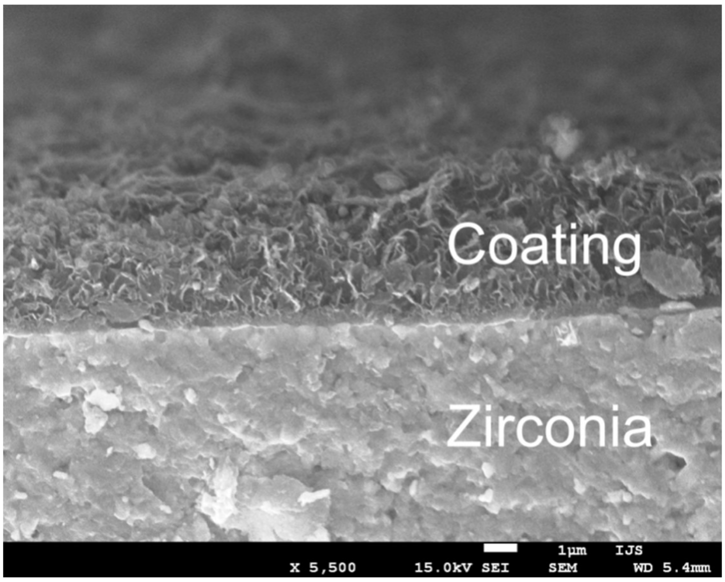

Figure 21. SEM image of the CaP coating that formed on the zirconia after 1.5 h of immersion in CPS2. The coating is composed of CDHA with a Ca/P ratio close to 1.5.

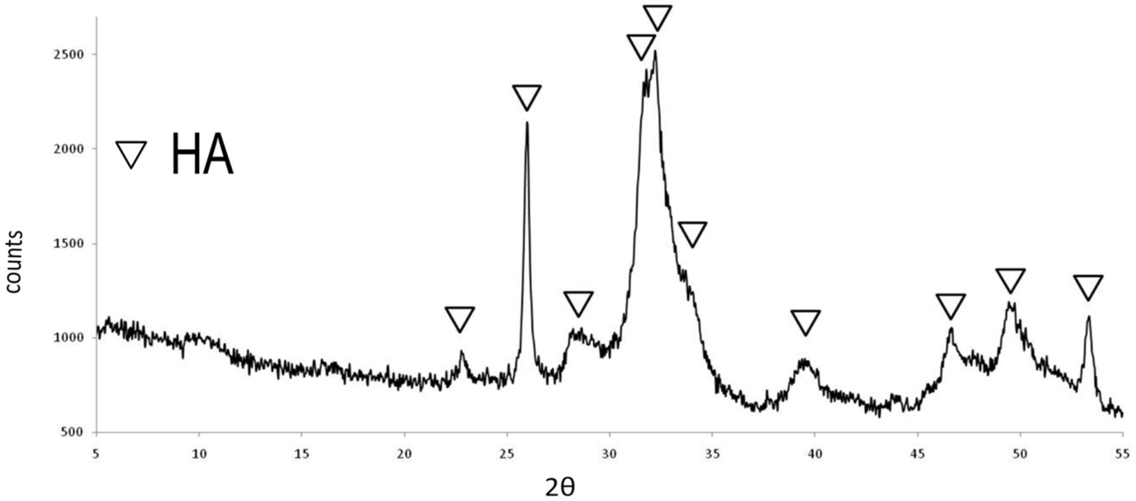

Figure 22. XRD of the lower part of the biomimetic CaP coating that formed on the zirconia after 1.5 h of synthesis in the second step. The diffraction lines correspond to the HA structure (JCPDS 09-0432).

TEM analysis revealed that precipitates that constitute the lower part of the coating are nanocrystals with a size of around 6 nm and SAED analysis confirmed that they have a HA crystal structure (Figure 23).

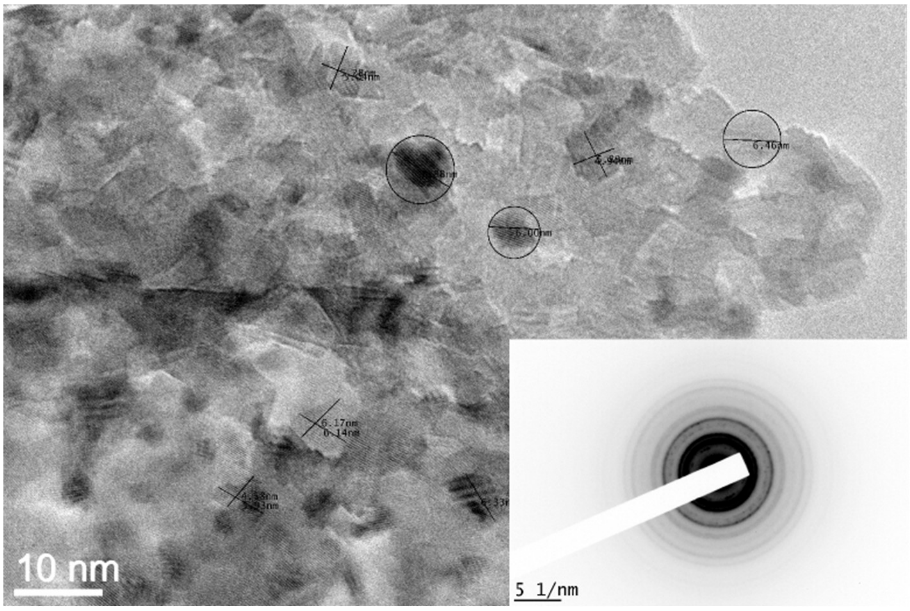

Figure 23. a) HR TEM image with corresponding SAED pattern of the precipitates that formed on the zirconia substrate after 1 hour of immersion in CPS2. The diameter of the individual nanocrystals was ≈6 nm. The SAED pattern of the precipitates matches the HA crystal structure.

In order to determine the stoichiometry of these HA deposits, an additional heat treatment of the sample was performed, because calcium deficient-HA (CDHA) cannot be differentiated from the stoichiometric HA based solely on the XRD analysis, but they can be distinguished after the heat treatment. Between 650 °C and 750 °C the CDHA decomposes according to the reaction described in [12], while the stoichiometric HA remains unchanged, as proposed by Ishikawa et al. [112].

$$Ca_{10-x}(HPO_4)_x(PO_4)_{6-x}(OH)_{2-x} \rightarrow (1-x)Ca_{10}(PO_4)_6(OH)_2 + 3xCa_3(PO_4)_2 + xH_2O \quad [12]$$

As can be seen from the XRD spectrum (Figure 24) of the deposits after 1.5 hours of immersion in the CPS2 and a heat treatment at 750 °C for 1 hour, β-TCP is the predominant phase and no HA peaks could be seen in the spectrum, confirming that the lower part of the biomimetic CaP coating was composed of CDHA, with a Ca/P ratio close to 1.5 and the molecular formula $Ca_9(HPO_4)(PO_4)_5(OH)$ [112].

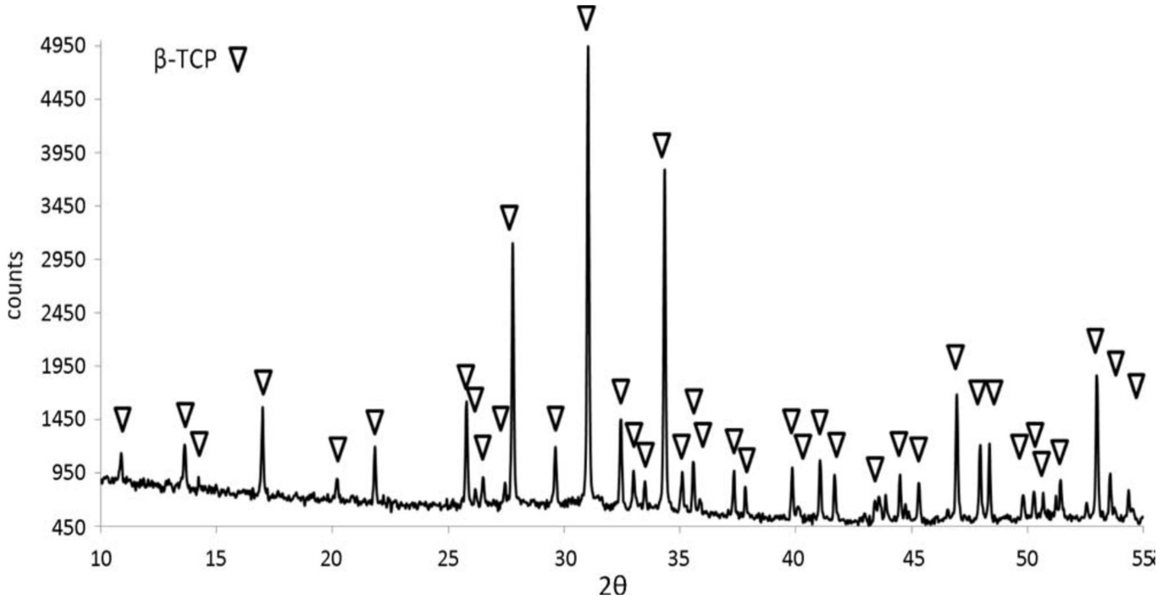

Figure 24. XRD of the lower and denser part of the biomimetic CaP coating, which formed on the zirconia surface after 1.5 h of immersion in CPS2 solution.

The topography of the biomimetic CaP coating was analysed with AFM and a stereometrical method. The values of surface topography parameters obtained with both methods are given in Table 8. The AFM image of the biomimetic CaP coating is shown in Figure 25.

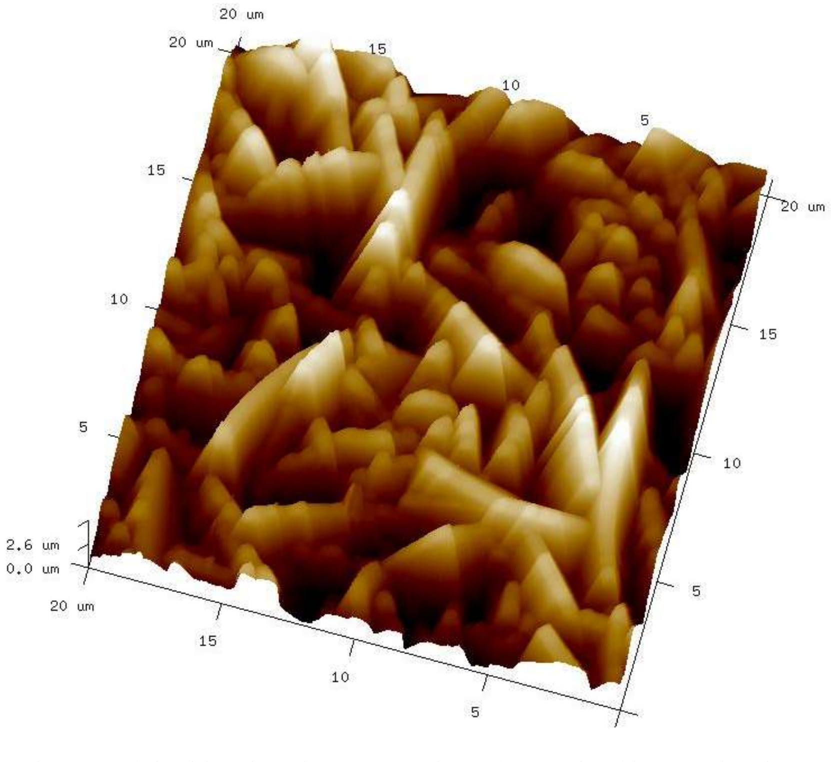

Figure 25. AFM image of the biomimetic CaP coating after 11 h of immersion in CPS2.

Table 8. The values of the surface topography parameters of the biomimetic CaP coating determined with AFM (left) and stereometrical analysis (right). R_a - average surface roughness; S_{dr} - developed surface area ratio.

AFM analysis		*Stereometrical analysis*
R_a (nm)	S_{dr}	S_{dr}
800 ± 200	145 %	900 %

The biomimetic CaP coating is composed of lamellar crystals that have the shape of a truncated deltoid and with an average width of 5.8 μm. For the calculation of the S_{dr} value based on the stereometrical analysis, as already mentioned in the Materials and Methods section, for the sake of simplified calculation, the lamellar crystals were approximated to squares with a thickness of 50 nm and an edge of length w. ΔS was determined from the sum of the surface areas of individual lamellae. The S_{dr} value of the biomimetic CaP coating, calculated from Equation 1, was 900 %.

4.1.3 Synthesis of biomimetic calcium phosphate coating on other inert biomaterials

Besides zirconia ceramics, some other inert biomaterials, which are used in medicine as bone implants, were also tested as substrates for CaP coating deposition. As shown in Figure 26, a homogenous CaP coating with a lamellar morphology formed on all the substrates tested that were immersed for 1 hour in CPS1 and for 4 hours in CPS2. Moreover, as seen in Figure 26 (l, n, p), the lamellar crystals uniformly covered individual fibres of the polymeric porous scaffolds.

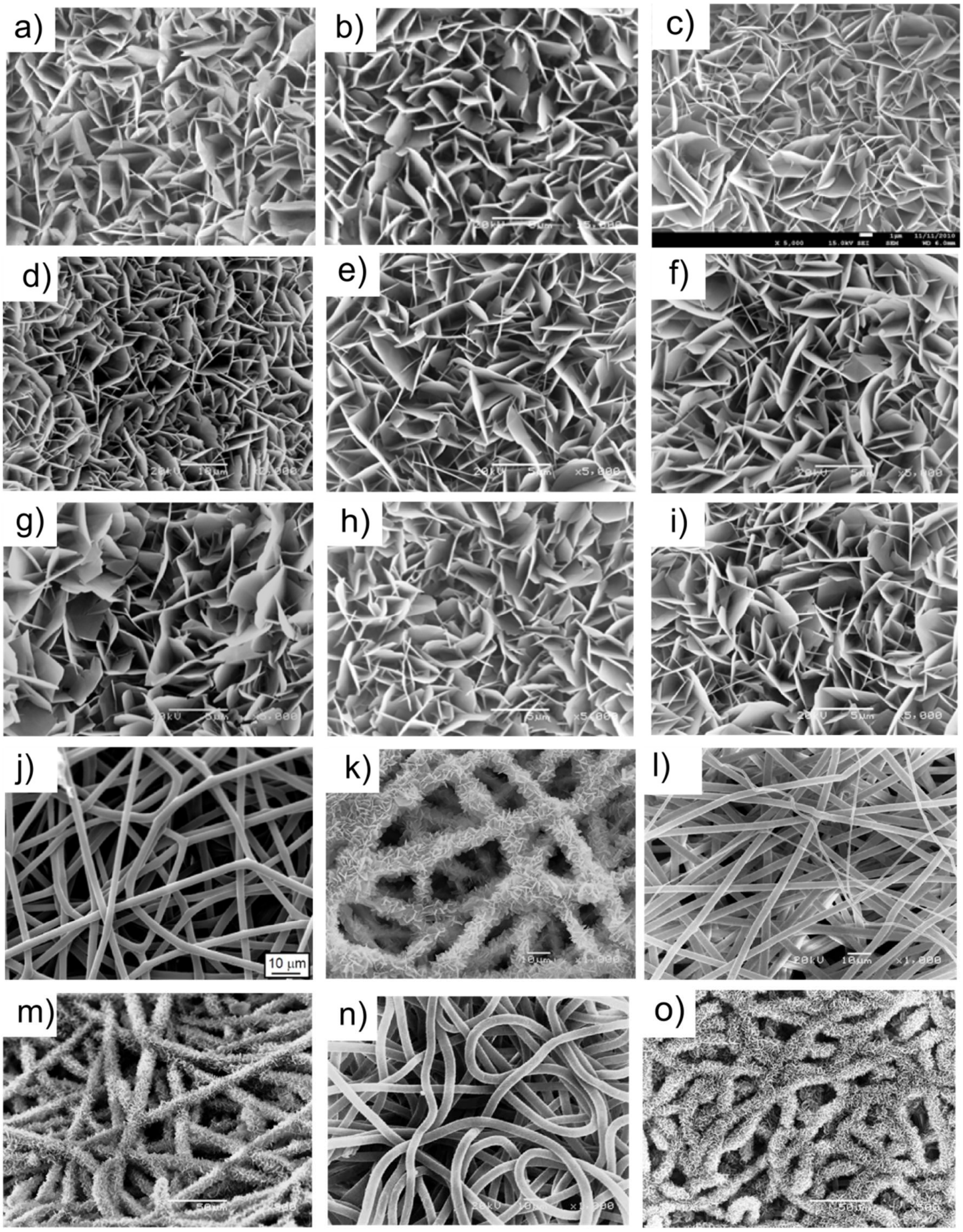

Figure 26. Synthesis of a biomimetic CaP coating on various bioinert materials used for bone regeneration.(a–j) substrates were dense discs or pellets; (k–p) substrates were porous polymeric scaffolds; (k, m, o) uncoated scaffolds; (l, n, p) coated scaffolds. a)TiAl4V6; b) stainless steel 316 L; c) alumina ceramics; d) PLGA; e) PEEK; f) PLLA; g) PCL; h) PMMA; i) UHMWPE; j) PLLA; k) PLLA; l) PLGA; m) PLGA; n) PCL; o) PCL.

XRD analyses showed that the coatings had the same composition on all the substrates tested and the diffraction lines that appeared on the spectra corresponded to both the HA and OCP crystal structures. Two representative XRD spectra of the coatings on PMMA and PEEK are shown in Figure 27. As in the case of the biomimetic CaP coating on zirconia, coatings on other substrates were also composed of a lower CDHA layer and an upper OCP layer with a lamellar morphology (Figure 28).

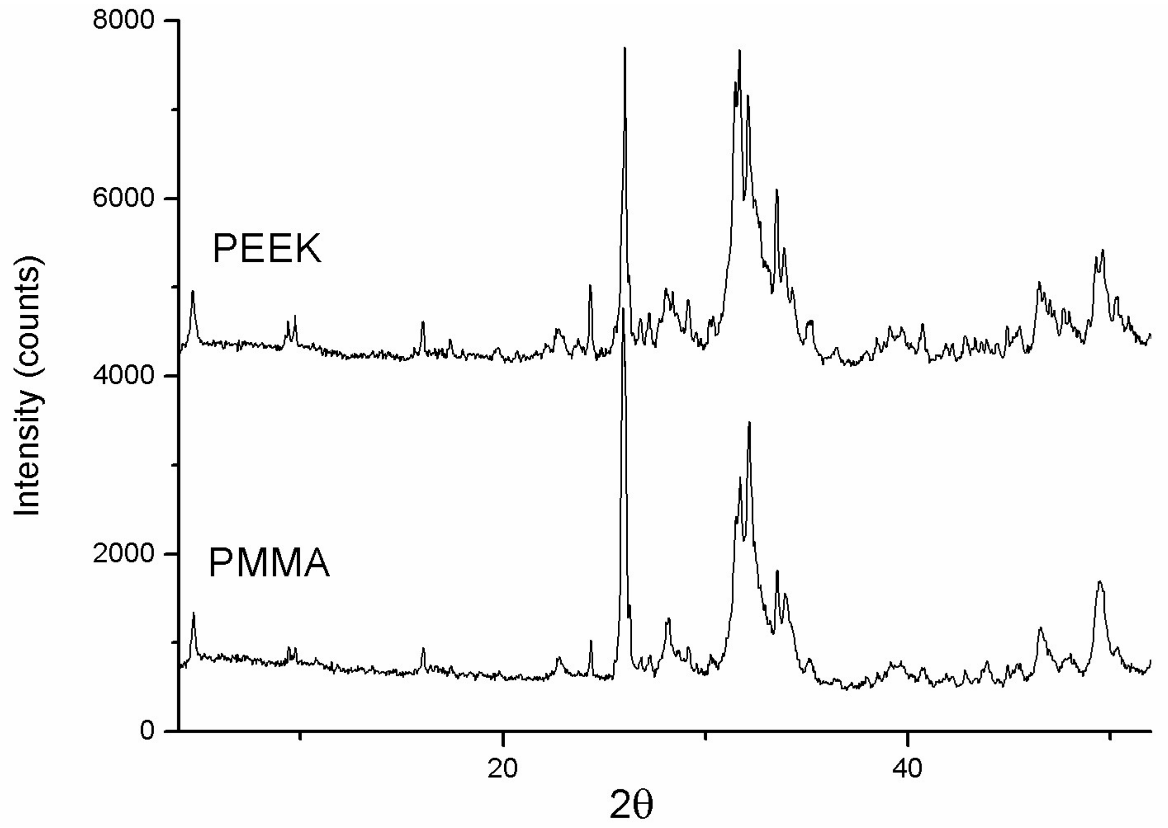

Figure 27. XRD spectra of the biomimetic CaP coating on PMMA and PEEK. The diffraction lines correspond to the OCP and HA crystal structure. The coatings were removed from the substrate for the XRD analysis. The SEM images of these coatings are shown in Figure 26.

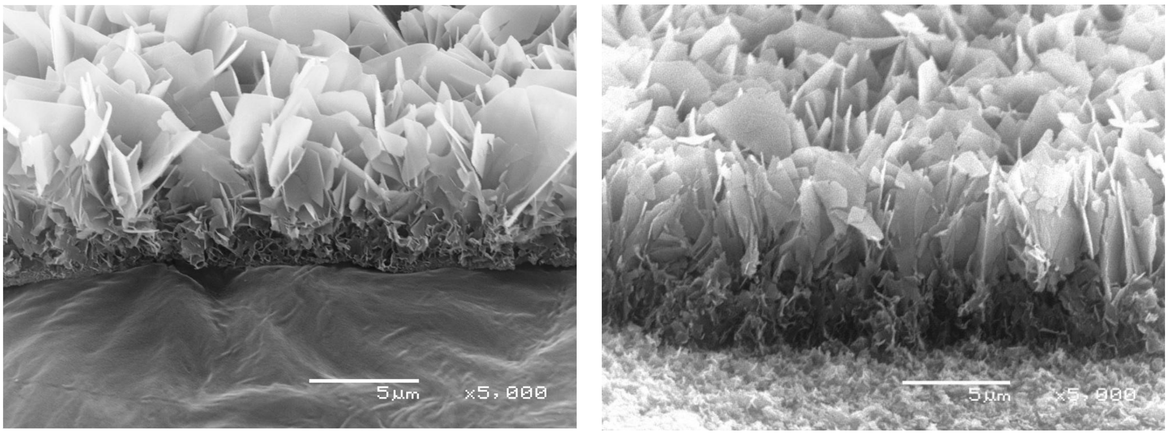

Figure 28. Side views of the biomimetic CaP coatings on PCL (left) and $TiAl_4V_6$ (right).

4.1.4 Physico-chemical properties of the biomimetic calcium phosphate coating on a zirconia substrate

In vitro experiments were conducted in order to predict the performance of the biomimetic CaP coating on zirconia after the implantation in living tissue. These included the SBF test, testing of the coating dissolution in the physiological solution, testing of the coating's wettability and testing of the coating's adhesion. The biomimetic CaP coating, which was deposited on zirconia after 11 h of immersion in CPS2, was used in all the tests mentioned above.

4.1.4.1 SBF test

Figure 29 shows a micrograph of the biomimetic CaP coating on zirconia after 4 days of immersion in the SBF. Globular agglomerates consisting of fine particles covered the lamellar OCP crystals. As can be seen in the XRD spectrum of the biomimetic coating after immersion in SBF (Figure 30) the (100) diffraction line of the OCP at 4.7° was absent while the intensity of peaks at 31.8° and 32.2°, which belong to the HA structure, increased, indicating that the deposits are composed of HA. Moreover, the EDS analysis detected Na and Mg in the coating.

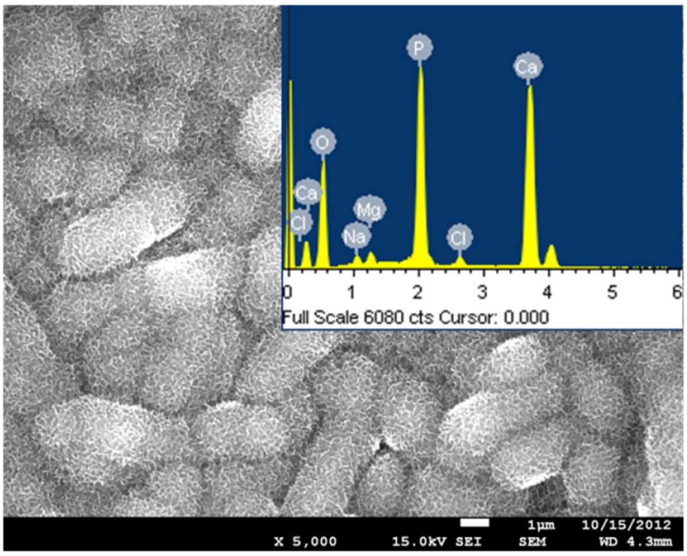

Figure 29. SEM micrograph of the biomimetic CaP coating on zirconia after 4 days of immersion in the SBF. Note the surface is covered by a layer with a typical globular morphology of bone-like HA. The corresponding EDS analysis is shown in the top right corner.

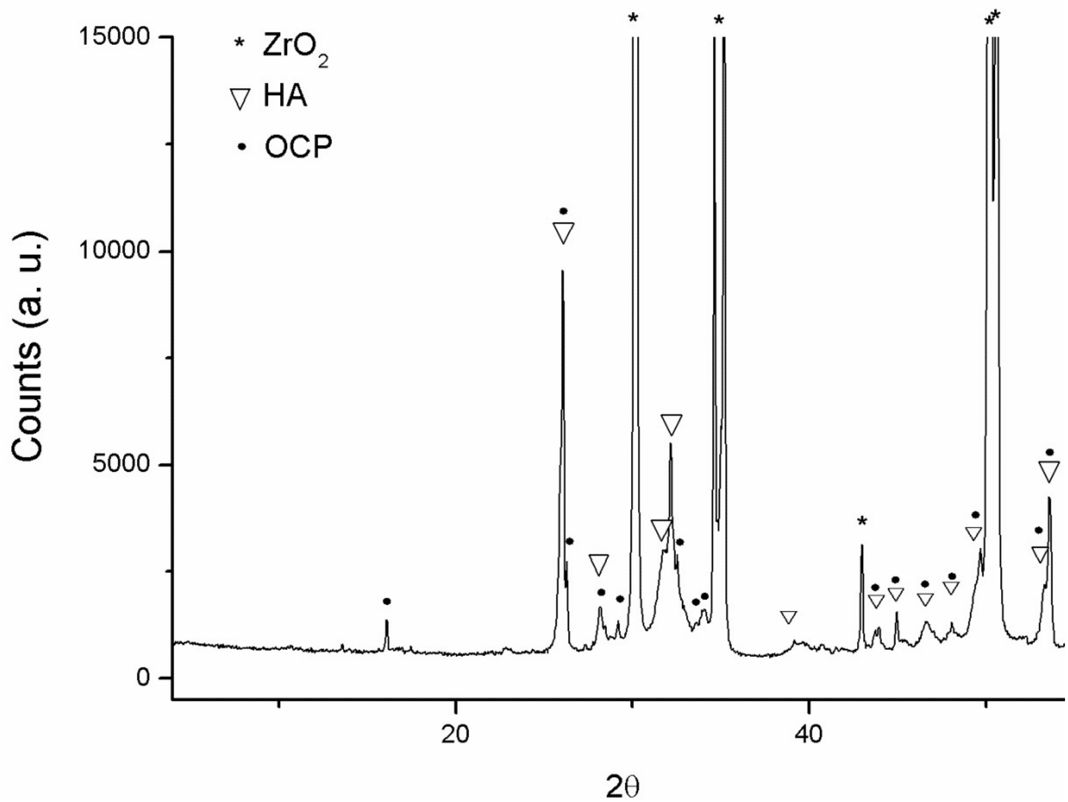

Figure 30. XRD spectrum of the biomimetic CaP coating on zirconia after 4 days of immersion in the SBF.

4.1.4.2 Dissolution of the biomimetic calcium phosphate coating in the physiological solution

As shown in Figure 31, the biomimetic CaP was soluble in PBS and Ca^{2+} ions were gradually released in the solution. The dissolution profile was almost linear.

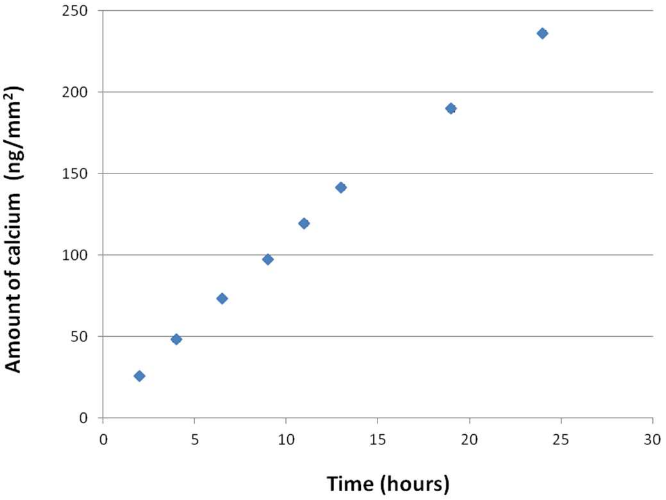

Figure 31. Calcium release from the biomimetic CaP coating to PBS at pH=7.4.

4.1.4.3 Wettability of the zirconia covered with the biomimetic calcium phosphate coating

The photographs in Figure 32 show the spreading of a water droplet on the uncoated zirconia substrate and the zirconia substrate covered with the biomimetic CaP coating. The contact angle of a water droplet on uncoated zirconia was 64.1° ± 3.4°. The coated zirconia displayed high hydrophilicity and as can be observed in Figure 32b the contact angle was strongly reduced to 2.6° ± 0.5°.

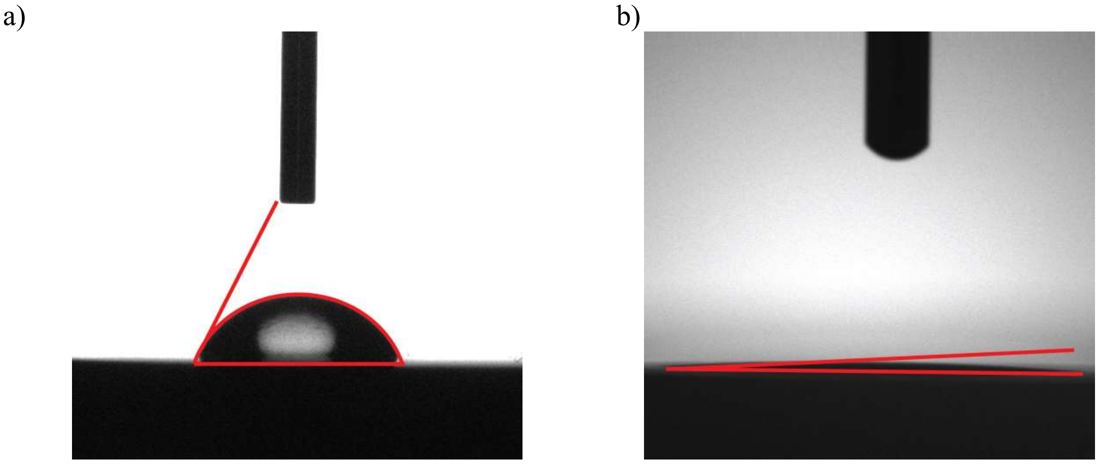

Figure 32. Image of the contact angle measurement for a water droplet spreading on (a) zirconia substrate and (b) zirconia covered with the biomimetic CaP coating.

4.1.4.4 Adhesion of the biomimetic calcium phosphate coating on zirconia substrate

The adhesion of the biomimetic CaP coating on zirconia was evaluated using a tape test, a tensile bond strength test, a scratch test and by assessing the coating damage after the implantation and explantation of the coated zirconia implants from the artificial bone.

4.1.4.4.1 Tape test

A standardized tape test (ASTM D-3359) was applied to evaluate the adhesion of the biomimetic CaP coating. Figure 33 shows the SEM image of the biomimetic CaP coating after the performance of the tape test. From the comparison of the micrographs of the biomimetic CaP coating before (Figure 16 c) and after the test (Figure 33 c) it can be seen that a small upper portion of the lamellar crystals was removed during the test. Nevertheless, the lamellar morphology of the coating was preserved. None of the squares from the cross-cut grid was detached from the ceramic surface. However, coating failures did occur on a few spots at the edges of cuts. These mostly included cohesive delaminations (Figure 33 A and B), which occurred at the interface between the upper lamellar and the lower denser part of the coating. According to the chart given in the standard, the coating adhesion was classified as 4B, i.e., more than 95 % of the coating was retained on the ceramic substrate. In addition, weighing the coated substrates before and after the test showed that 94 % of the initial mass of the coating remained on the substrates after the test, indicating good adhesion of the coating.

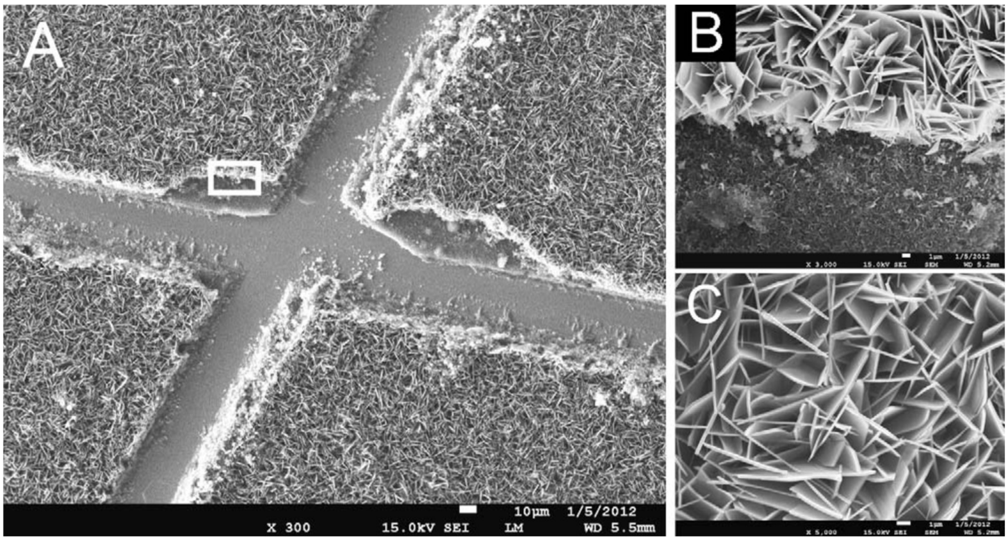

Figure 33. SEM images of the coating after the performance of the tape test at the cross-cut region. (A) Cohesive delamination was mostly observed near the edges of the cuts. (B) Detailed inspection of the coating at the spot of a cohesive delamination marked with a square in (A). (C) Note that the upper portion of OCP lamellas was removed during the test.

4.1.4.4.2 Tensile strength test

The tensile bond strength of the biomimetic CaP coating was 1.8 ± 0.4 MPa. During the tensile testing of the biomimetic CaP coatings only adhesive fractures occurred at the coating-substrate interface and the coating was retained on the iron rod (Figure 34). No trace of the epoxy adhesive was detected on the zirconia substrates after the tensile test, demonstrating the absence of penetration of the adhesive to the substrate.

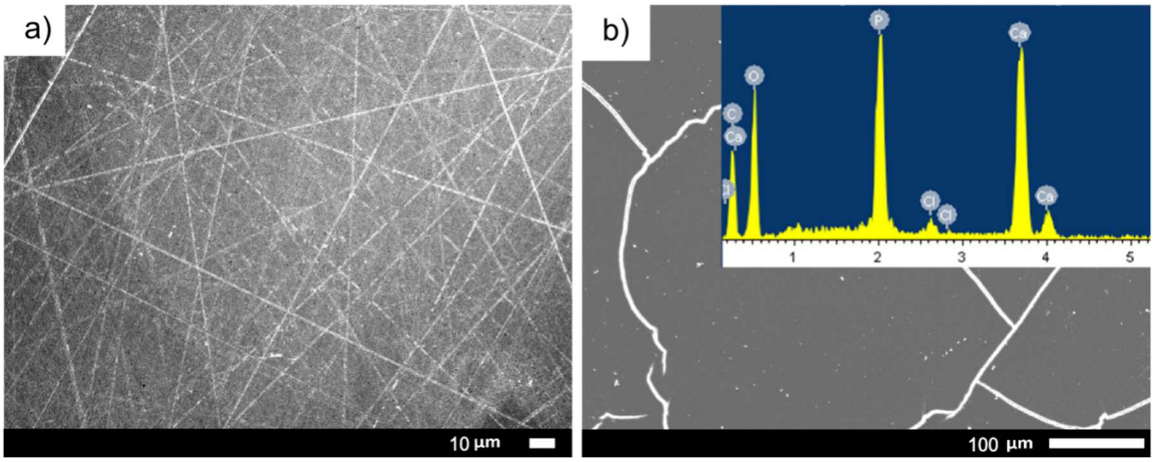

Figure 34. a) SEM micrograph of the zirconia surface after tensile testing of the biomimetic CaP coating on zirconia. During the tensile test the coating was removed from the substrate. No trace of the epoxy adhesive was detected on the substrates after the tensile test, demonstrating the absence of penetration of the adhesive to the substrate. The superficial scratches that can be observed on the surface of the zirconia are a consequence of polishing. b) SEM micrograph and EDS analysis of the iron rod that was used to pull-out the coating. The biomimetic CaP coating was retained on the iron rod after the test and the EDS analysis confirmed the presence of Ca and P elements on the iron rod.

4.1.4.4.3 Scratch test

Figure 35 shows an SEM micrograph of a scratch groove, which was produced on the biomimetic CaP coating during the scratch test. The critical load (L_c), at which the coating was completely separated from the substrate, was 5.3 ± 0.6 N.

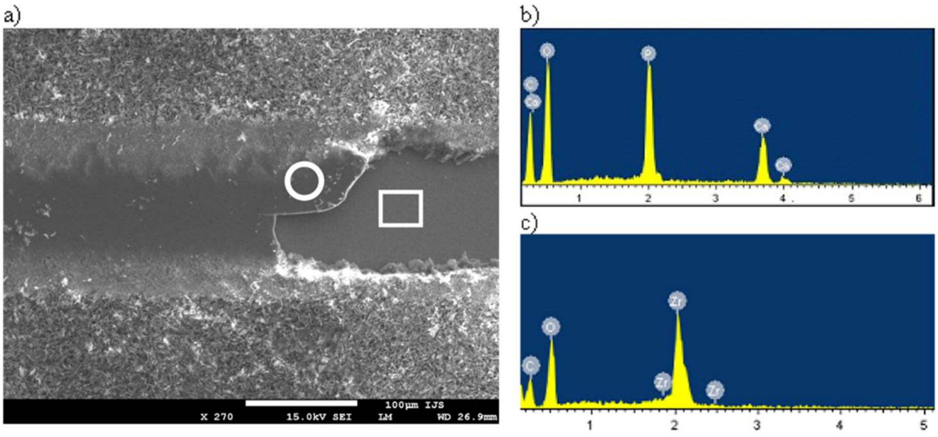

Figure 35. a) SEM micrograph of the biomimetic CaP coating after the scratch test and with the corresponding EDS analyses. (b) EDS analysis of the coating at the spot marked with a circle in a). (c) EDS analysis of the substrate at the spot marked with a square in a). L_c at which the coating was fully separated from the substrate was 5.3 ± 0.6 N.

4.1.4.4.4 Implantation in the artificial bone

Figure 36 shows SEM images of threaded parts of the CaP-coated zirconia implant before (Figure 36(a, b)) and after (Figure 36 (c, d)) implantation in an artificial bone. As seen on the SEM micrographs, the biomimetic CaP coating was homogenous over the entire surface of the implant. However, the coating did not preserve the topographical features of the underlying substrate. The coating was damaged after im- and explantation as shown in Figure 36 (c, d). The lamellar crystals, which constituted the major part of the biomimetic CaP coating, were removed and only a thin CaP layer remained on the surface of the zirconia implant. In addition, cracks and delaminations of large areas of coating were observed, mainly on the tips of the threads. Weighing the coated implants before and after the implantation showed that 36 % ± 9 % of the initial mass of the biomimetic CaP coating remained on the implant after im- and explantation from the artificial bone.

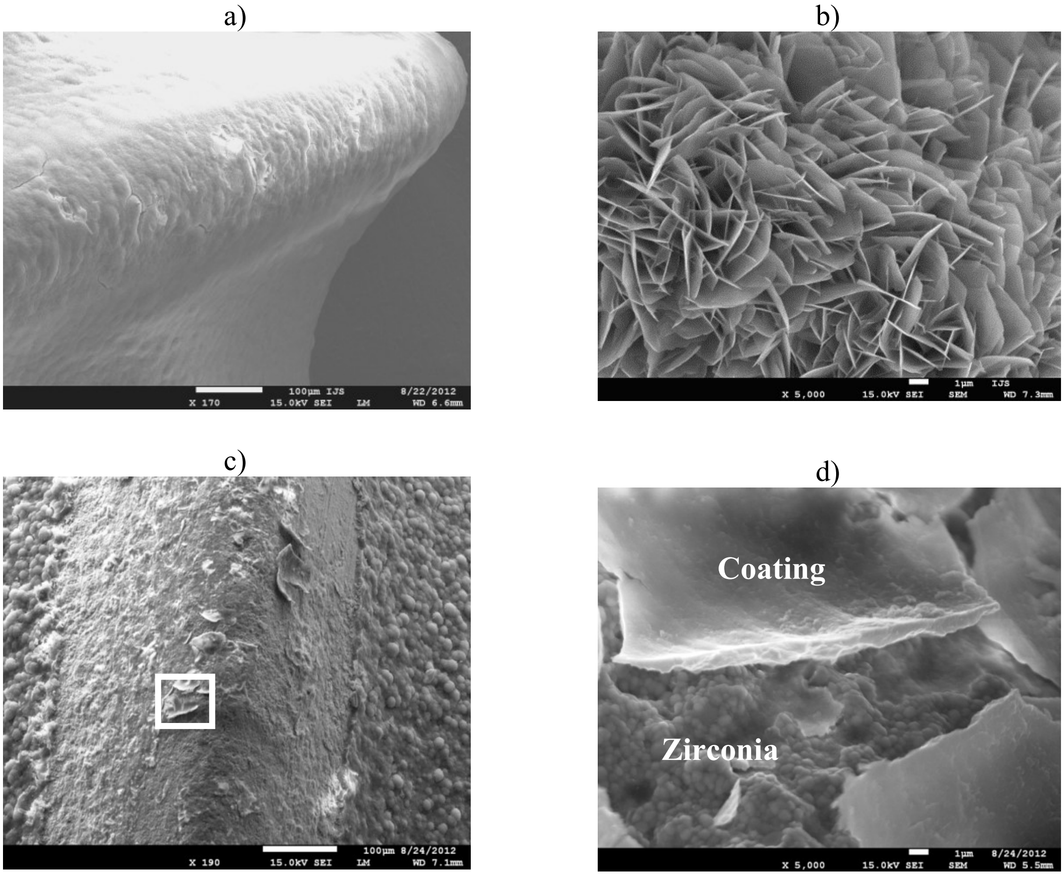

Figure 36. SEM micrographs of the zirconia implant coated with biomimetic CaP coating before (a,b) and after (c,d) implantation in the artificial bone. c) Note that the lamellar crystals of the biomimetic CaP coating were removed during the insertion of the implant in the artificial bone. In addition, severe cracks and delaminations of the coating mostly occurred at the tips of the threads. d) Enlarged area, which is marked with a square in c).

4.2 Post-deposition processing of the biomimetic calcium phosphate coatings

The second part of the thesis is focused on the post-deposition thermal processing of the biomimetic CaP coating on zirconia. Since there has not been any systematic study performed on the heating of biomimetic CaP coatings I was interested in how heating of the biomimetic CaP coating at various temperatures influences the properties of the obtained CaP coatings. Moreover, I investigated the possibility of combining heating and ultra-sound treatment to prepare novel CaP coatings.

The post-deposition processing of biomimetic CaP coatings on zirconia involved heating in the range between 600 °C and 1200 °C. Moreover, an ultra-sound treatment was applied to the coatings that were heated between 800 °C and 1200 °C.

Figure 37a shows an SEM image of the CaP coating that was prepared by heating the biomimetic CaP coating at 600 °C. After heating at 600 ºC (HA-600) the lamellar topography of the original biomimetic CaP coating (Figure 16) was preserved. The R_a value of the coating, as determined with the AFM was 700 nm. Figure 37b shows an AFM image of the coating.

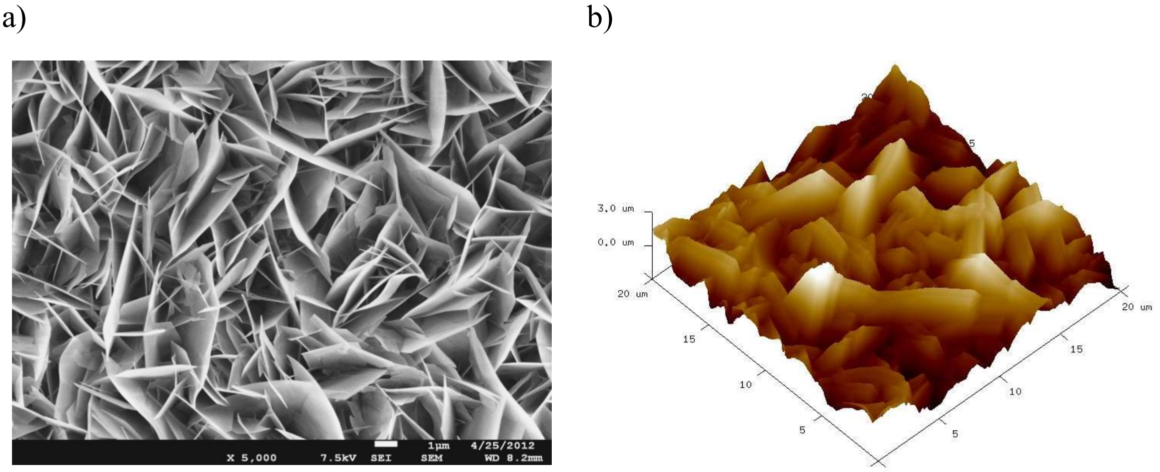
a) b)

Figure 37. SEM micrograph (left) and AFM image (right) of the HA-600 coating, which was obtained after heating the biomimetic CaP coating on zirconia at 600 °C.

An FTIR spectrum of the HA-600 coating is shown in Figure 38. In the spectrum ν_3 phosphate bands appeared at 1020 and 1088 cm^{-1}, ν_4 phosphate bands at 597 and 558 cm^{-1} and a shoulder at 625 cm^{-1} and hydroxyl stretch appeared at 3570 cm^{-1}. These signals are typical for the HA structure [110-111]. The broad water band at 3600 cm^{-1} disappeared, suggesting that crystal water was removed during the heating. Besides the HA peaks, additional peaks arose between 1150 and 1230 cm^{-1}, at 980 cm^{-1}, 950 cm^{-1}, and 746 cm^{-1} with a shoulder at 720 cm^{-1}. These bands correspond to the calcium pyrophosphate structure, $Ca_2P_2O_7$ (CPP) [111, 155]. The XRD pattern of the HA-600 coating showed peaks typical for the HA crystal structure (JCPDS 09-0432) (Figure 39).

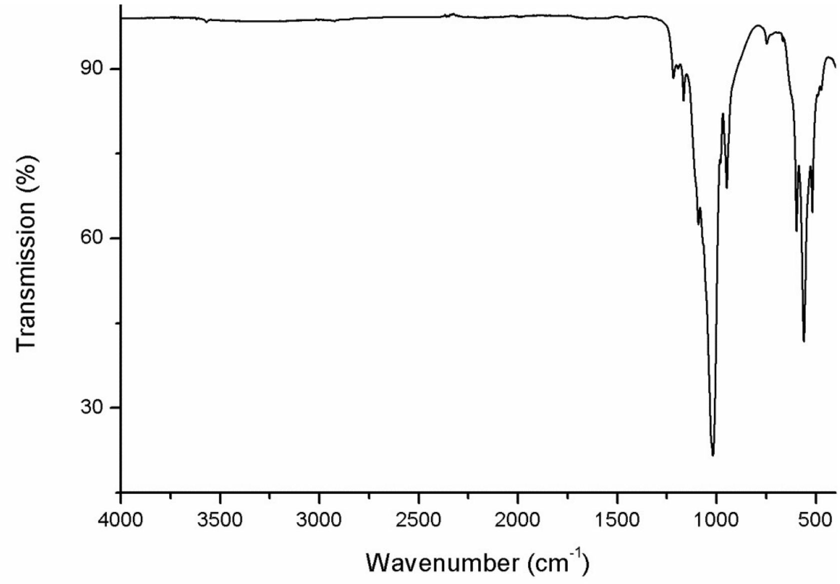

Figure 38. FTIR spectra of the HA-600 coating.

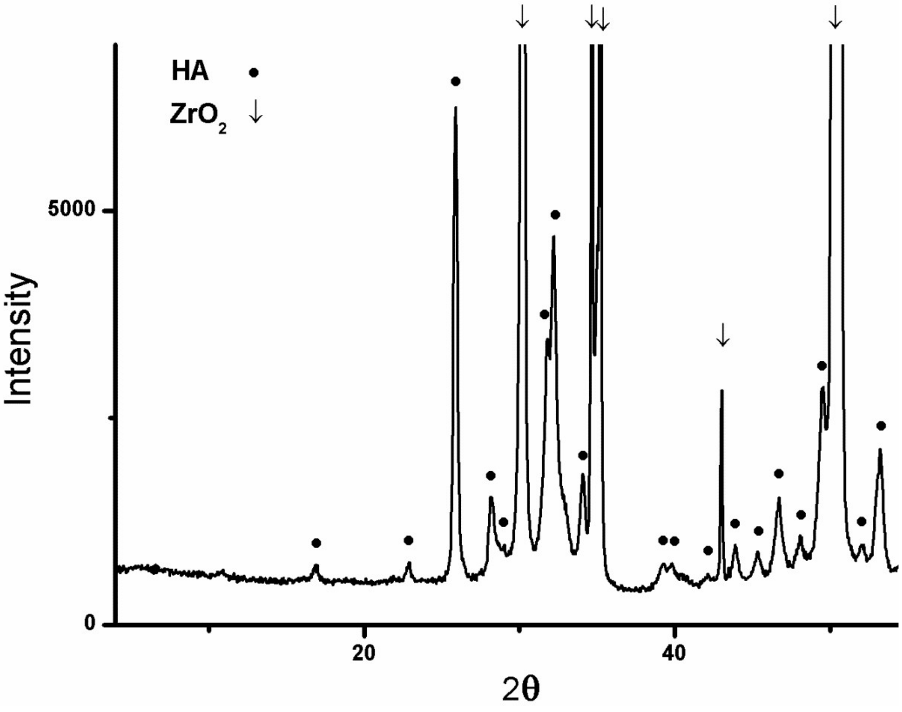

Figure 39. XRD diffractogram of the HA-600 coating on the zirconia substrate.

As can be seen from the SEM micrograph in Figure 40 the heating of the biomimetic CaP coating at 800 ºC, 900 ºC, 1100 ºC and 1200 ºC considerably changed the topography of the coatings. After heating at 800 ºC and 900 ºC the lamellar crystals became porous, but the lamellar topography of the coating was still partly preserved. Heating at 1100 ºC and 1200 ºC caused a collapse in the lamellar morphology. The coating was constituted of smaller crystals that formed a reticular morphology.

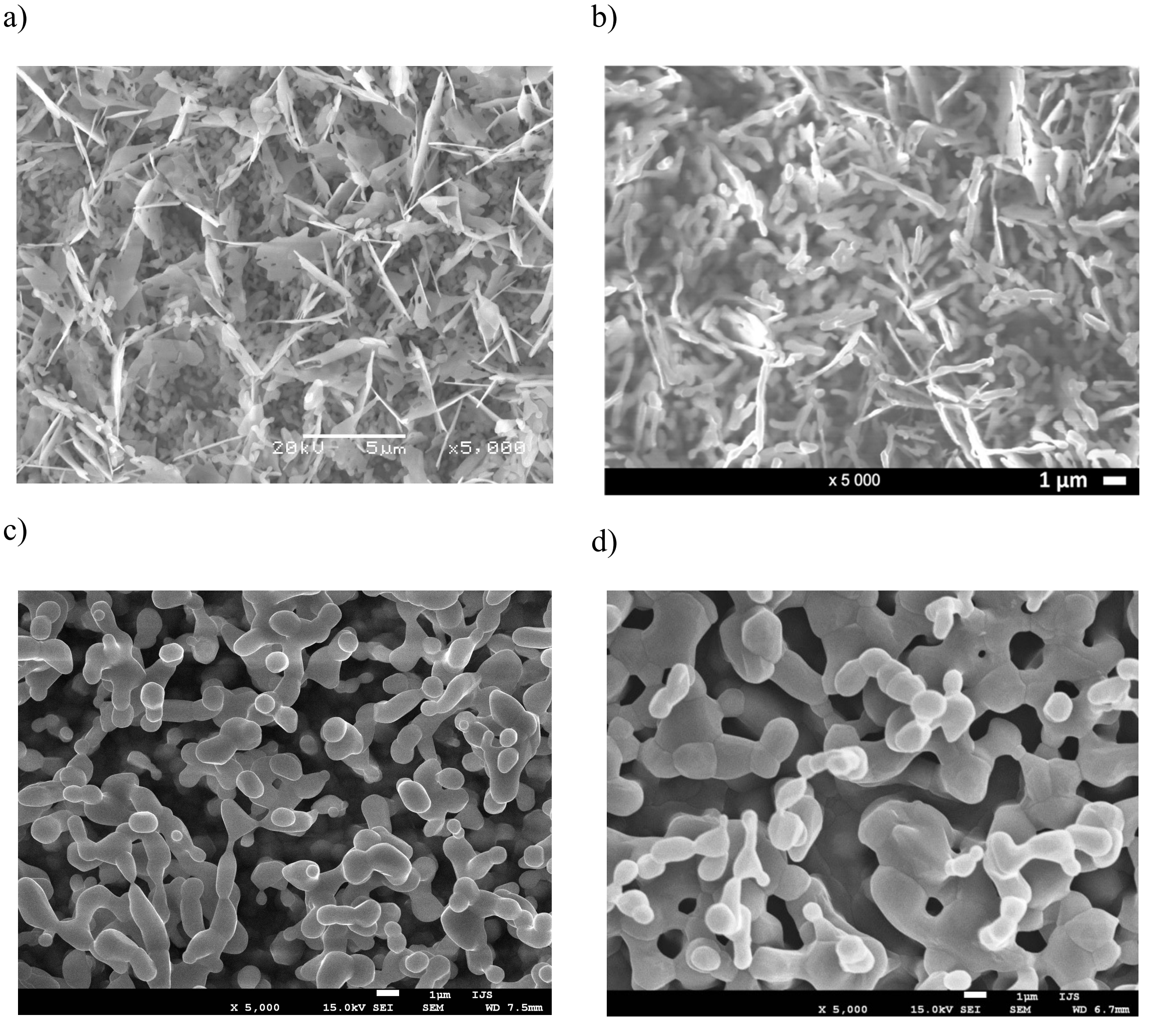

Figure 40. SEM micrograph of the coating that was obtained after heating the biomimetic CaP coating at 800 °C (a), 900 °C (b), 1100 °C (c), 1200 °C (d).

The FTIR spectra of coatings heated at 800 ºC and 900 ºC displayed a similar pattern (Figure 41). The hydroxyl stretch at 3570 cm^{-1}, which is typical for the HA structure disappeared, indicating that HA was not present in the coatings. In contrast, CPP bands remained at the same positions in the spectrum. New ν_3 PO_4 bands appeared at 1080 cm^{-1}, 970 cm^{-1}, shoulder at 1015 cm^{-1}, and ν_4 bands at 590 cm^{-1} and 542 cm^{-1}, which correspond to the β-TCP structure. After heating the biomimetic CaP coating at 1100 °C and 1200 °C only absorption bands typical for the β-TCP structure were observed.

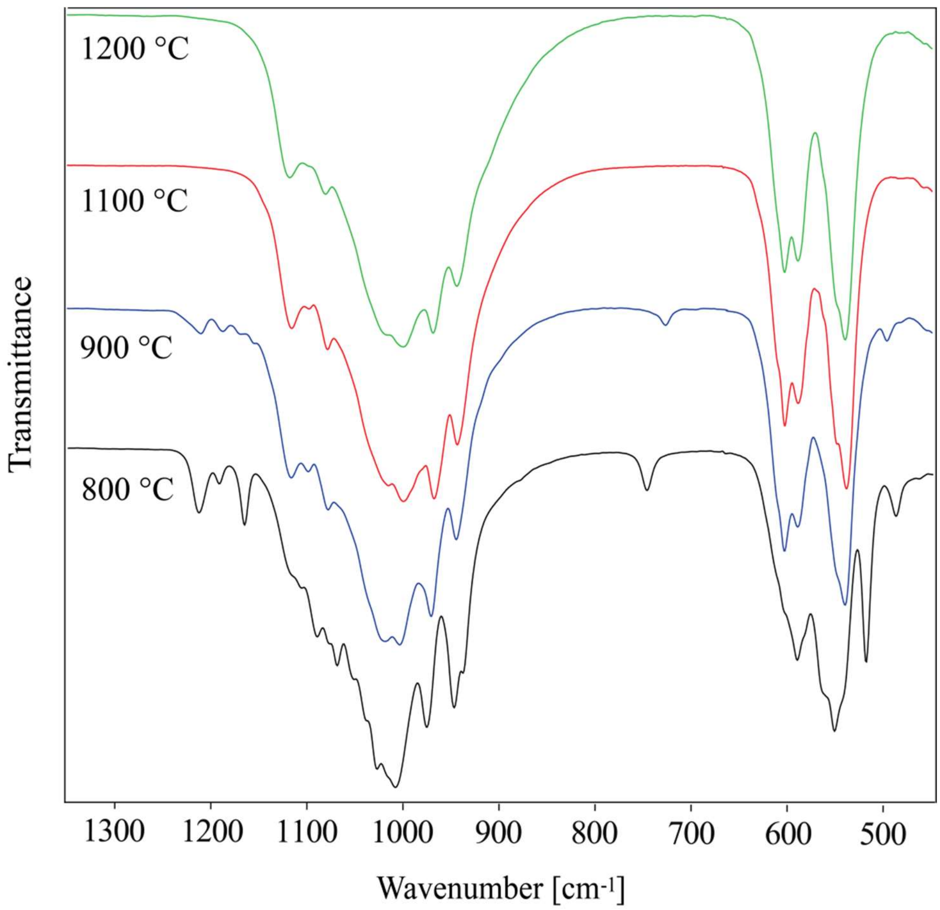

Figure 41. FTIR spectra of the coatings, which were obtained after heating the biomimetic CaP coating at 800 °C, 900 °C, 1000 °C and 1200 °C.

The XRD analysis of the coating heated at 800 °C revealed that β-TCP is the main phase in the coating (Figure 42). Beside the β-TCP peaks, low intensity signals appeared at 30.1°, 31.9°, 40.2°, 40.6°, 42°, 46,3 and 49.1°, which correspond to the β-CPP crystal structure (JCPDS 09-0346). After heating at 900 °C, the intensity of these CPP signals was reduced and after heating at 1100 °C and 1200 °C β-TCP was the only phase present in the coating (Figure 42).

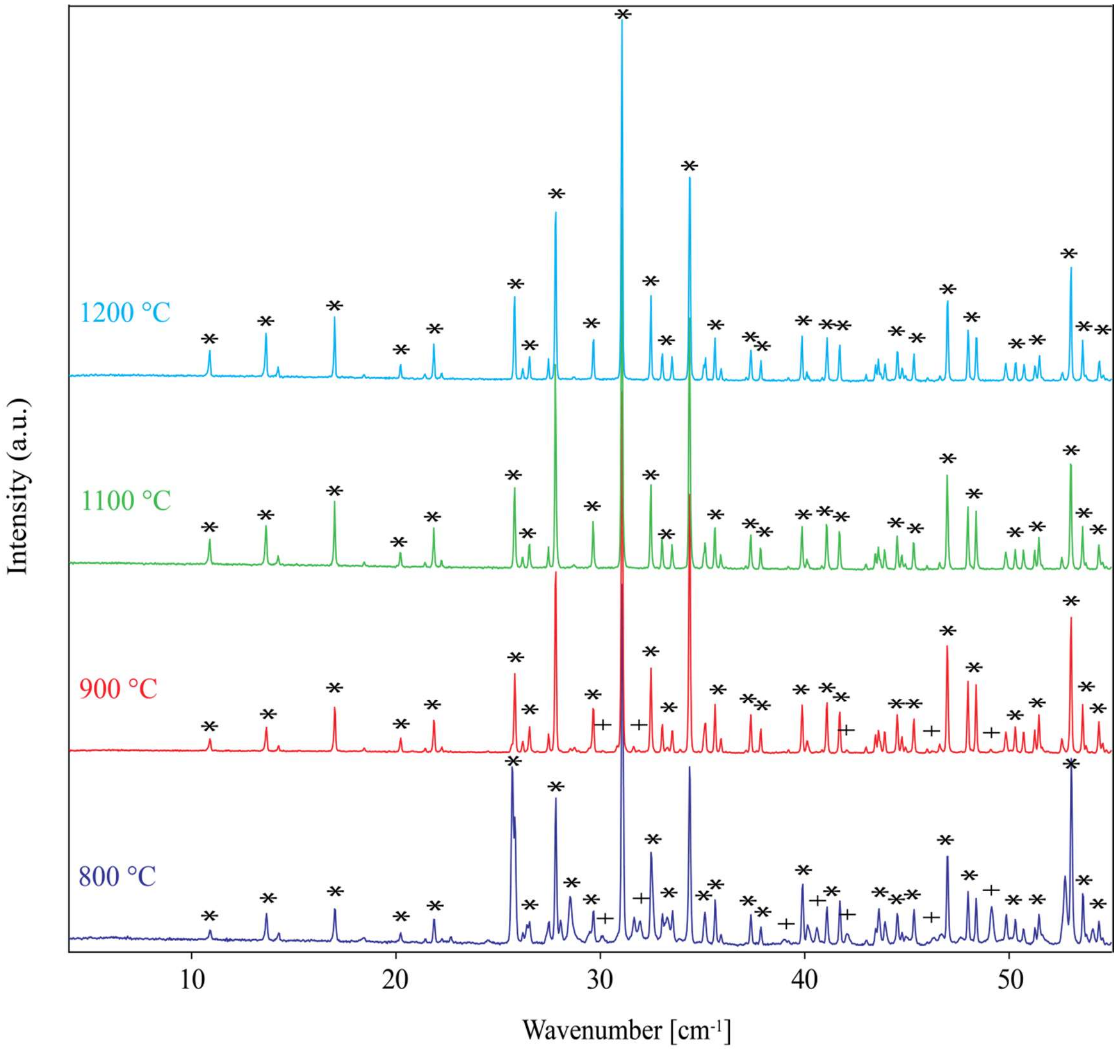

Figure 42. XRD spectra of the coatings after heating the biomimetic CaP coating at 800 °C, 900 °C, 1100 °C and 1200 °C. + β-CPP (JCPDS 09-0346); * β-TCP (JCPDS 09-0169). The CaP coatings were removed from the zirconia substrate for the XRD analysis.

The coatings that were heated above 800 ºC lost their mechanical integrity, such that by applying a relatively small force to the coating, for example, a stream of tap water or short (≈1 minute) sonication in a water bath, a majority of the coating could be removed, except for the thin CaP coating remaining on the zirconia surface. These thin coatings were used and evaluated in further experiments and depending on the heating temperature they will be abbreviated as βTCP-800, βTCP-900, βTCP-1100 and βTCP-1200. The XRD spectra of the coated zirconia specimens revealed that the coatings were composed of β-TCP. In the diffractograms of the βTCP-1100, βTCP-1200 coatings the diffraction lines of monoclinic zirconia appeared beside the peaks of tetragonal zirconia and β-TCP. The relative amount of transformed monoclinic zirconia on the specimens' surfaces was determined according to the method of Garvie and Nicholson [156]. The amount of monoclinic zirconia phase in the βTCP-1100 and βTCP-1200-coated zirconia samples was in both cases approximately 3 %.

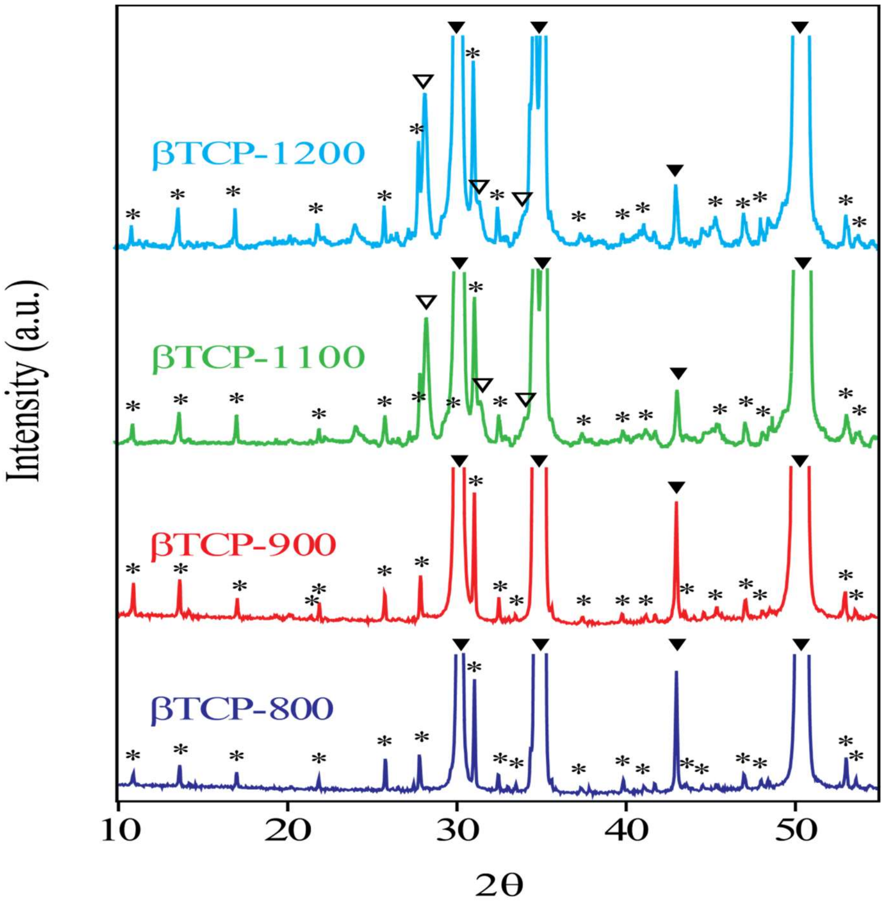

Figure 43. XRD spectra of the βTCP-800, βTCP-900, βTCP-900-9h, βTCP-1100 and βTCP-1200. ▼ tetragonal zirconia (JCPDS 88-1007); * β-TCP (JCPDS 09-0169); ∇ monoclinic zirconia (JCPDS 37-1484).

The βTCP-800 coating was composed of interwined particles that formed a reticular topography and had a thickness ≈500 nm. The βTCP-800 coating exhibited a roughness in the nanometre range (R_a = 46 nm, S_{dr} = 18 %) (Table 9). A SAED analysis of the coating revealed that each particle that constitutes the coating is a β-TCP monocrystal (Figure 44 c). The βTCP-900 had a similar thickness but displayed a different topography. It was composed of individual grains with diameters between 100-800 nm, which formed a fully dense structure. From the profile image of the βTCP-900 coating (Figure 45(c)) it can be observed that it is composed of a monolayer of grains. The surface roughness of the βTCP-900 coatings was in the same range as in the case of βTCP-800, i. e., R_a = 42 nm and S_{dr} = 15 % (Table 9).

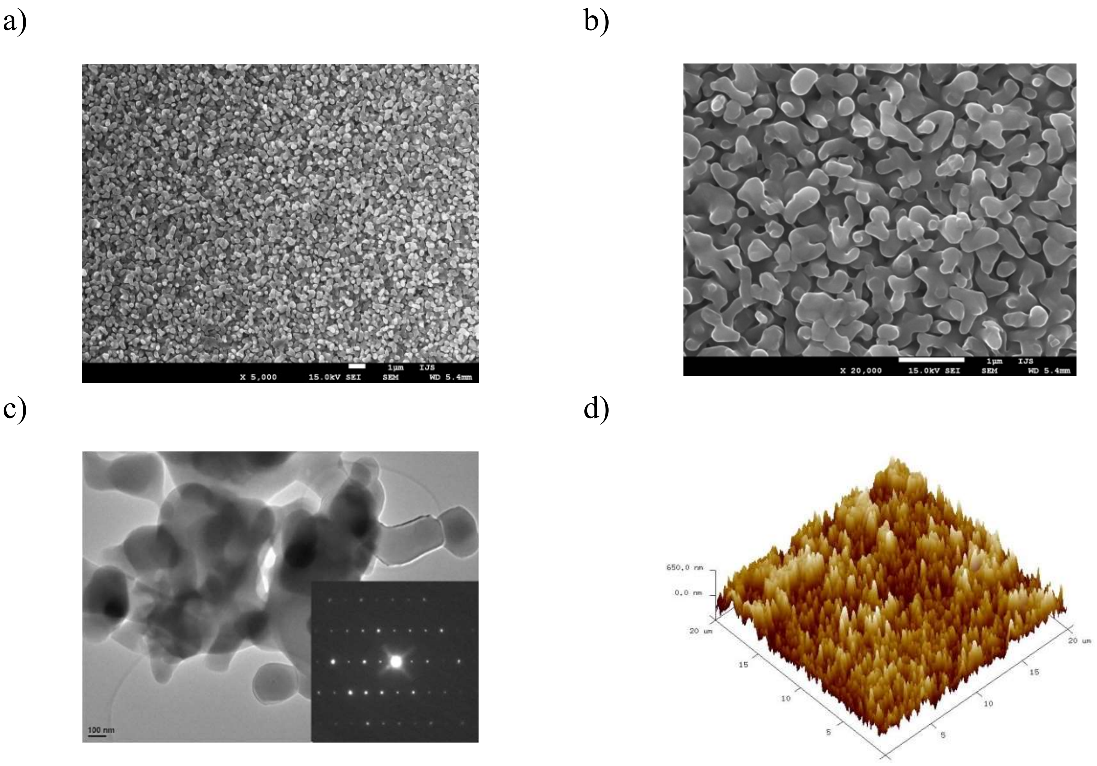

Figure 44. SEM micrographs (a,b), TEM/SAED analysis (c) and AFM image (d) of the βTCP-800 coatings. The coating was prepared by heating the biomimetic CaP coating at 800 °C and subsequently removing the upper part of the coating using sonication.

Table 9. Surface topography parameters for different CaP coatings prepared by applying post-deposition processing to a biomimetic CaP coating. For comparison, the topography parameters of the biomimetic CaP and HA-600 coatings are also shown.

Coating	*Average surface roughness (R_a) (μm)*	*Developed surface area ratio (S_{dr}) (μm)*
βTCP-800	46 ± 5	18 %
βTCP-900	42 ± 5	15 %
βTCP-1100	270 ± 20	35 %
βTCP-1200	370 ± 20	44 %
Biomimetic CaP	800 ± 200	900 % *
HA-600	700 ± 200	900 % *

* S_{dr} of the biomimetic CaP and HA-600 coatings with a lamellar topography was determined with the stereometrical method.

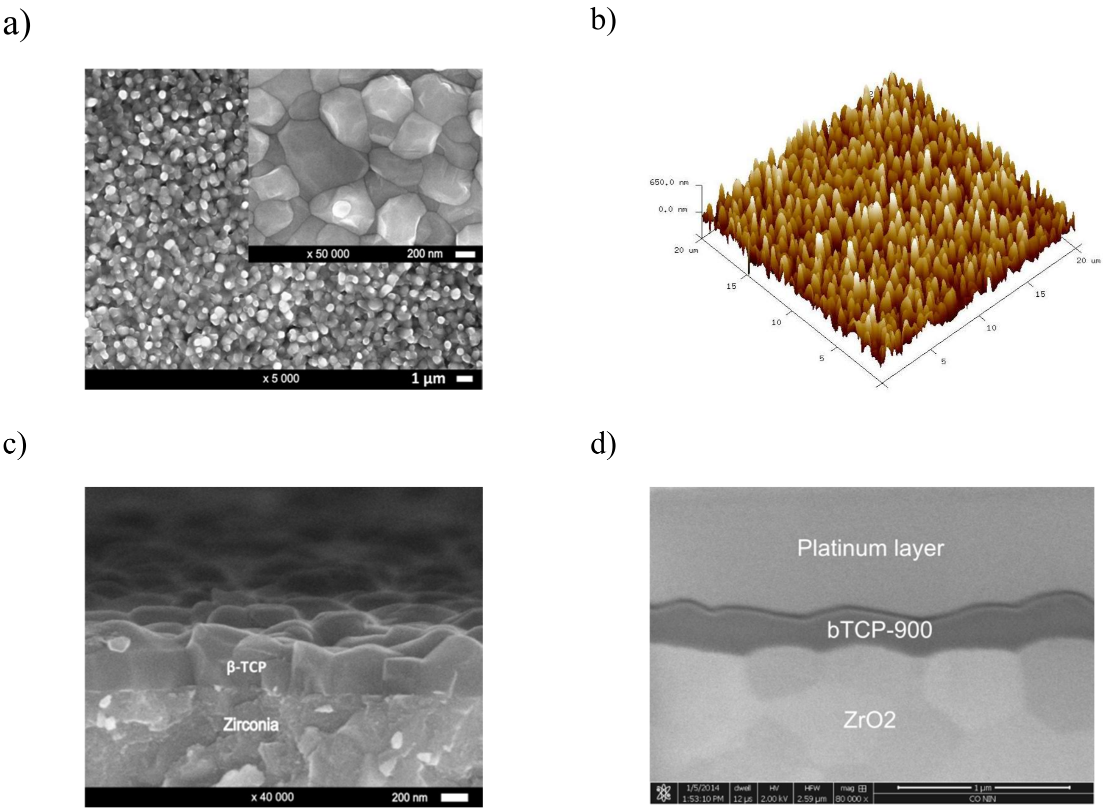

Figure 45. SEM micrographs (a, c, d) and AFM image (b) of the βTCP-900 coating. The coating was prepared by heating the biomimetic CaP coating at 900 °C and subsequently removing the upper part of the coating using sonication. d) A FIB was used to prepare a cross-section of the βTCP-900 coating on zirconia substrate. Note the grains that constitute the zirconia substrate. A platinum layer was deposited on the coatings in order to protect them from the high-energy ion beams.

The βTCP-1100 and βTCP-1200 coatings were also dense and composed of grains (Figure 46, Figure 47), but additional crystals formed on the ground monolayer, resulting in an increased thickness and surface roughness of these coatings compared to the βTCP-900 (Table 9).

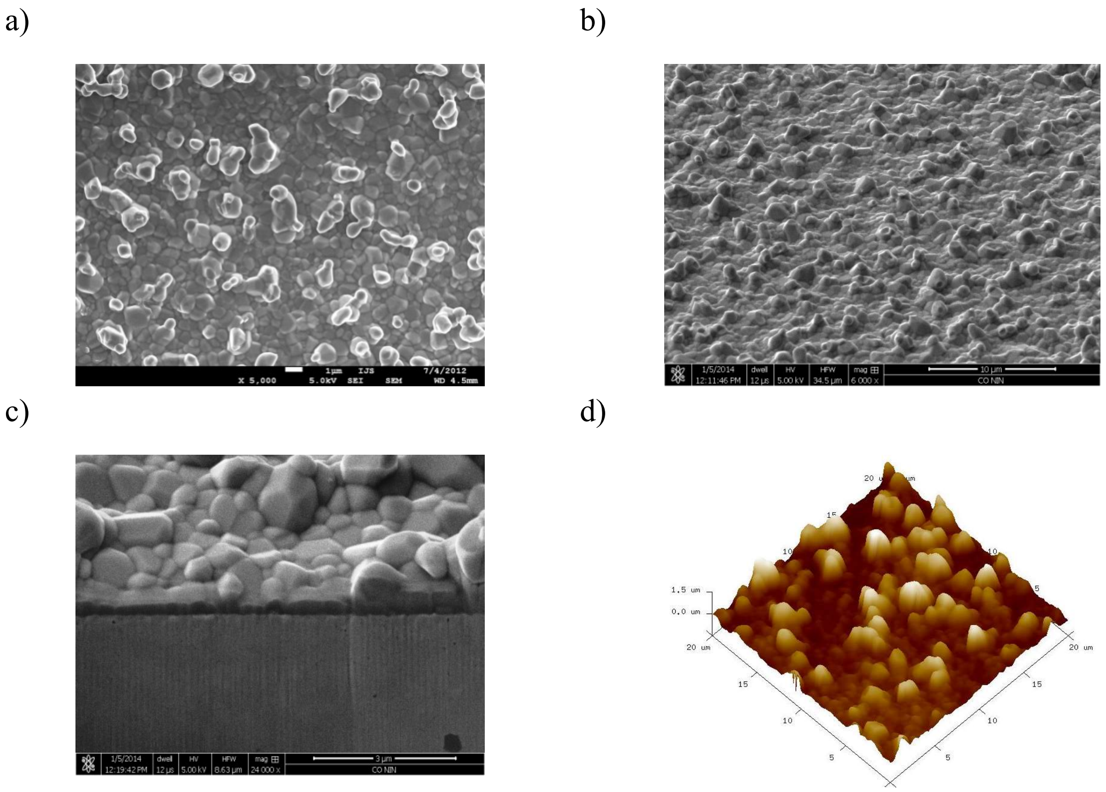

Figure 46. SEM images (a, b, c) and AFM image (d) of the βTCP-1100 coating at different magnifications. The coating was prepared by heating the biomimetic CaP coating at 1100 °C and subsequently removing the upper part of the coating using sonication. (a) Upper view; (b,c) side-view of the coating. c) FIB was used to prepare a cross-section of the coating.

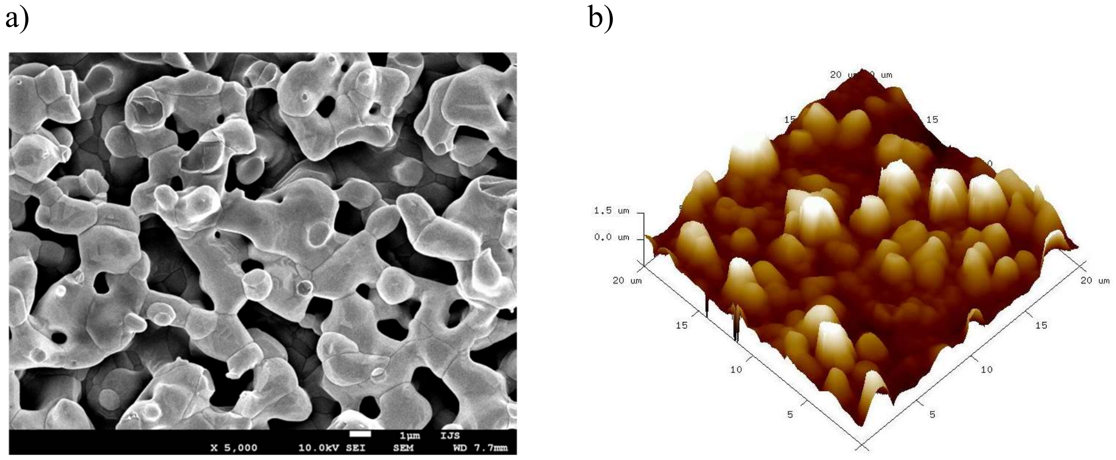

Figure 47. SEM (a) and AFM image (b) of the βTCP-1200 coating. The coating was prepared by heating the biomimetic CaP coating at 1200 °C and subsequently removing the upper part of the coating using sonication.

In order to test the influence of heating rate and dwell time on the topography of prepared coatings two additional heating regimes of the biomimetic CaP coating were examined: i) heating at 800 °C, 1h with a heating rate 600 °C/h; and ii) heating at 900 ºC for 9 hours (heating rate = 300 °C/h). After heat treatment the samples were sonicated. As can be observed in Figure 48, the increased heating rate produced a more porous coating after heating at 800 °C (comparison with βTCP-800) and the increased dwell time resulted in the increased grain size of the coating and changed the shape of grains, which became more sharp-edged and faceted (comparison with the βTCP-900 coating). The XRD analysis (Figure 43) revealed that prolonged heating at 900 °C did not change the phase composition of the coating and the β-TCP crystal structure was preserved.

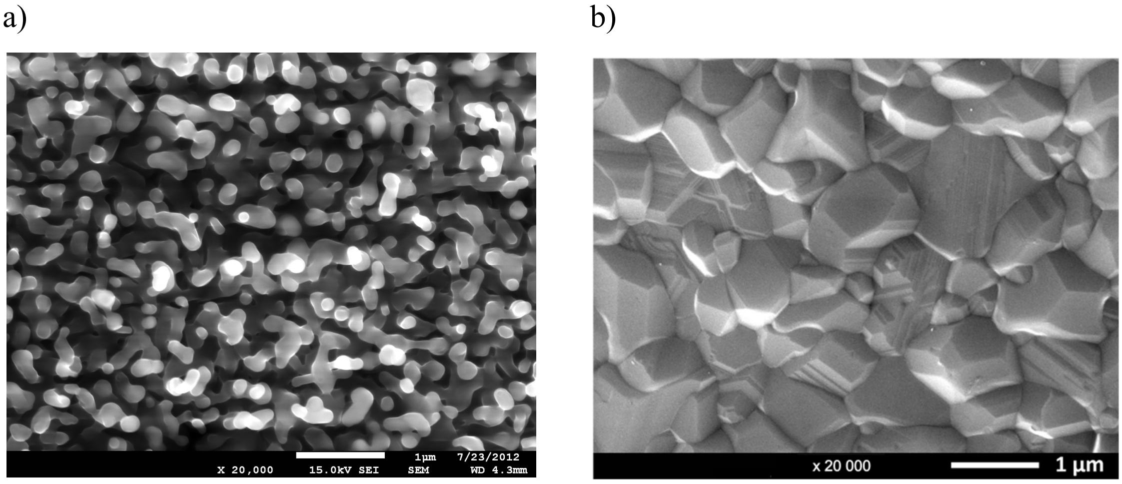

Figure 48. SEM image of the β-TCP coatings on the zirconia substrate that were synthesized by heating the biomimetic CaP coating at a) 800 °C (1 h, rate = 600 °C/h) and b) 900 °C (9 h, rate = 600 °C/h) and subsequent sonication.

4.2.1 Mechanical properties

The results of the mechanical tests are gathered in Table 2.

Table 10. Mechanical properties of biomimetic CaP coating and different CaP coatings prepared by post-deposition processing of the biomimetic CaP coating.

Coating	*Scratch test Critical load-L_c (N)*	*Tensile strength test (MPa)*	*Implantation and explantation of the coated implant from the artificial bone Remaining mass of the coating (%)*
Biomimetic CaP coating	5.6 ± 0.6	1.8 ± 0.3	36 ± 9
HA-600	/	3.2 ± 0.6	*
βTCP-800	/	47.8 ± 4.7	*
βTCP-900	97 ± 9	52.3 ± 3.8	92 ± 7
βTCP-1100	/	32.9 ± 7.2	/
βTCP-1200	/	27.6 ± 5.1	/

* In the case of HA-600 and βTCP-800 coatings the damage to the coatings during implantation and explantation from the artificial bone was determined qualitatively using SEM.

4.2.1.1 Tensile bond testing

Figure 49 presents measured values of the tensile bond strength for various CaP coatings. For comparison, also the bond-strength value of the biomimetic CaP coating is shown. During tensile testing fractures occurred at the substrate-coating interface in the case of the HA-600, βTCP-900, βTCP-1100 and βTCP-1200, indicating that the cohesion strength of these coatings is stronger than the adhesion strength. In contrast, as can be observed in Figure 50, in the case of βTCP-800 the failure occurred at the coating-adhesive interface at 47.8 ± 4.6 MPa. The measured value therefore certainly represents a lower limit for the adhesion bond strength of the coating on the substrate. No trace of the adhesive was detected on the zirconia substrates after the tensile tests were performed, demonstrating the absence of penetration of the adhesive to the substrate.

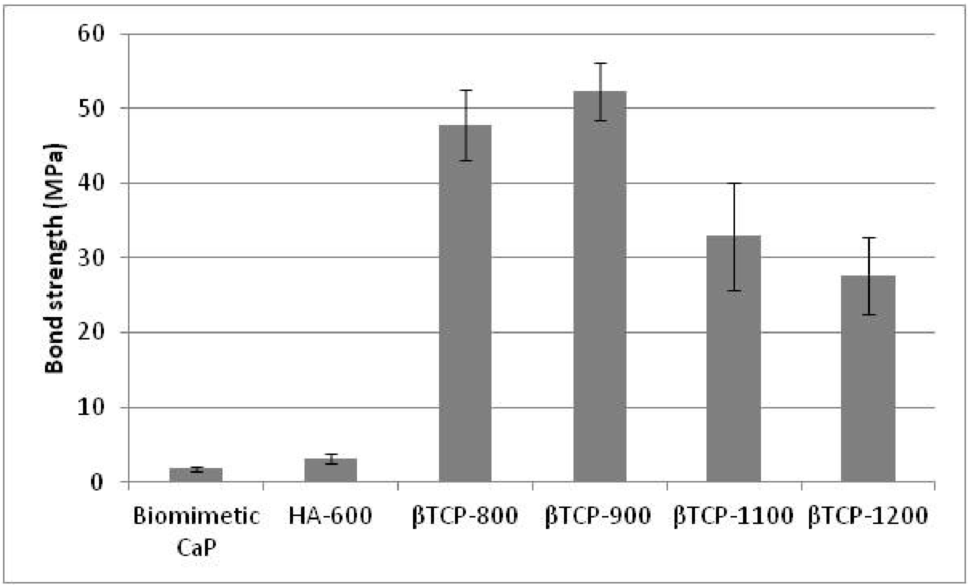

Figure 49. Measured values for tensile bond strength of different CaP coatings.

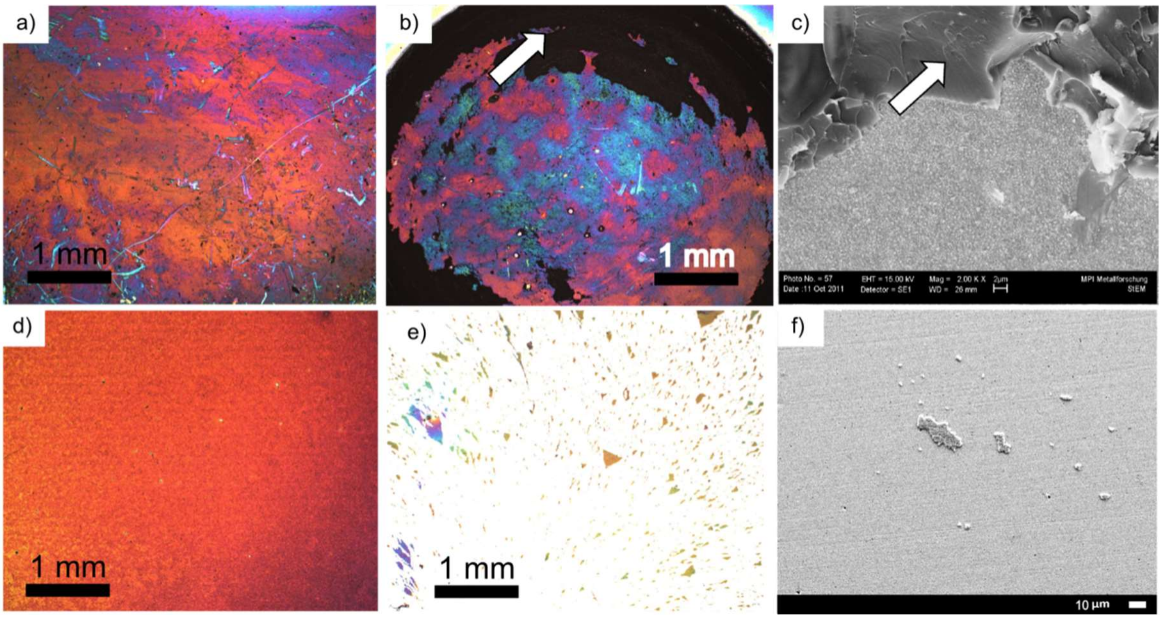

Figure 50. Optical micrographs (a, b, d, e) and SEM micrographs (c, f) of βTCP-800 (a-c) and βTCP-900 (d-f) coatings before (a, d) and after (b, c, e, f) tensile testing. White arrows show the remains of the adhesive that was used in the tensile test.

4.2.1.2 Scratch test

A scratch test was performed on the βTCP-900 coating. As is clear from the optical micrograph that shows a panoramic view of the scratch in the βTCP-900 (Figure 51a) the coating was not separated from the zirconia substrate, even at the final load of 120 N. Nevertheless, the microscopic analysis of the scratch groove at a higher magnification revealed that coating chipping occurred at the edges of the groove, starting at the load 59 N ± 4 N (Figure 51 b). At higher loads, starting at 97 N ± 9 N, chipping occurred in the scratch groove and the white zirconia substrate became visible (L_c) (Figure 51 c) (Table 10). No other mode of coating failure was observed in the β-TCP coating (Table 10).

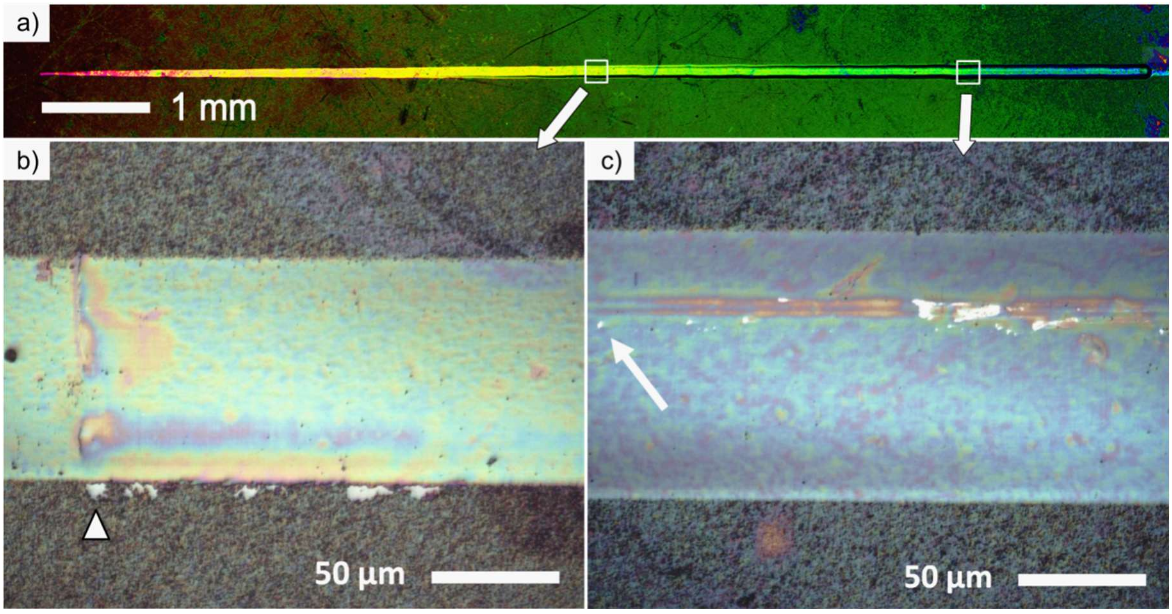

Figure 51. Optical micrographs of the β-TCP coating on zirconia ceramics after the scratch test. a) Panoramic view of the scratch. No form of coating failure could be observed in the coating. b) Coating chipping occurred at the edge of the scratch groove, starting at 59 N ± 4 N (arrowhead). c) Critical load (L_c) at which the β-TCP coating was removed in the scratch groove and white zirconia substrate became exposed was at 97 N ± 9 N (white arrow).

4.2.1.3 Implantation of the coated implant in the artificial bone

Figure 52 and Figure 53 show the SEM images of the zirconia implants with different CaP coatings before and after implantation and explantation from the artificial bone. As can be seen, all the CaP coatings tested were homogenous over the entire surface of the implants. While the βTCP-800 and βTCP-900 coatings preserved the micrometer-range surface topography of the underlying substrate (Figure 53), the thicker HA-600 coating (Figure 52) completely covered the surface features of the underlying implant. The HA-600 coating was strongly damaged after im- and explantation (Figure 52). The lamellar crystals, which constituted the major part of the biomimetic CaP coating, were removed and only a thin CaP layer remained on the surface of zirconia implant. In addition, cracks and delaminations of large areas of coating were observed, mainly on the tips of the threads. The βTCP-800 coating remained homogenous over the surface of the implant but detailed SEM analysis at higher magnification revealed that the individual crystals that constitute the coating were damaged during the implantation (Figure 53). The crystals exhibited an internal structure composed of nanocrystals with a size of ≈20 nm. A TEM/ED analysis of these nanocrystals (Figure 54) showed that they have a β-TCP crystal structure. The βTCP-900 coating exhibited even better mechanical stability compared to the βTCP-800 and no form of coating cracking or delamination was observed. The only deformations observed were squashings of the coating on a few areas on the peaks of the implant threads. Weighing the βTCP-900-coated implants before and after im- and explantation from the artificial bone showed that 92 ± 7 % of the initial mass of the coating was preserved on the implant. The observed squashings could be the reason for the observed loss in the coating mass (Figure 53).

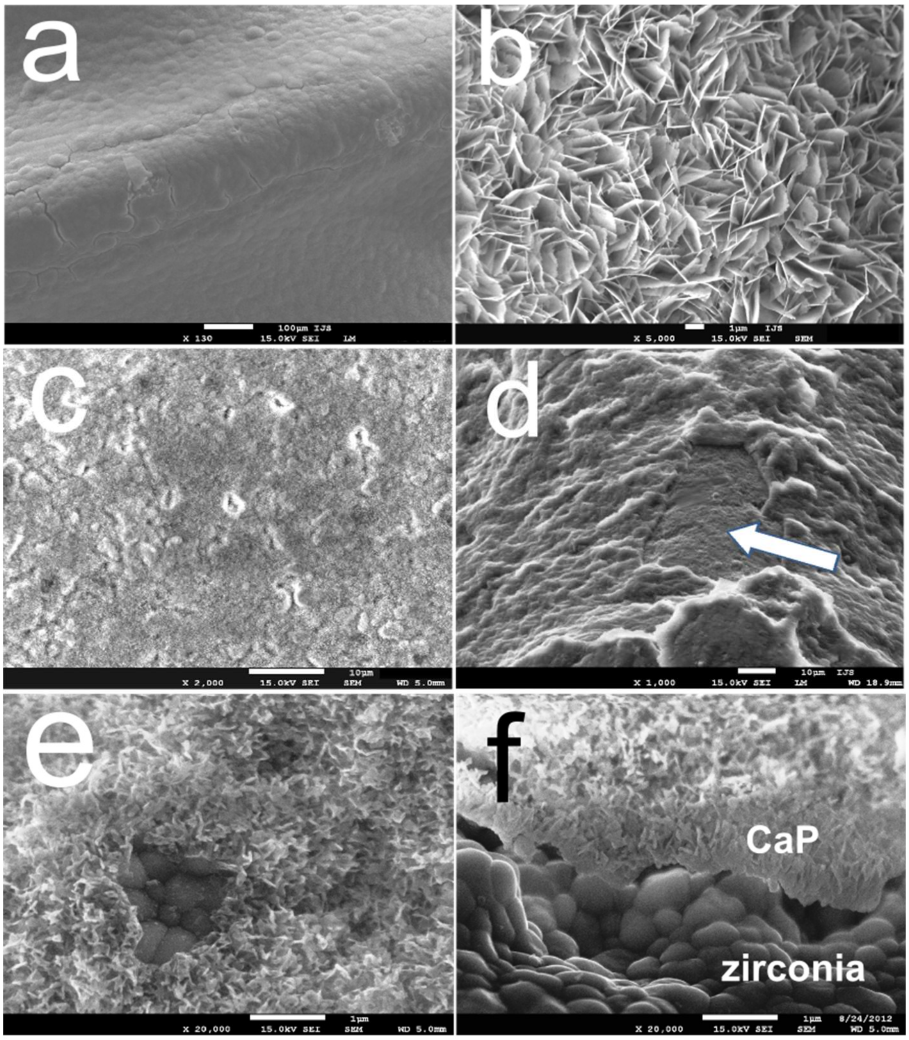

Figure 52. SEM micrographs of zirconia implants coated with HA-600 coating before (a, b) and after (e, f) implantation in the artificial bone. d) The white arrow shows on the spot where the coating was removed and the zirconia substrate became visible.

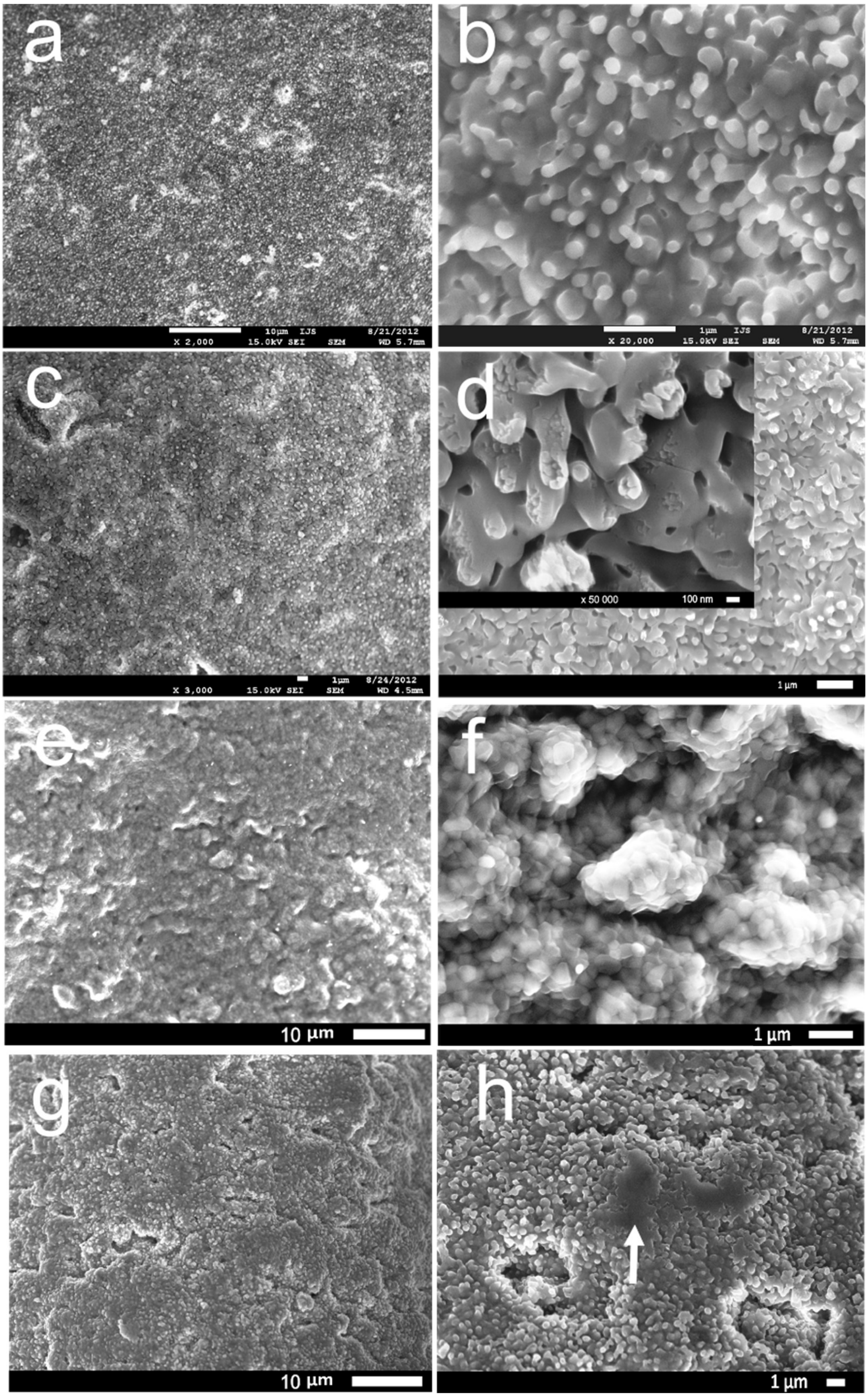

Figure 53. SEM micrographs of zirconia implants coated with βTCP-800 (a–d) and βTCP-900 (e–h) coating before (a, b, e, f) and after (c, d, g, h) implantation in the artificial bone. h) The white arrow shows an area of squashed βTCP-900 coating.

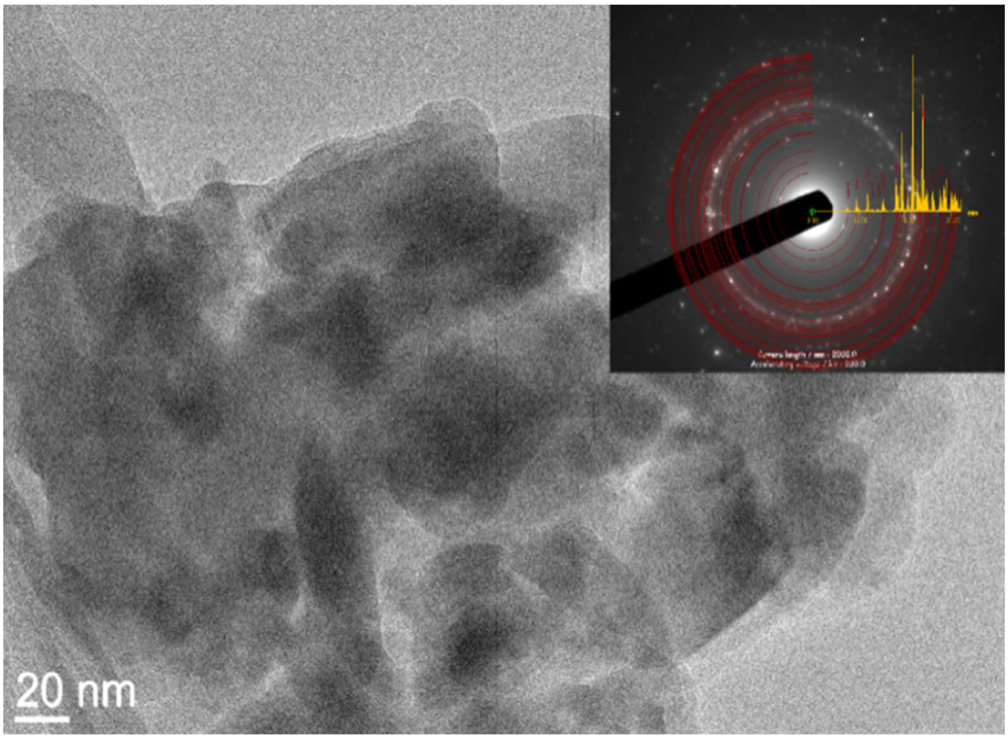

Figure 54. TEM bright-field image of the βTCP-800 coating scratched from the zirconia surface after implantation and explantation from the artificial bone. Note the nanocrystals with sizes ranging from 20 to 50 nm. The experimental SAED pattern is in agreement with the calculated electron diffraction of the β-TCP crystal structure.

4.2.1.3.1 Implantation of a titanium implant coated with βTCP-800 in a pig's jaw bone

In order to test the prepared coatings in a more realistic situation, the βTCP-800 coating was deposited on a commercial titanium implant (Ankylos$^{\text{TM}}$). Figure 55 shows photographs taken during the implantation of the implant into a pig's bone. In Figure 56, SEM images of the implant after implantation are represented. No damage to the coating could be observed after a thorough inspection of the surface.

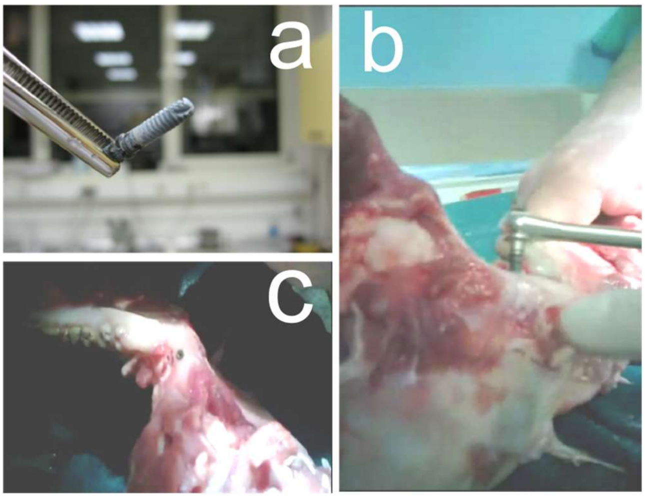

Figure 55. Implantation of Ankylos^{TM} titanium implant in the pig’s cadaver bone. a) Photograph of the implant with βTCP-800 coating. b) image taken during the implantation procedure. c) Note the implant inserted into the jaw bone.

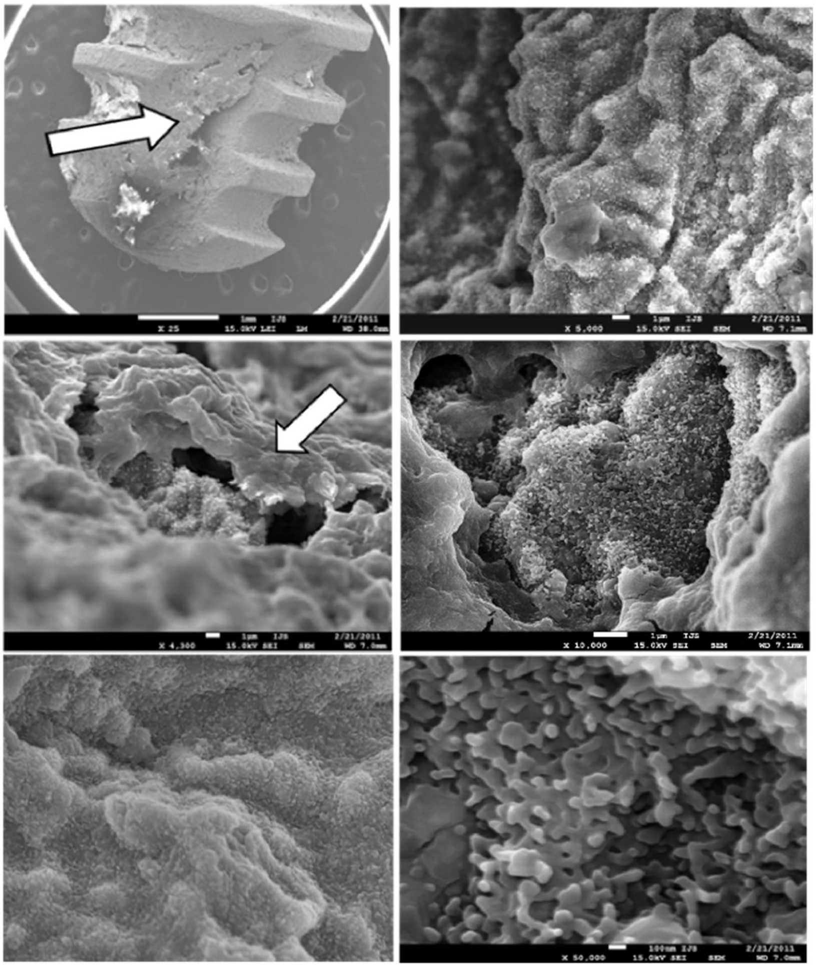

Figure 56. SEM images of the titanium implant (Ankylos^{TM}) coated with βTCP-800 after implantation and explantation from the pig's cadaver jaw bone. The white arrows show the remnants of the biological tissue on the implant’s surface.

4.3 Dissolution of calcium phosphate coatings in a physiological solution

Figure 57 and Figure 58 show the dissolution profiles of Ca^{2+} for the studied CaP coatings after immersion in the PBS for 24 hours. For the sake of clarity the dissolution profiles of the less soluble β-TCP coatings (β-TCP-800, β-TCP-900, β-TCP-1100, β-TCP-1200) are presented separately in Figure 58. The dissolution rate sequence was: HA-600 > OCP > TCP-1200 > TCP-1100 > TCP-800 > TCP-900. The HA-600 and biomimetic OCP coatings had a much higher dissolution rate than the β-TCP coatings.

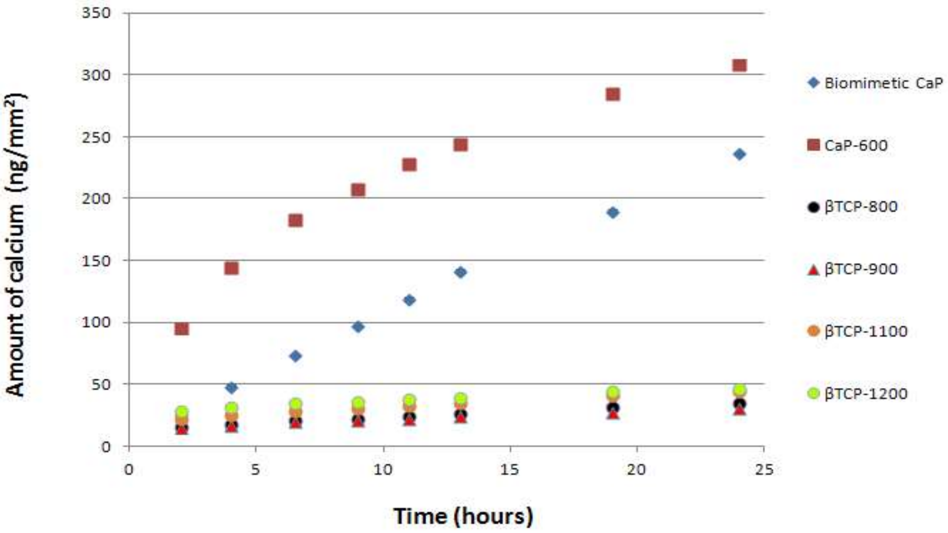

Figure 57. Release rate of Ca^{2+} ions in PBS from different CaP coatings.

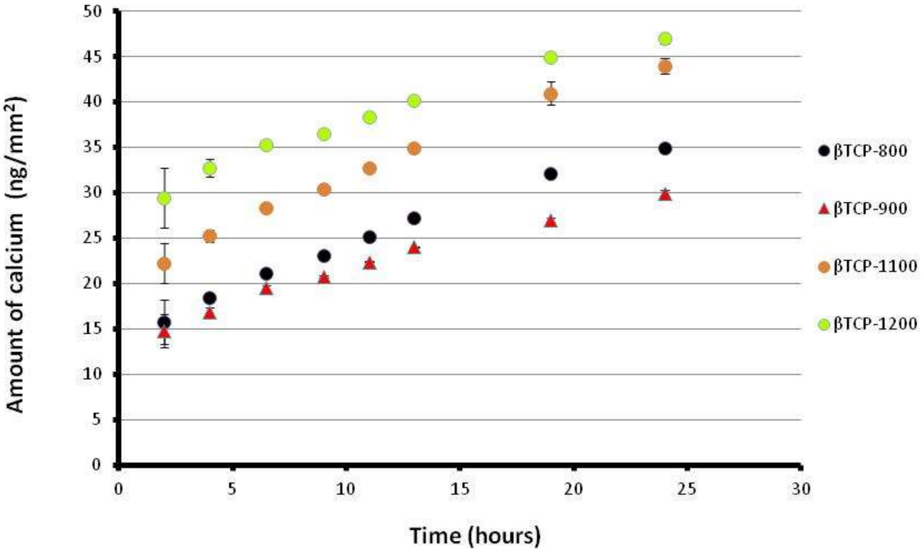

Figure 58. Release rate of Ca^{2+} ions in PBS from βTCP-800, βTCP-900, βTCP-1100 and βTCP-1200 coatings.

Knowing that coatings prepared by heating the biomimetic OCP coating between 600 °C and 900 °C are composed of calcium orthophosphate and calcium pyrophosphate (Figure 38, Figure 42, Figure 41), an additional experiment was performed in order to examine whether the dissolution rate of these two phases in PBS is different. A zirconia disc coated with the HA-600 coating was immersed in deionized water for several days and afterwards analysed with FTIR spectroscopy. Deionized water was chosen as the dissolution medium due to its lower ionic strength compared to PBS, resulting in increased dissolution of the coating and a more pronounced difference in the dissolution rate between the calcium orthophosphate and CPP phases. As can be observed in the FTIR spectra of the HA-600 coating after three days of immersion in water (Figure 59), the pyrophosphate peaks around 740 and 1200 cm^{-1} disappeared and only orthophosphatic bands remained in the spectrum.

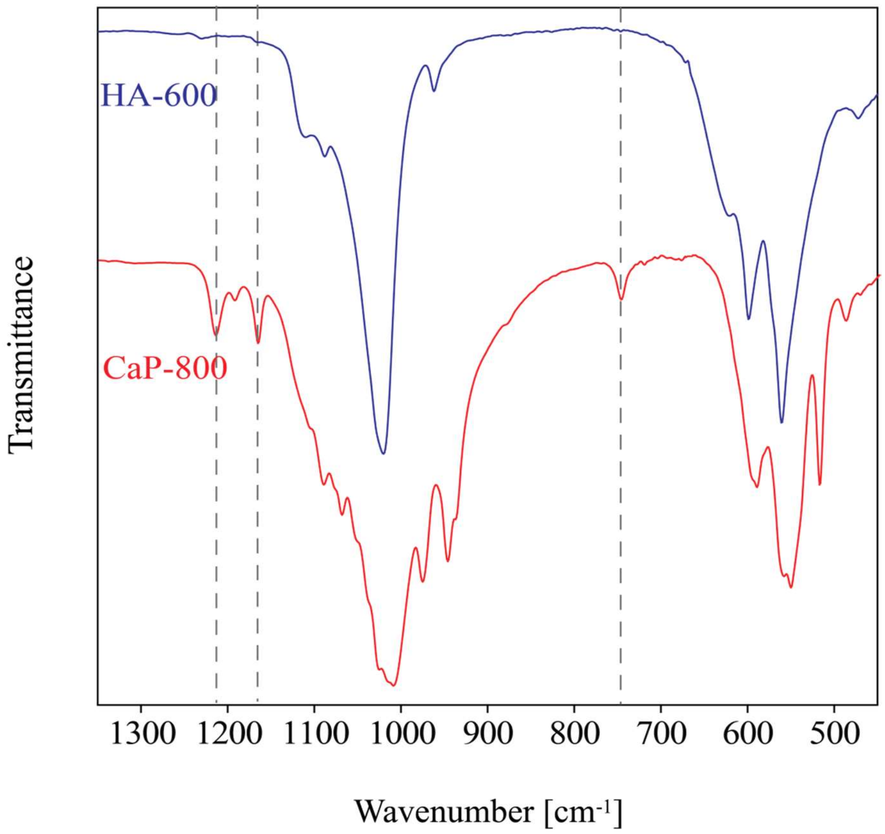

Figure 59. FTIR spectra of the HA-600 and CaP-800 coatings after immersion in deionized water for three days (HA-600) and six days (CaP-800), respectively. Note the absence of CPP peaks at 740 cm^{-1} and around 1200 cm^{-1} in the case of the HA-600 coating. The CaP-800 coating was

prepared by heating the biomimetic CaP coating at 800 °C.

With the aim to test the dissolution behaviour of the CPP phase formed after heating at higher temperatures, an additional dissolution experiment in water was performed with the coating that was prepared by heating the biomimetic CaP coating at 800 °C (no sonication after heat treatment) (abbreviation: CaP-800). The SEM image of the coating is represented in Figure 40. The CaP-800 coating was composed of β-TCP and β-CPP, as determined with XRD (Figure 42) and FTIR (Figure 41) analyses. After six days of immersion in water the relative intensity of the pyrophosphate bands compared to the orthophosphate bands remained unchanged, indicating that heating of biomimetic CaP at 800 °C produces CPP groups with a lower dissolution rate than after heating at 600 °C.

4.4 Test of bioactivity

Figure 60 shows micrographs of different CaP coatings on zirconia substrates after immersion in the SBF for 7 days (HA-600, βTCP-800) or 2 months (βTCP-900). A biological-like HA layer precipitated on all the CaP coatings tested.

a)

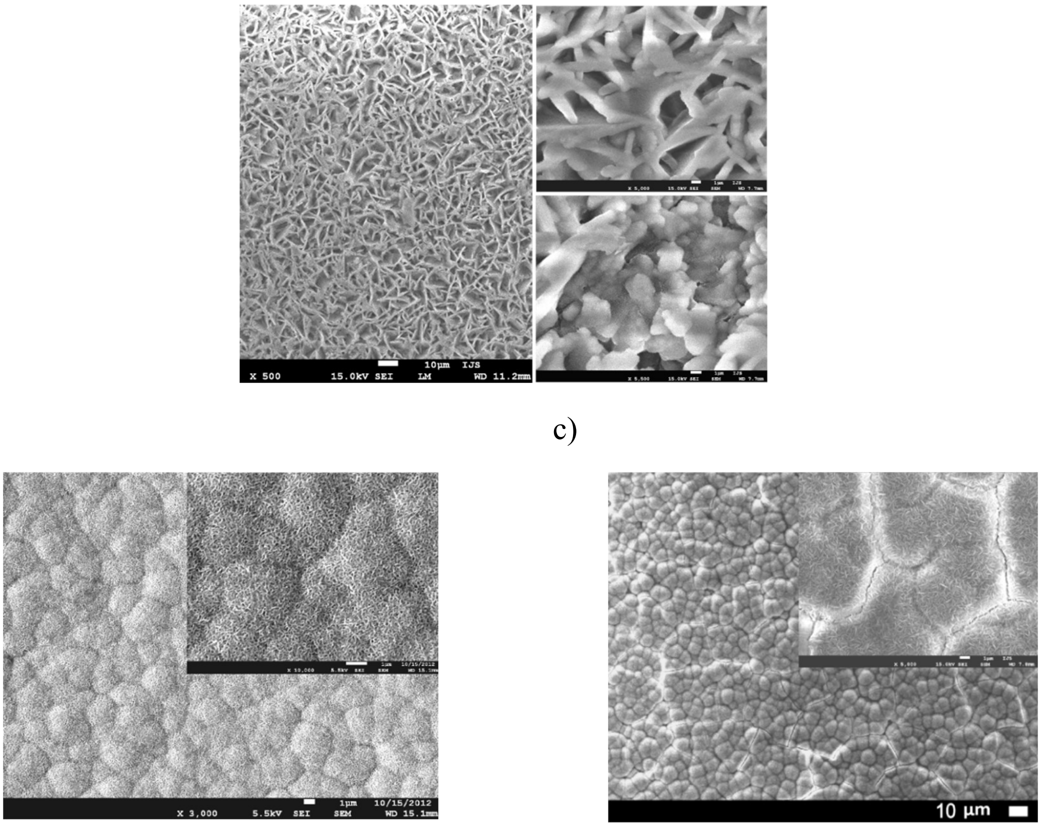

b)

c)

Figure 60. SEM micrographs of the zirconia substrates with different CaP coatings after

immersion in SBF for 7 days (HA-600 and βTCP-800) and 2 months (βTCP-900). a) HA-600; b) βTCP-800; c) βTCP-900.

In the case of the βTCP-800 and βTCP-900 coatings the HA layer was uniform and composed of agglomerates that consisted of fine crystals. Moreover, the layer covered the texture of the underlying coating. In contrast, in the case of the HA-600 coating, the original lamellar morphology was still preserved. The apatite crystals precipitated on the surface of the plates causing an increase in their thickness from an initial ≈50 nm to ≈1µm. In addition, on some areas the precipitates covered the lamellar crystals. On the XRD diffractograms of the HA-600 coating after the SBF test the relative intensity of the HA peaks in the XRD diffractogram increased compared to the coating before the SBF test. In the XRD diffractograms of the βTCP-800 and βTCP-900 coatings, new peaks appeared at 22.9°, 25.9°, 28.1°, 29°, 31.8°, 32.2°, 32.9°, 34°, 39.2°, 46.7°, 52.1°, which correspond to the HA crystal structure.

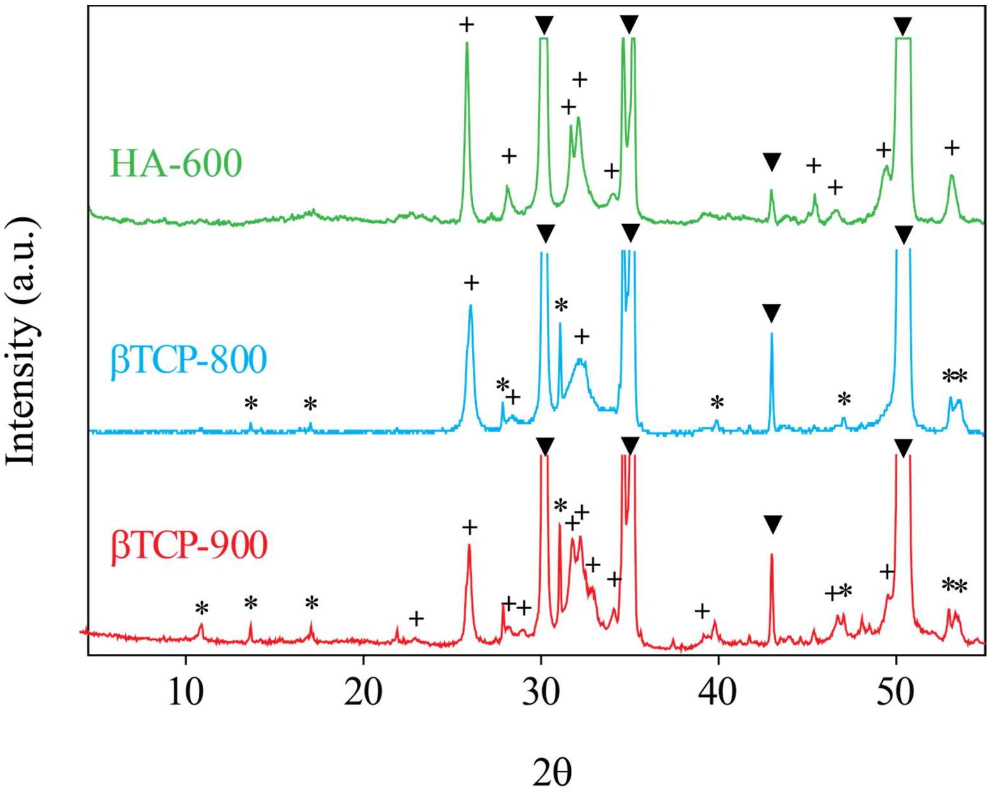

Figure 61. XRD diffractograms of zirconia substrates with different CaP coatings after immersion in SBF for 7 days (HA-600, βTCP-800) and 2 months (βTCP-900). Note the appearance of diffraction lines typical for the HA structure in the case of theβTCP-800 and βTCP-900 coating. ▼ Tetragonal zirconia; * β-TCP; + HA.

5 Discussion

5.1 Biomimetic synthesis of calcium phosphate coatings on zirconia ceramics

First step of the biomimetic synthesis

In the first step of the synthesis, after 1 h of immersion in the CPS1, a thin apatite seeding layer was deposited on the zirconia substrate. In addition to the heterogeneous nucleation on the layer on the zirconia substrate, a homogenous precipitation of HA crystals also occurred in the solution, resulting in its cloudy appearance. The precipitation was accompanied by a pH decrease. The shape of the pH curve is similar to the one obtained by Ofir et al. [153], but the pH changes are far less pronounced because we used buffered solutions in our experiments. Stage I was characterized by a constant pH (Figure 9) and lasted for 40 min. The first CaP phase that precipitates from neutral and alkaline calcium phosphate solutions is usually amorphous CaP (ACP) and depending on the solution's temperature, pH, reactant concentration and the impurities present, the amorphous phase can transform into either OCP or apatite [157]. Under the conditions used in the first step of our synthesis, i.e., pH=7.4 and 37 °C, ACP is likely to be formed initially. The results of the FTIR NGIA analysis confirmed this assumption. The spectrum of the precipitates that formed on a substrate after 20 min (stage I) of immersion in CPS1 matches that of ACP. The precipitation of ACP is usually accompanied by a slight decrease in pH [153]. However, as mentioned above, due to buffered reaction solution, a pH decrease was not detected in stage I. The analysis of the precipitates after 45 min of immersion (stage II) showed that OCP formed on the substrate. The formation of OCP, as described by Equation 5, is accompanied by a pH decrease:

$$8Ca^{2+} + 6HPO_4^{2-} + 5H_2O \rightarrow Ca_8H_2(PO_4)_6 \cdot 5H_2O + 4H^+ \qquad [13]$$

In stage III, the OCP/CDHA transformation took place. This event was not accompanied by a pH change, which indicates that the transformation occurred through the reorganization of ions in the OCP crystal lattice, resulting in the exclusion of H_2O and HPO_4^{2-} ions from the crystal lattice, as proposed by Eanes et al. [157].

Second step of the biomimetic synthesis

The seeding CDHA layer deposited in the first step (Figure 12) later served as a template for the secondary nucleation of CaP during the second step of the synthesis. Moreover, it enabled the formation of a homogeneous coating over the entire surface of the zirconia substrate. Figure 62 illustrates the impact of this layer on the structure of the final coating. When the substrate was immersed in CPS2 without the first step, only individual CaP agglomerates with a lamellar morphology formed on its surface. Furthermore, a thin CDHA seeding layer could also additionally accelerate the nucleation of CaP crystals in the second step of synthesis by dissolving and increasing the degree of supersaturation in the local environment.

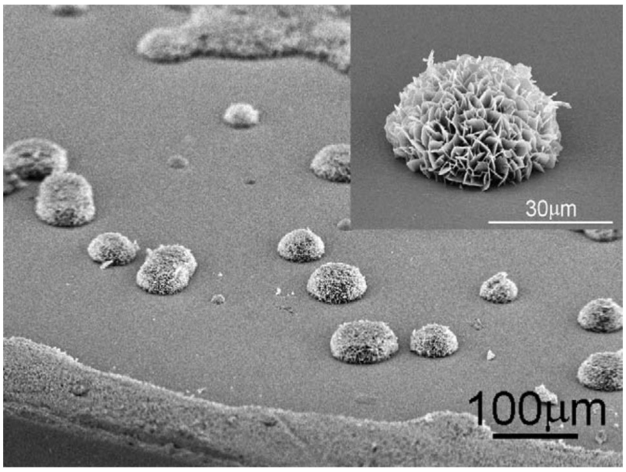

Figure 62. SEM image of the substrate that was immersed in CPS2 for 24 h without pre-immersion in CPS1. Only individual CaP islands are formed on the surface.

The pH drop of the CPS2 solution (Figure 15) during the second step of the synthesis is consistent with the formation of both CDHA and OCP, as described by Equations 5 and 6.

$$10\ Ca^{2+} + 6\ PO_4^{3-} + 2OH^- \rightarrow Ca_{10-x}(HPO_4)_x(PO_4)_{6-x}(OH)_{2-x} \qquad [14]$$

HA is thermodynamically the most stable phase in the CPS2 solution, while other phases, such as the OCP, DCPD and ACP phases, are kinetically more favourable [158]. At first glance, the composition of our layered coating tends to contradict this theory, since at the beginning of the reaction, when the supersaturation level of the CPS2 was higher, the thermodynamically more stable CDHA was deposited on the substrate and after a certain time of the reaction, when the supersaturation level of the CPS2 was lower, the kinetically more stable OCP started to precipitate. A similar phenomenon was observed by Reiner et al. [159] who studied the wet-chemical precipitation of biomimetic CaP coatings on a titanium substrate in different supersaturated CaP reaction solutions (5X SBF). Their hypothesis was that, initially, the OCP nucleation rate is higher than the crystal growth rate and, as a result, a large number of very small OCP crystals are formed, which are quickly transformed into CDHA by the hydrolysis reaction. Due to the depletion of ions with the propagating reaction, the solution becomes less supersaturated with respect to the OCP and when a certain critical supersaturation is reached, the nucleation of OCP becomes impossible and crystal growth becomes the dominant mechanism. Consequently, large crystals form, which are less prone to hydrolysis. This mechanism could be the reason for the deposition of a layered (CDHA/OCP) biomimetic CaP coating in the CPS2 solution studied in this thesis.

As can already be assumed from the SEM images (Figure 16), the biomimetic CaP coating possesses a high surface roughness and specific surface area. AFM and the stereometrical method were applied to obtain characteristic parameters of the surface topography (Table 8). From the comparison between the AFM image (Figure 25) and the SEM image (Figure 16) of the coating it is clear that the AFM technique is not precise enough to detect the whole surface of the lamellas that constitute the coating. The AFM image is obtained by scanning the surface with the sharp tip, but due to the finite aspect ratio of the tip the end of the tip does not reach the whole surface of lamellas. The obtained AFM image therefore does not reflect properly the surface of lamellas and it is more flattened compared to the real surface. Therefore, the lamellar crystals in the AFM scan image (Figure 25 and Figure 37) do not have a sharp-edged shape. Moreover, the cantilever was not able to detect all the crystals, especially the smaller ones. These limitations of the AFM method significantly affected the S_{dr} value of the coating, which is in reality larger than 145 %. The stereometrical analysis gave more accurate values about the S_{dr} value of the coating since all the crystals that constitute the upper part of the biomimetic CaP coating were considered. As a result the S_{dr} value increased to 900 %. The main drawback of the stereometrical analysis lies in the determination of the dimensions of the lamellar crystals. While from the SEM images we could easily determine the thickness w of lamellar crystals, we could not determine their height and the angles of their geometric shape, due to the fact that the density of crystals within the coating was very high and individual crystals were obscured by other crystals. In addition, the crystals were very brittle and when trying to isolate and analyse individual lamella by scrapping-off the coating, the crystals were severely damaged and it was impossible to obtain any information about their dimensions. Therefore, for the sake of an easier calculation of S_{dr} we approximated that the lamellae have the shape of a square with an edge *w*.

The developed biomimetic procedure is also efficient for the deposition of a CaP coating on other bioinert materials used in medicine for the regeneration of bone defects. As demonstrated in Figure 26, the OCP layer was successfully deposited on various ceramic, metallic and polymer substrates. A clear benefit of the synthesis procedure is its ability to coat polymers, which is impossible to achieve with high-temperature procedures, such as plasma spraying. Moreover, a homogenous CaP coating was deposited selectively on individual fibres that constitute the porous polymer scaffolds and also in the interior of the scaffolds, regardless on their chemical composition. Moreover, the coating did not close the pores of the scaffold, which is crucial for providing cell migration and vascularisation across the scaffold.

An important property of CaP bioceramics, which has a strong influence on their biological performance, is their dissolution in a physiological environment. During dissolution, the degradation products of calcium phosphate bioceramics (calcium and phosphate ions) are naturally metabolized and they do not induce abnormal calcium or phosphate levels in urine, serum, or organs [160]. The biomimetic CaP coating exhibited high solubility in a physiological solution. As can be seen in Figure 31, the dissolution rate in PBS remained almost linear for a period of 24 hours. It is believed that the high solubility of CaP bioceramics phases is the key reason for their bone-bonding ability [8, 161-162]. Various studies have shown that Ca^{2+} and phosphate ions released in the biological fluid have a strong influence on the behaviour of osteoprogenitor cells and bone cells (osteoblasts and osteoclasts), affecting their proliferation, adhesion and differentiation and consequently have an influence on de novo bone formation. Moreover, liberated Ca^{2+} and phosphate ions increase the supersaturation level in the microenvironment of the biological fluid, causing precipitation of the biological apatite on the surface of the CaP implant, which is considered as a key element for the bone-bonding ability of implants [7, 72, 117]. Hence, the high dissolution rate of the biomimetic OCP coating may be the reason for the precipitation of HA crystals on its surface after 4 days of immersion in SBF (Figure 29). The deposited HA crystals had a characteristic morphology and composition of biological-like HA. Due to the fact that the

EDS analysis detected Mg^{2+} and Na^{+} ions in the deposited HA layer, it can be assumed that these ions were incorporated into the crystal lattice of the HA crystals, which is typical for HA crystals present in bone [8].

Besides the bioactive characteristics, another benefit of the biomimetic CaP coating could be the strong improvement of the zirconia surface's wettability. As can be observed in Figure 32, the contact angle of a water droplet on zirconia was markedly reduced from 64° (uncoated zirconia) to 2.5° for the coated zirconia, revealing the superhydrophilic character of the biomimetic CaP coating. The high wettability of the coating can be attributed to its high surface roughness. It is known that surface roughness has a considerable influence on the contact angle and that increased surface roughness can amplify the hydrophobic or hydrophilic nature of the surface. Since CaP are hydrophilic the increase in surface roughness of the CaP material will result in increased hydrophilicity and a reduced contact angle of a water droplet [163]. Various in vitro and in vivo studies have clearly related the improved biological response of bone implants to increased hydrophilicity [61-63, 164-167]. The surface wettability of implants influences the degree of contact with body fluids and therefore, more hydrophilic surfaces seem more desirable than hydrophobic ones in view of their interactions with proteins, cells and tissues.

Yet another important aspect of the application of CaP coatings on load-bearing implants is their mechanical stability and bonding to the substrate. The CaP coatings on the load-bearing implants must survive the forces acting during handling and during the implantation of the implant in the bone in order to perform their bioactive function at the site of the surgical installation. For this purpose, good mechanical stability of the CaP coatings on the load-bearing implants is of great importance. The tape test (ASTM D-3359) showed that biomimetic CaP coatings on zirconia have good adhesion to the substrate and on a 0 to 5 scale described in the standard it could be classified as 4B, which corresponds to a very good adhesion.

The scratch test is intended to assess the mechanical integrity, failure modes, and practical adhesion strength of a coating on a substrate. The test method does not measure the fundamental adhesion strength between the coating and the substrate but rather provides the critical load (L_c) at which the failure occurs at the substrate-coating interface or in the coating [168]. In this study we determined L_c as the load where the coating was removed from the substrate in the scratch groove and the substrate became visible. The L_c for the biomimetic CaP coating was 5.3 ± 0.6 N. We could not find any data in the literature about the scratch testing of CaP coatings on zirconia substrates. In contrast, there have been many reports about the scratch testing of CaP coatings on metallic substrates and a few studies focused on biomimetic CaP coatings on titanium [169-172]. The reported L_c for the CaP coatings on metallic substrates obtained with various coating technologies ranged from 1 N to 30 N [117, 171, 173]. Wang et al. [169] reported on an L_c between 9 N and 12 N for biomimetic CaP coatings with a similar lamellar morphology on a titanium substrate, which is comparable with the L_c for the biomimetic CaP coating that was investigated here.

According to some opinions the pull-out tensile test is inappropriate for coatings thinner than 380 µm due to possible penetration of the adhesive through the porous coating to the substrate-coating interface, which could result in inaccurate measurements of the coating-substrate bonding strength [116]. Despite this, several authors applied the method to test the adhesion of thin coatings [170, 174-175]. In the present study relevant information about the coating's adhesion was successfully obtained using this method due to the fact that the epoxy adhesive did not penetrate through the biomimetic CaP to the substrate, which was proven by the SEM analysis. The biomimetic CaP fractured at the substrate-adhesive interface during the tensile test, suggesting that the cohesive strength of the coating was stronger than the interfacial bond strength. The tensile strength of biomimetic CaP coatings on deposited zirconia is low (≈1.8 MPa) and comparable to the bond strength of biomimetic CaP coatings on titanium [132, 174].

Since CaP coatings experience combined shear, tensile and compressive stresses in vivo, the tape test, tensile test and scratch test represent an over simplification of the in vivo situation [116]. For this purpose, implantation of the CaP-coated implants into the bone [176-177] or artificial bone [177] and characterization of the implant's surface after explantation have been proposed as a valuable method for an evaluation of the mechanical properties of CaP coatings since it provides more realistic information about the mechanical behaviour of the coatings in vivo. The mechanical strength of the biomimetic CaP coatings was not sufficient to withstand the forces present during the implantation. The SEM analysis of the implant's surface after the test revealed that a large portion of the coating was removed with only a thin and dense CaP layer remaining on the ceramic surface. In addition, cracking and severe delaminations of the coating were observed on the tips of the implant threads. Only 36 % ± 9 % of the coating mass remained on the implant after the insertion. Hagi et al. [177] obtained a similar result for the biomimetic coatings on titanium implants. In their experiments, they used less dense artificial bone (density: 32 g/cm^3) from the same manufacturer and prepared their biomimetic CaP coatings according to a different wet-chemical biomimetic procedure by applying 5X-SBF as the reaction solution. In their study, the percentage of the biomimetic coating remaining on the implants after im- and explantation from the artificial bone was 39 % ± 13 %.

Among the mechanical tests applied, only the results of the tape test imply good properties of the biomimetic CaP coatings. The other three methods applied indicate the low mechanical strength of biomimetic CaP coatings. The scratch test, tensile test and implantation test appear more appropriate than tape test for testing the adhesion of the CaP coating since they give more realistic informations about the CaP coating adhesion.

The obtained results show that a biomimetic CaP coating on zirconia possesses promising biological characteristics and could elicit a favourable biological response from the surrounding tissue after implantation and improve the bone anchorage of the zirconia implant by establishing chemical bonds across the bone-implant interface. Nevertheless, they possess low mechanical strength, which could be a limiting factor for their application in clinics.

5.2 Post-deposition processing of biomimetic calcium phosphate coatings

The second part of my doctoral research was devoted to the development of novel CaP coatings by applying post-deposition processing of the biomimetic CaP coatings and to the characterization of the complex phase-transformations occurring in the CaP coating during heating. Moreover, particular attention was given to the development of CaP coatings with good adhesion to the zirconia substrate, which would be able to withstand the mechanical stresses present during the handling and implantation in the bone.

There have been many attempts to improve the adhesion of CaP coatings prepared by various wet-chemical biomimetic procedures. An often reported approach is the surface treatment of substrates prior to the immersion in the reaction solution in order to introduce more functional groups on the substrate's surface and improve the chemical bonding between the substrate and the coating [174, 178-181]. Another possible approach is post-deposition processing. For example, thermal annealing is a well-established procedure for improving the crystallinity and adhesion of sprayed or sputtered Ca-P coatings [117, 182-185]. In contrast, the post-deposition processing of biomimetic CaP coatings has not been substantially studied. To the best of our knowledge there have only been two reports on the post-deposition thermal processing of biomimetic CaP coating [68, 186], and only one of them focused on an improvement of the coating adhesion [68]. Probably the main reason, why it has not been explored more, is the fact that a key advantage of the biomimetic coatings is their compositional and morphological resemblance with bone apatite and to act as a carrier of drugs, which are sensitive to high temperatures.

5.2.1 Composition

The biomimetic CaP coating was composed of two distinct phases, i. e. lower CDHA and upper OCP. While coatings with a similar structure have already been reported and described before [159, 187-188] there have not yet been any reports on the characterization of such coatings after thermal treatments. However, thermal studies have been performed separately on both CDHA and OCP, and mostly on powders. Therefore, the results of this doctoral work that are related to the heating of biomimetic CaP coating will be compared to previous studies that were dealing with the heating of CaP powders.

With respect to the composition of our biomimetic coating and previous studies on the thermal behaviour of CDHA and OCP, one could expect that heating between 600 ºC and 900 ºC will result in the formation of a coating with HA (600 ºC) and β-TCP (800 ºC, 900 ºC) crystal structure, respectively, and with the presence of $P_2O_7^{4-}$ groups in all cases. Moreover, according to the literature, a higher content of $P_2O_7^{4-}$ for the samples fired at 600 ºC would be anticipated [110-111, 113, 189-190]. After heating the CDHA with a Ca/P ratio 1.5 above 900 ºC a complete conversion of $P_2O_7^{4-}$ to PO_4^{3-} takes place, resulting in the formation of pure β-TCP without the presence of CPP [112-113, 191]. There have not been any reports on heating OCP at temperatures higher than 900 ºC. Nevertheless, due to the fact that OCP heated at 900 °C is composed of CPP and β-TCP [111], one can expect that heating at higher temperatures will, like in the case of CDHA (≈1.5), result in the formation of pure β-TCP.

As expected from the literature, the FTIR analysis showed that the heating of a biomimetic CaP coating at 600 ºC resulted in the formation of a coating that was composed of HA and CPP (HA-600) (Figure 38). The broad water band at 3600 cm^{-1} disappeared, suggesting that the crystal-bound water was removed during heating. The XRD diffractogram of the HA-600 coating partly correlated with the FTIR analysis and displayed peaks at positions typical for the HA crystal structure, but no peaks typical for crystalline CPP were observed (Figure 42).

According to the literature reports an amorphous, γ or β crystal structure of CPP could be anticipated upon heating the biomimetic CaP coating at 600 °C [103, 111, 190, 192]. The fact that γ- or β-CPP peaks could not be observed on the XRD diffractogram of the HA-600 suggests that CPP exists in an amorphous form (Figure 42). Another result that supports the formation of an amorphous CPP phase in the coating after heating at 600 ºC was the much higher solubility of the CPP compared to the coating that was prepared by heating the biomimetic CaP at 800 ºC (Figure 57, Figure 59). For the latter, the XRD analysis showed that it contains crystalline β-CPP (Figure 38). After the HA-600 coating was immersed in water for three days the typical CPP bands at ≈740 cm^{-1} and ≈1200 cm^{-1} completely disappeared from the FTIR spectrum. In contrast, in the case of the coating that was heated at 800 °C and which contains crystalline β-CPP, no reduction in the CPP signals was observed after six days of immersion in water, indicating that crystalline β-CPP in these coating is much less soluble when compared to the CPP phase present in the HA-600 coating (Figure 59).

The heating of the biomimetic CaP coating at 800 ºC and 900 ºC resulted in the formation of a crystalline mixture of β-TCP and β-CPP and after heating at 1100 ºC and 1200 ºC β-TCP was found as the only phase present in the coating, which matches with the other reports from the literature (Figure 42)[111, 155, 189]. The heating of the biomimetic CaP coating did not affect the morphology of the coating up to 600 ºC (Figure 37). At higher temperatures, an increase in the temperature was accompanied by a significant change in the morphology of coating (Figure 40). The temperature range where the lamellar morphology started to collapse overlaps with the range at which the reaction between HA and CPP takes place for the formation of β-TCP. Structural rearrangements that occurred during the formation of β-TCP were accompanied by a change in the coating morphology. The heating of the biomimetic CaP coating between 800 ºC and 1200 ºC caused a reduction in the mechanical stability of the upper part of the coating and after applying a small force to the coating, such as a stream of tap water or sonication, it could easily be removed from the substrate with only a thin β-TCP layer remaining on the surface of the zirconia. This thin β-TCP layer was used in our subsequent studies (Figure 44, Figure 45, Figure 46 and Figure 47). It was formed from CDHA nanocrystals with an average size of 6 nm (Figure 23) that constituted the lower part of the biomimetic CaP coating and which transformed to β-TCP during heat treatment (Figure 24).

While the β-TCP crystal structure of the coating remained stable in the range between 800 ºC and 1200 ºC (Figure 43), the topography of the β-TCP coating was changing with heating regime, i.e. heating temperature, rate and dwell time. The βTCP-800 coating was composed of particles that formed a reticular morphology and exhibited a roughness in the nanometre range (R_a=46 ± 5 nm). There have not been any reports in the literature about the preparation of β-TCP coating with such a reticular morphology. Heating at higher temperatures (900 ºC – 1200 ºC) resulted in fully dense coatings which were composed of grains (Figure 45, Figure 46, Figure 47). The grain size and the surface roughness of the coating were increasing by increasing the temperature of the heating (Table 9).

Regardless of the composition of the implant, the surface topography is considered as a critical component in achieving implant stability for sufficient osseointegration [16]. The smooth or machined implant surfaces used in the past, which possessed macro-range and micro-range surface roughness, have been replaced by modified surfaces, which also include topographic features in the nanometre range. Moreover, a possible common mechanism behind the strong bone response to many new implants is a nano-roughness pattern [16]. The surface topographies of the CaP coatings that were studied here strongly varied in the sense of surface roughness (Ra), developed surface area (Sdr) and texture (Table 9). The biomimetic CaP and HA-600 coatings had a lamellar morphology and exhibited the highest surface roughness. Due to the fact that coatings with similar topography have already been studied before, the influence of such a lamellar topography on the biological response can be predicted on the basis of previous works. Various studies have shown that such a lamellar topography is beneficial for the adhesion, proliferation and differentiation of cells [169, 193] and strongly improves the osseointegration of metal implants [194-196]. Moreover, Habibovic et al. [197] demonstrated that CaP coatings with a lamellar morphology on various kinds of porous metal and polymer implants can induce the bone formation in a muscle, thus revealing their osteoinductive potential. Nevertheless, a possible drawback for biomimetic CaP and HA-600 coatings could be the observation that they completely covered the micrometer-range surface features of the underlying implants (Figure 52, Figure 36). The micrometre-range roughness of implants is crucial for providing the mechanical interlocking between the mineralized bone and the surface of the implant after the implantation [24]. Moreover, the final topography of the coating, which will be in a contact with bone tissue and body fluids after surgical installation, is questionable, since the experiment of implantation in the artificial bone revealed that the coating topography is considerably changed after the implantation in the artificial bone (Figure 52, Figure 36).

We could not find any reports in the literature about the preparation of CaP coatings with a topography similar to β-TCP coatings (βTCP-800, βTCP-900, βTCP-1100, βTCP-1200). Therefore, the prediction of a biological response based on their topography is much harder than in the case of the biomimetic CaP and HA-600 coatings. When applied on the zirconia implant, it also covered the micrometre-range surface features of the underlying implant's surface (Figure 52). In contrast to biomimetic CaP and HA-600 coatings, βTCP-800 and βTCP-900 coatings followed the topography of the underlying implant and did not interrupt its micrometre-range topography (Figure 53). Among the studied CaP coatings, βTCP-800 and βTCP-900 presented the lowest surface roughness ($R_a \approx 40–50$ nm) (Table 9). Roughness in the nanometer range could be an advantage and may have a strong impact on the protein adsorption and implant osseointegration. Webster et al. [198] demonstrated that nano-rough materials had higher adsorption capacities for the proteins vitronectin and fibronectin, which are extra-cellular matrix proteins that play a key role in cell adhesion, growth, migration and differentiation [199-200]. The higher adsorption capacity for these proteins resulted in enhanced osteoblast attachment, compared to conventional micro-rough materials. Moreover, various studies showed that nano-structured materials decrease inflammation as well as accelerate wound healing and angiogenesis around implants [25]. Kondo et al. [201] prepared porous β-TCP bone implant in the shape of a block with the reticular morphology similar to the βTCP-800 coating and in vivo tests in dogs and rats demonstrated have a strong potential to repair critical-size defects and an osteoinductive capacity. Nevertheless, there are still big differences between their material and the βTCP-800 coating, since their implant was a porous β-TCP monolith and therefore precautions should be taken when comparing the two materials. The post-deposition processing procedures of biomimetic CaP coating, that we developed and studied, allow the possibility to control the surface topography of the CaP coatings. Although we studied the topography of only seven different CaP coatings on zirconia, obviously even more different topographies can be obtained by controlling the heating regime, i.e., heating rate and dwell time. For example, prolonging the dwell time at 900 °C from 1 hour to 9 hours results in the formation of a β-TCP coating with increased grain size. Moreover, by increasing the heating rate to a temperature of 800 °C from 300 °C/h to 600 °C/h, a more porous β-TCP coating with reticular morphology can be obtained (Figure 48). The ability to control the topography of the CaP coating on implants could represent a great benefit for future applications of coatings since the topography can be tailored to elicit the optimal biological response. At this stage it is impossible to predict which topography would be optimal to induce the best biological response. Further in vitro and possibly in vivo biological tests would be necessary to get informations about the optimal topography of CaP coatings on a zirconia implant.

Another important surface property of implants that it is believed to play a major role in the process of healing and osseointegration, is their surface chemistry [24, 202-203]. There is a vast number of reports in the literature that relate the favourable biological response of CaP bioceramics to their chemistry. Therefore, it can be expected that the CaP coatings developed and studied in this doctoral work will elicit favourable response from cells after implantation and enhance the osseointegration of zirconia implants.

5.2.2 Mechanical properties

Tensile test

As seen from Table 10, the post-deposition processing of biomimetic coatings resulted in a significant improvement of the CaP coating's bond strength to the substrate. All the coatings exhibited a statistically higher bond strength than the biomimetic CaP coating. Heating at 600 °C resulted in slightly higher bond strength compared to the biomimetic CaP coating (3.2 MPa vs. 1.8 MPa). In contrast, thin βTCP-800 and βTCP-900 coatings demonstrated a substantially higher bond strength. During the tensile testing of βTCP-900 a fracture occurred at the coating-substrate interface, while in the case of βTCP-800 coating the fracture occurred at the coating-adhesive interface, indicating that the actual bond strength of βTCP-800 coating is even higher than 47.8 ± 4.7 MPa. Fractures at the CaP coating-adhesive interface during tensile testing have already been reported [175, 204-205]. In order to obtain the actual value about the bond strength of βTCP-800 coating could be the usage of a different adhesive, surface treatment of the metallic rod that was used to pull-out the coating, different measuring conditions etc. Heating at higher temperatures, i.e. 1100 °C and 1200 °C, did not change the composition of the coatings but had a strong impact on their adhesion. The measured bond strength of the βTCP-1100 and βTCP-1200 coatings was ≈20 MPa, which is approximately half of the value of the βTCP-800 and βTCP-900 coatings.

Scratch test

Among the CaP coatings, which were prepared by post-deposition processing of the biomimetic CaP coating, only the βTCP-900 coating was tested with a scratch test. As in the case of the biomimetic CaP coating, the L_c was determined as the load where the coating was removed from the substrate in the scratch groove and the substrate became visible. The βTCP-900 coating exhibited much better scratch resistance than the biomimetic CaP coating and during scratch propagation the β-TCP coating deformed plastically without being fully detached from the substrate, even at a load of 120 N. The L_c measured for the βTCP-900 coating was higher than those reported in the literature for chemically deposited apatite coatings (13 N) [170], electrolytically deposited CaP coatings (12 N [169] and 20 N [170]), plasma-sprayed CaP coatings (22N) [169] and PLD-deposited CaP coatings (9.6 N) [171], where also a Rockwell C diamond stylus of 200-µm radius was used in the tests. Nevertheless, it is hard to compare the absolute values of L_c for different coatings because of the differences in terms of roughness, thickness, morphology, crystallinity, homogeneity, substrate used, etc.

Implantation and explantation of implants from the artificial bone and pig's cadaver bone

The experiment of im- and explantation of coated zirconia implants in the artificial bone have shown marked differences in the mechanical properties between the different CaP coatings. When the HA-600 coating was screwed into the artificial bone the damage that occurred to the coating was similar to the one observed for the biomimetic CaP coating (Figure 52). The lamellar crystals were completely removed from the coating over the entire surface area of the implant and on a few spots on the tips of the implant threads the coating was completely removed and the zirconia substrate became exposed. The βTCP-800 and βTCP-900 coatings demonstrated better resistance towards the forces present during implantation when compared to other CaP coatings and were not removed from the substrate (Figure 53). The only defects observed for the βTCP-900 coating were squashings on a few spots which could also be the reason for the observed loss in the mass of the coating. In contrast, crystals that constitute the βTCP-800 coating were damaged during the implantation experiment and they exhibited an internal structure composed of nanocrystals (Figure 53). The fact that the TEM/ED analysis of these nanocrystals (Figure 54) showed that they have a β-TCP crystal structure, indicates that β-TCP nanocrystals are splintered fragments that formed from β-TCP monocrystals (Figure

44) as a consequence of mechanical forces present during implantation in the artificial bone. To the best of our knowledge, there have not been any reports on such a tribological behaviour of β-TCP or any other CaP phase until now. It can be expected that such β-TCP nanocrystals are more soluble compared to larger β-TCP monocrystals due to the higher surface-to-volume ratio. The formation of nanocrystals upon surgical installation of β-TCP coated implant in the bone could have a beneficial effect on the implant osseointegration due to the larger amount of Ca^{2+} and phosphate ions released in the surrounding tissue.

In order to test the βTCP-800 coating in a more realistic situation, the commercial titanium implant with the βTCP-800 coating was implanted in the pig's cadaver jaw bone by the surgeon under the standard procedure for the said implant and afterwards it was immediately explanted. The fact that no form of βTCP-800 coating damage could be observed suggests that the mechanical loading during screwing and unscrewing of the coated ceramic implant in the artificial bone was different than in the real situation. In order to compare the forces present during implantation in the real or artificial bone a newton-meter should be used to measure the torque forces present during drilling. In addition, the utilization of the newton-meter could also reduce the deviation in the loss of the coating mass during implantation among the parallels in the individual experimental group. However, the reason for deviation in the coating damage may not be only in the application of different forces during screwing since different substrates used in the implantation experiments and different conditions during implantation (dry conditions in the case of artificial bone and the presence of blood and biological molecules in the case of cadaver's bone) could also significantly contribute to the difference in the mechanical behaviour of the βTCP-800 coating upon implantation. The advantage of the implantation in the artificial bone compared to the cadaver's bone is its simplicity from the point of view that it is more practical procedure and that the characterization of the implant after the experiment is easier. The remains of the polyurethane on the implant after the experiment could be easily removed by washing the implant in water. In contrast, after implantation in a cadaver's bone and a thorough cleaning in an ultrasound bath, the majority of the implant was still covered with a layer of adherent biological tissue. Hence, a quantification of the loss of a coating mass after im- and explantation is hampered.

The different mechanical tests showed that the βTCP-800 and βTCP-900 coatings possess an excellent mechanical strength. Such a mechanical strength can be attributed to the formation of strong chemical bonds at the substrate-coating interface during the heat treatment and to the formation of dense, defect-free and uniform coatings.

A possible explanation for the lower bond strength of the βTCP-1100 and βTCP-1200 compared to βTCP-800 and βTCP-900 coatings could be the heating at higher temperature, resulting in the evolution of higher residual stresses in the coatings and increased tendencies for coating debonding. The residual stresses develop in the CaP coatings due to a mismatch in the coefficients of thermal expansions (CTE) between the zirconia substrate (10 ppmK^{-1} [206]) and the β-TCP (13 ppmK^{-1} [207]) coating. Moreover, at temperatures between 1100 °C and 1200 °C β-TCP reversibly transforms to α-TCP, which has a considerably higher CTE (60 ppm K^{-1} [207]). Due to a mismatch in the CTE a considerable residual tensile stress is induced in the coating upon cooling, which can result in a formation of cracks and reduced coating adhesion at the interface [77]. The thermal stress, σ_{Rt}, can be calculated using Equation 7 [208].

$$\sigma_{Rt} = \frac{\Delta\alpha \cdot \Delta T \cdot E_c}{1 - v_c} \qquad [15]$$

where Δα is the difference of CTE between the CaP coating and the zirconia substrate (=3 ppmK^{-1}), ΔT is the temperature difference between ambient temperature and the heating temperature, E_f is the Young's modulus of the coating (60 GPa [209]) and ν is the Poisson's ratio of the β-TCP coating (0.24 [210]).

According to Equation 7 the increase in heating temperature will result in an increase of the residual tensile stresses in the coating upon cooling. For example, the σ_{rt} of the β-TCP coatings heated at 800 °C was 185 MPa and for the coatings that were heated at 1200 ºC, the σ_{rt} was 280 MPa. The mismatch in the CTE has been frequently reported for the reduced adhesion of CaP coatings on titanium [211-215] and for bioglass coatings on zirconia and alumina ceramics [77, 89].

The reduced bond strength of βTCP-1100 and βTCP-1200 coatings compared to βTCP-900 was accompanied by the appearance of a monoclinic zirconia phase (Figure 43). However, on the basis of the obtained results, the direct relation between these two quantities cannot be established. Krajewski et al. [85] also reported on the formation of a monoclinic zirconia phase upon heating of a silica-based biological glass coating on a zirconia (Y-TZP) substrate. After heating of glass-coated zirconia at 1300 °C a large amount of monoclinic phase formed together with the $CaZrO_3$ and $ZrSiO_4$. They suggested that the reason for the formation of a monoclinic phase was the permeation of the glass into the zirconia microstructure and the partial dissolution of zirconia grains, which was accompanied by the dispersion of Y_2O_3 in the glass phase. As a result, in the cooling stage, the ZrO_2 inside the vitreous bulk tended to crystallize, but because it did not have a sufficient amount of Y_2O_3 ions to stabilize the network, it was crystallized directly in its monoclinic form. Nevertheless, they did not perform any additional experiments to confirm or reject these assumptions. This mechanism cannot be an explanation for our system (β-TCP coatings on zirconia), since there is no glassy phase in the coating in which zirconia would dissolve.

Kim et al.[216] also observed changes in the zirconia (Y-TZP) substrates after heating HA-coated zirconia substrates at 1100 °C and 1200 °C. They deposited HA coating on a zirconia using the slurry-dipping method and heated the coated substrates between 1000 °C and 1300 °C to consolidate the coating and improve its adhesion. Based on the XRD analyses (Figure 63) they concluded that additional $CaZrO_3$ phases form at the zirconia-coating interface. However, it should be mentioned that their observation of $CaZrO_3$ in the XRD diffractogram is based only on one low intensity peak ($2\theta = 31.4°$) which overlaps with the peak of monoclinic zirconia and which was present in the diffractograms of the βTCP-1100 and βTCP-1200 coatings studied in this doctoral work. Due to the fact that the XRD diffractograms they showed in the paper include only a narrow 2θ range (28.5°–33.5°) where the peak of the monoclinic zirconia overlaps with the $CaZrO_3$ peak, the presence of a monoclinic zirconia in their samples cannot be excluded.

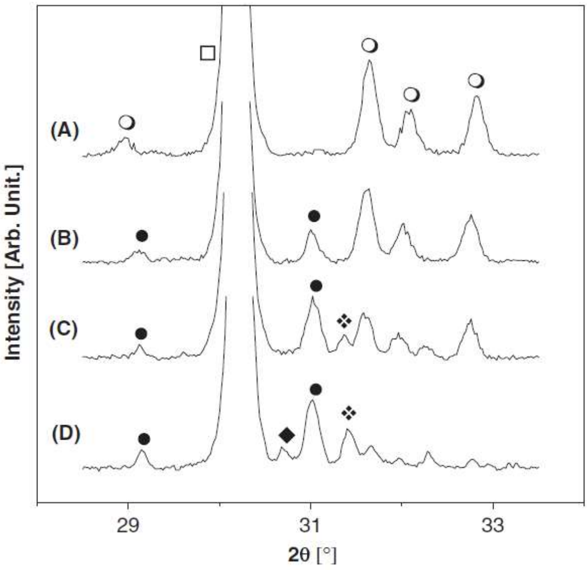

Figure 63. XRD diffractograms of HA layers on zirconia substrates after heat treatment at various temperatures: (A) 1000 °C, (B) 1100 °C, (C) 1200 °C, and (D) 1300 °C: (o) HA, (●) TCP, (□) tetragonal ZrO_2, and (❖) $CaZrO_3$. The study was performed by Kim et al. [216].

Klopčič et al. [217] also observed the transformation of zirconia from tetragonal to monoclinic form after heating the composite of $CaTi_4(PO_4)_6$ (CTP) and tetragonal zirconia (Y-TZP). After heating the composite at 1280 ºC they observed the formation of a large amount of monoclinic zirconia phase together with YPO_4. They concluded that the consumption of Y_2O_3 doping for the formation of YPO_4 was the reason for the transformation of the tetragonal zirconia to the monoclinic phase upon cooling. However, due to the fact that YPO_4 peaks were not observed in the XRD diffractograms of the βTCP-1100 and βTCP-1200 coatings this mechanism cannot be attributed to our system.

Kosmač and Dakskobler [218] prepared layered composites of tricalcium phosphate (TCP) and Y-TZP and sintered them at 1300 ºC. They did not observe the formation of monoclinic phase upon heat treatment. Moreover, during autoclaving in water at 200 ºC for 24 hours no transformation of the tetragonal zirconia to the monoclinic phase took place, indicating full stability of the porous zirconia layers in these composites under hydrothermal conditions.

Obviously, complex events take place during the heating of biomimetic CaP coatings at 1100 °C and 1200 °C. On the basis of the results obtained during this doctoral work, the mechanisms underlying the relatively low bond strength of the βTCP-1100 and βTCP-1200 coatings compared to βTCP-800, βTCP-900 and the formation of the monoclinic zirconia cannot be explained. Further work will need to be performed to understand and explain these phenomena.

5.2.3 Dissolution in physiological solution

Post-deposition processing of the biomimetic CaP coating had a substantial impact on the dissolution rate of the CaP coatings in PBS. As can be observed in Figure 57 and Figure 58 the dissolution of the HA-600 coating was higher when compared to a biomimetic CaP coating while the dissolution of all the β-TCP coatings was much lower. The higher dissolution of the HA-600 can be attributed to the presence of a highly soluble CPP phase in the coating. Moreover, the HA-600 coating exhibited a progressive reduction in the Ca^{2+} release rate. While in the first 9 h of immersion the HA-600 coating exhibited a higher dissolution rate than the biomimetic CaP coating, after longer immersion times the Ca^{2+} release rate from the HA-600 coating was considerably reduced and lower than in the case of the biomimetic CaP coating. The reason for the higher solubility of HA-600 in the first 9 h could be the presence of the highly soluble CPP phase. In contrast to the HA-

600 coating, the biomimetic CaP coating exhibited a constant dissolution rate during the whole experiment resulting in a linear dissolution profile. In the last measuring interval, which was 5 h long, the amount of Ca^{2+} released from the biomimetic CaP coating (47 ng/mm^2) was significantly higher than in the case of HA-600 (23 ng/mm^2). A possible explanation for the constant dissolution rate of biomimetic CaP and non-linear dissolution rate of HA-600 could be that the biomimetic CaP coating is uniform and mainly composed of OCP crystals while the HA-600 coating contains a highly soluble CPP phase besides the HA crystals. The dissolution of the β-TCP coatings was much lower than in the case of the HA-600 and biomimetic CaP coatings (Figure 58). The dissolution rate sequence of the β-TCP coatings was: βTCP-1200 > βTCP-1100 > βTCP-800 > βTCP-900. From the comparison between the dissolution rates and the values of the surface topography (Table 2) it can be observed that the increase in the coating S_{dr} results in the increase in the coating's dissolution rate. Clearly, the dissolution rate of the β-TCP coatings is related to the area of the coating in contact with the PBS solution.

5.2.4 Test of bioactivity

HA-600, βTCP-800 and βTCP-900 coatings were tested for bioactivity with the in vitro SBF test [219]. All the CaP coatings tested exhibited an apatite-forming ability in SBF. The ability of the material to induce apatite nucleation in the SBF has been proposed as a method for testing the bone-bonding ability of materials (bioactivity). Despite the fact that the experiments with SBF represent a simplification of the real in vivo situation and that many authors expressed concerns regarding the method [20-21], it has been frequently used and became a widely accepted approach for testing the bioactivity of materials. According to the results of the SBF test, the prepared CaP coatings could improve the bone anchorage of the zirconia implant by establishing chemical bonds across the bone-implant interface. The SBF test showed differences among the tested CaP coatings. While the HA layer formed on the HA-600 and βTCP-800 after 7 days of immersion in SBF, it did not form on the βTCP-900 even after 21 days of immersion. This observation could indicate that βTCP-900 coating is less bioactive compared to the other coatings. However, precaution should be taken when interpreting the results of the SBF test due to the reported inconsistencies, particularly related to the reactions of β-TCP ceramics in SBF and in vivo. Several studies revealed that β-TCP ceramics do not form apatite on the surface in SBF, but despite this bond to a living bone in vivo [19]. Hence, in order to accurately predict the performance of β-TCP-coated zirconia implants in humans, more biological tests would need to be conducted.

6 Conclusions

In my doctoral work I developed a biomimetic procedure for the deposition of calcium phosphate (CaP) coatings on zirconia ceramics. The benefits of the synthesis procedure are its simplicity, reproducibility and a high deposition rate. The synthesis procedure involved two steps. In the first step, zirconia substrates were immersed in the supersaturated CaP solution with a pH = 7.4 and after 1 hour of soaking a thin (200 nm) calcium hydroxyapatite (HA) seeding layer formed on the zirconia substrates. This deposition took place in three stages: i) precipitation of an amorphous CaP; ii) precipitation of octacalcium phosphate (OCP); iii) transformation of the OCP to the HA. The subsequent immersion of these coated zirconia substrates in a fresh solution with a similar composition but a lower pH (pH = 7.0) led to a rapid growth of the biomimetic CaP coating (second step). After 11 hours of immersion in this solution a 12 μm-thick biomimetic CaP coating with a lamellar topography was deposited on the zirconia. It had a lamellar topography and its average surface roughness (R_a) was 800 nm. It was composed of two layers. The lower part of the coating was composed of HA nanocrystals with an average size of 6 nm, while the upper layer was composed of octacalcium phosphate (OCP) monocrystals that had a lamellar shape. The deposited biomimetic CaP coating on the zirconia was superhydrophilic and had a constant dissolution rate in a physiological solution. After the immersion of the zirconia substrates with biomimetic CaP coatings in a simulated body fluid, the biological-like HA crystals precipitated on their surface, implying the bioactive capacity of the biomimetic CaP coating. The bond strength of the biomimetic CaP coating to the zirconia substrate was 1.8 MPa, which represents a relatively low adhesion for applications in clinics.

The thermal treatment of the biomimetic CaP coating at temperatures between 600 °C and 1200 °C induced complex phase transformations in the original biomimetic CaP coating and changed its surface topography. After heating at 600 °C the lamellar topography of the coating was preserved, but the phase composition of the coating was changed to a mixture of HA and calcium pyrophosphate (CPP). Moreover, coatings that were heated at 600 °C exhibited a higher dissolution rate in the physiological solution than the biomimetic CaP coating due to the presence of the highly soluble CPP phase. Heating between 800 °C and 1200 °C resulted in a gradual loss of the lamellar topography. After heating at 800 °C and 900 °C the coatings were composed of β-tricalcium phosphate (β-TCP) and β-CPP, and after heating at 1100 °C and 1200 °C the β-TCP was the only phase present in the coating.

By applying a short ultra-sound treatment to the coatings that were heated between 800 °C and 1200 °C a majority of the upper part of the coating was removed, such that only a thin β-TCP coating with good adhesion was obtained on the zirconia substrate. The surface roughness of this thin β-TCP coating, as well as its dissolution rate in a physiological solution could be controlled by regulating the heating regime and the end temperature. An increase in the heating temperature resulted in an increase of the R_a value of the coating, from about 50 nm (800 °C and 900 °C) to 370 nm (1200 °C), and in an enhanced coating dissolution rate. Moreover, the heat treatment improved the adhesion of the CaP coatings to the zirconia substrate, thereby confirming the initial hypothesis. The bond strength of the coating after heating at 600 °C was 3.2 MPa. The thin β-TCP coatings prepared by heating at 800 °C and 900 °C and the subsequent sonication exhibited the highest adhesion, with a bond strength of approximately 50 MPa. The bond strength of the β-TCP coatings prepared by heating at 1100 °C and 1200 °C was lower and reached values of approximately 30 MPa.

7 Acknowledgements

I would like to express my sincere gratitude to my supervisor and mentor, Prof. Dr. Tomaž Kosmač for his guidance and patience during my doctoral studies, and for all the discussions and advices.

I would like to thank my co-supervisor, Asst. Prof. Kristoffer Krnel, for valuable discussions and useful suggestions.

I would like to acknowledge various people who have contributed to my research and to the work presented herein. I would like to thank all my co-workers at the Engineering Ceramics Department for their help and valuable discussions. I would like to thank Darko Eterovič and Roman Bevc for their technical assistance. I would like to thank Dr. Irena Pribošič for TEM analyses and for introducing me to the science of calcium phosphates in the beginning of my doctoral studies. I would like to extend my thanks to Asst. Prof. Goran Dražič and Janez Zavašnik for TEM analyses, Asst. Prof. Srečo Škapin and Dejan Klement for XRD measurements, Dr. Marjeta Maček Kržmanc for TG-DTA measurements, Asst. Prof. Miha Škarabot and Dr. Hana Uršič Nemevšek for AFM analyses, Dr. Mira Polajnar for protein quantification, Prof. Dr. Boris Orel and Dr. Angela Šurca Vuk for FTIR analyses, Prof. Dr. Radmila Milačič for AAS measurements, Dr. Paskvale, Asst. Prof. Čekada and Prof. Dr. Peter Panjan for their help with the mechanical testing of CaP coatings. I would also like to thank Prof. Dr. Ralf Kohal and Dr. Brigitte Altmann for performing the biological tests on my samples. Thank you Lovro, my room-mate, for all the fruitful discussions and for being a nice company.

I would like to thank the committee members for devoting their time to read the dissertation and for their valuable suggestions.

I would also like to thank my family and friends for their love and support. Lastly, I would like to thank to Andreja for her continued support, encouragement, patience and for love and understanding throughout my doctoral studies.

8 References

[1] Ratner, B. D.; Hoffman, A. S.; Schoen, F. J.; Lemons, J. E. Biomaterials Science: An Introduction to Materials in Medicine (Academic Press, New York, 1996).

[2] Ratner, B. D.; Bryant, S. J. Biomaterials: where we have been and where we are going. *Annual Review of Biomedical Engineering* **6**, 41–75 (2004).

[3] Hench, L. L.; Polak, J. M. Third-generation biomedical materials. *Science* **295**, 1014–1017 (2002).

[4] Navarro, M.; Michiardi, A.; Castaño, O.; Planell, J. A. Biomaterials in orthopaedics. *Journal of the Royal Society Interface* **5**, 1137–1158 (2008).

[5] Hench, L. L.; Wilson, J. Introduction. In: *An introduction to bioceramics*. 1–24 (World Scientific, London, 1999).

[6] Osborn, J. F.; Newesely, H. Dynamic aspects of the implant–bone interface. In: *Dental implants*. 111–123 (Carl Hansen Verlag, Munchen Germany, 1980).

[7] Hench, L. L.; Wilson, J. An introduction to bioceramics (World Scientific, London, 1999).

[8] LeGeros, R. Z. Calcium phosphates in oral biology and medicine. *Monographs in Oral Science* **15**, 1–201 (1991).

[9] LeGeros, R. Z. Calcium phosphate-based osteoinductive materials. *Chemical Reviews* **108**, 4742–4753 (2008).

[10] Puleo, D. A.; Nanci, A. Understanding and controlling the bone-implant interface. *Biomaterials* **20**, 2311–2321 (1999).

[11] Paital, R. S.; Dahotre, N. B. Calcium phosphate coatings for bio-implant applications: Materials, performance factors, and methodologies. *Materials science and engineering - R* **66**, 1–70 (2009).

[12] Kingery, W. D.; Uhlmann, D. R.; Bowen, H. K. Introduction to ceramics (Wiley, New York, 1976).

[13] Albee, F. H. Studies in Bone Growth: Triple Calcium Phosphate as a Stimulus to Osteogenesis. *Annals of Surgery* **71**, 32–39 (1920).

[14] Carter, C. B.; Norton, M. G. Ceramics in Biology and Medicine. In: *Ceramic Materials: Science and Engineering*. 635–651 (Springer, New York, 2007).

[15] Chevalier, J.; Gremillard, L. Ceramics for medical applications: A picture for the next 20 years. *Journal of the European Ceramic Society* **29** 1245–1255 (2009).

[16] Wennerberg, A.; Albrektsson, T. Effects of titanium surface topography on bone integration: a systematic review. *Clinical Oral Implants Research* **20**, 172–184 (2009).

[17] Albrektsson, T.; Wennerberg, A. Oral implant surfaces: Part 1–review focusing on topographic and chemical properties of different surfaces and in vivo responses to them. *International Journal of Prosthodontics* **17**, 536–543 (2004).

[18] Anil, S.; Anand, P. S.; Alghamdi, H.; Jansen, J. A. Dental Implant Surface Enhancement and Osseointegration. In: *Implant Dentistry – A Rapidly Evolving Practice*. 83–108 (InTech, Turkyilmz, 2011).

[19] Kokubo, T. *In vitro* evaluation of bone bioactivity In: *Bioceramics and their clinical applications*. 165–182 (Woodhead Publishing Cambridge, 2008).

[20] Bohner, M.; Lemaitre, J. Can bioactivity be tested in vitro with SBF solution? *Biomaterials* **30**, 2175–2179 (2009).

[21] Pan, H. B.; Zhao, X. L.; Darvell, B. W.; Lu, W. W. Apatite-formation ability - Predictor of "bioactivity"? *Acta Biomaterialia* **6**, 4181–4188 (2010).

[22] Kim, K.-h.; Narayanan, R.; Rautray, T. R. Surface Modification of Titanium for Biomaterial Applications (Biomaterials - Properties, Production and Devices) (Nova Science Pub Inc, 2010).

[23] Tomsia, A. P. et al. Nanotechnology approaches to improve dental implants. *International Journal of Oral and Maxillofacial Implants* **26**, 25–44; discussion 45–29 (2011).

[24] Le Guehennec, L.; Soueidan, A.; Layrolle, P.; Amouriq, Y. Surface treatments of titanium dental implants for rapid osseointegration. *Dental Materials* **23**, 844–854 (2007).

[25] Ainslie, K. M.; Thakar, R. G.; Bernards, D. A.; Desai, T. A. Inflammatory Response to Implanted Nanostructured Materials: Understanding and Controlling Protein, Cell, and Tissue Responses. In: *Biological Interactions on Materials Surfaces*. 356–372 (Springer, New York, 2009).

[26] Blaschke, C.; Volz, U. Soft and hard tissue response to zirconium dioxide dental implants - A clinical study in man. *Neuroendocrinology Letters* **27**, 69–72 (2006).

[27] Kohal, R. J.; Weng, D.; Bachle, M.; Strub, J. R. Loaded custom-made zirconia and titanium implants show similar osseointegration: an animal experiment. *Journal of Periodontology* **75**, 1262–1268 (2004).

[28] Kohal, R. J. et al. In vitro reaction of human osteoblasts on alumina-toughened zirconia. *Clinical Oral Implants Research* **20**, 1265–1271 (2009).

[29] Bachle, M. et al. Behavior of CAL72 osteoblast-like cells cultured on zirconia ceramics with different surface topographies. *Clinical Oral Implants Research* **18**, 53–59 (2007).

[30] Gahlert, M. et al. Biomechanical and histomorphometric comparison between zirconia implants with varying surface textures and a titanium implant in the

maxilla of miniature pigs. *Clinical Oral Implants Research* **18**, 662–668 (2007).

[31] Hoffmann, O.; Angelov, N.; Zafiropoulos, G. G.; Andreana, S. Osseointegration of zirconia implants with different surface characteristics: an evaluation in rabbits. *International Journal of Oral and Maxillofacial Implants* **27**, 352–358 (2012).

[32] Schliephake, H. et al. Mechanical anchorage and peri-implant bone formation of surface–modified zirconia in minipigs. *Journal of Clinical Periodontology* **37**, 818–828 (2010).

[33] Wang, G. C.; Liu, X. Y.; Zreiqat, H.; Ding, C. X. Enhanced effects of nano-scale topography on the bioactivity and osteoblast behaviors of micron rough ZrO2 coatings. *Colloids and Surfaces B-Biointerfaces* **86**, 267–274 (2011).

[34] Hempel, U. et al. Response of osteoblast-like SAOS-2 cells to zirconia ceramics with different surface topographies. *Clinical Oral Implants Research* **21**, 174–181 (2010).

[35] Sennerby, L.; Dasmah, A.; Larsson, B.; Iverhed, M. Bone tissue responses to surface-modified zirconia implants: A histomorphometric and removal torque study in the rabbit. *Clinical Implant Dentistry and Related Research* **7**, S13–S20 (2005).

[36] Oliva, J.; Oliva, X. V.; Oliva, J. D. One-year follow-up of first consecutive 100 zirconia dental implants in humans: A comparison of 2 different rough surfaces. *International Journal of Oral & Maxillofacial Implants* **22**, 430–435 (2007).

[37] Park, Y. S.; Cung, S. H.; Shon, W. J. Peri-implant bone formation and surface characteristics of rough surface zirconia implants manufactured by powder injection molding technique in rabbit tibiae. *Clinical Oral Implants Research* **24**, 586–591 (2012).

[38] Delgado-Ruiz, R. A. et al. Femtosecond laser microstructuring of zirconia dental implants. *Journal of Biomedical Materials Research Part B–Applied Biomaterials* **96B**, 91–100 (2011).

[39] Barsch, N. et al. Femtosecond laser microstructuring of hot-isostatically pressed zirconia ceramic. *Journal of Laser Applications* **19**, 107–115 (2007).

[40] Kosmac, T. et al. Strength and reliability of surface treated Y-TZP dental ceramics. *Journal of Biomedical Materials Research* **53**, 304–313 (2000).

[41] Piconi, C.; Maccauro, G. Zirconia as a ceramic biomaterial. *Biomaterials* **20**, 1–25 (1999).

[42] Hao, L. et al. The formation of a hydroxyl bond and the effects thereof on bone-like apatite formation on a magnesia partially stabilized zirconia (MgO-PSZ) bioceramic following CO_2 laser irradiation. *Journal of Materials Science-Materials in Medicine* **15**, 967–975 (2004).

[43] Hao, L.; Lawrence, J.; Chian, K. S. Osteoblast cell adhesion on a laser modified zirconia based bioceramic. *Journal of Materials Science-Materials in Medicine* **16**, 719–726 (2005).

[44] Webster, T. J. et al. Enhanced functions of osteoblasts on nanophase ceramics. *Biomaterials* **21**, 1803–1810 (2000).

[45] Namavar, F. et al. Lotus effect in engineered zirconia. *Nano Letters* **8**, 988–996 (2008).

[46] Sabirianov, R. F.; Rubinstein, A.; Namavar, F. Enhanced initial protein adsorption on engineered nanostructured cubic zirconia. *Physical Chemistry Chemical Physics* **13**, 6597–6609 (2011).

[47] Tanahashi, M.; Matsuda, T. Surface functional group dependence on apatite formation on self-assembled monolayers in a simulated body fluid. *Journal of Biomedical Materials Research* **34**, 305–315 (1997).

[48] Uchida, M. et al. Apatite-forming ability of a zirconia/alumina nano-composite induced by chemical treatment. *Journal of Biomedical Materials Research* **60**, 277–282 (2002).

[49] Faga, M. G. et al. Chemical treatment on alumina-zirconia composites inducing apatite formation with maintained mechanical properties. *Journal of the European Ceramic Society* **32**, 2113–2120 (2012).

[50] Fischer, H. et al. Bioactivation of inert alumina ceramics by hydroxylation. *Biomaterials* **26**, 6151–6157 (2005).

[51] Li, P. J. et al. The Role of Hydrated Silica, Titania, and Alumina in Inducing Apatite on Implants. *Journal of Biomedical Materials Research* **28**, 7–15 (1994).

[52] He, X.; Zhang, Y. Z.; Mansell, J. P.; Su, B. Zirconia toughened alumina ceramic foams for potential bone graft applications: fabrication, bioactivation, and cellular responses. *ournal of Materials Science-Materials in Medicine* **19**, 2743–2749 (2008).

[53] Bertazzo, S.; Rezwan, K. Control of alpha-Alumina Surface Charge with Carboxylic Acids. *Langmuir* **26**, 3364–3371 (2009).

[54] Bertran, C. A.; Bertazzo, S.; Almeida, L. L.; Souza, A. V. Hydroxyapatite Formation on Alumina Surface Modified by Aluminoxane. *Key Engineering Materials* **330–332**, 753–756 (2007).

[55] Bertazzo, S. et al. Bioactivation of alumina by surface modification: a possibility for improving the applicability of alumina in bone and oral repair. *Clinical Oral Implants Research* **20**, 288–293 (2009).

[56] Liang, H. et al. Bioactivity of Mg-ion-implanted zirconia and titanium. *Applied Surface Science* **253**, 3326–3333 (2007).

[57] Zhao, Q. et al. Surface modification of Al2O3 bioceramic by NH2+ ion implantation. *Biomaterials* **20**, 595–599 (1999).

[58] Zreiqat, H.; Evans, P.; Howlett, C. R. Effect of surface chemical modification of bioceramic on phenotype of human bone-derived cells. *Journal of Biomedical Materials Research* **44**, 389–396 (1999).

[59] Zreiqat, H. et al. Mechanisms of magnesium-stimulated adhesion of osteoblastic cells to commonly used orthopaedic implants. *Journal of Biomedical Materials Research* **62**, 175–184 (2002).

[60] Liang, H. et al. Enhanced calcium phosphate precipitation on the surface of mg-ion-implanted ZrO2 bioceramic. *Surface Review and Letters* **14**, 71–77 (2007).

[61] Att, W. et al. Enhanced osteoblast function on ultraviolet light-treated zirconia. *Biomaterials* **30**, 1273–1280 (2009).

[62] Wang, R. et al. Light-induced amphiphilic surfaces. *Nature* **388**, 431–432 (1997).

[63] Aita, H. et al. The effect of ultraviolet functionalization of titanium on integration with bone. *Biomaterials* **30**, 1015–1025 (2009).

[64] Cortes, D. A.; Nogiwa, A. A.; Almanza, J. M.; Ortega, S. Biomimetic apatite coating on Mg-PSZ/Al2O3 composites. Effect of the immersion method. *Materials Letters* **59**, 1352–1355 (2005).

[65] Kokubo, T. Apatite formation on surfaces of ceramics, metals and polymers in body environment. *Acta Materialia* **46**, 2519–2527 (1998).

[66] Rambo, C. R. et al. Biomimetic apatite coating on biomorphous alumina scaffolds. *Materials Science & Engineering C-Biomimetic and Supramolecular Systems* **26**, 92–99 (2006).

[67] Klopcic, S. B.; Kovac, J.; Kosmac, T. Apatite-forming ability of alumina and zirconia ceramics in a supersaturated Ca/P solution. *Biomolecular Engineering* **24**, 467–471 (2007).

[68] Pribosic, I.; Klopcic, S. B.; Kosmac, T. Biomimetic Preparation and Characterization of Bioactive Coatings on Alumina and Zirconia Ceramics. *Journal of the American Ceramic Society* **93**, 288–294 (2010).

[69] Bigi, A. et al. Nanocrystalline hydroxyapatite coatings on titanium: a new fast biomimetic method. *Biomaterials* **26**, 4085–4089 (2005).

[70] Jiang, G. W.; Shi, D. L. Coating of hydroxyapatite on porous alumina substrate through a thermal decomposition method. *Journal of Biomedical Materials Research* **48**, 117–120 (1999).

[71] Jiang, G. W.; Shi, D. G. Coating of hydroxyapatite on highly porous Al2O3 substrate for bone substitutes. *Journal of Biomedical Materials Research* **43**, 77–81 (1998).

[72] Kim, H. W. et al. Calcium phosphates and glass composite coatings on zirconia for enhanced biocompatibility. *Biomaterials* **25**, 4203–4213 (2004).

[73] Wang, Z. Q. et al. Mechanical and biomedical properties of hydroxyapatite-based gradient coating on alpha-Al2O3 ceramic substrate. *Journal of Non–Crystalline Solids* **351**, 1675–1681 (2005).

[74] Suzuki, T. et al. Ability of zirconia double coated with titanium and hydroxyapatite to bond to bone under load-bearing conditions. *Biomaterials* **27**, 996–1002 (2006).

[75] Rocchietta, I. et al. Surface-modified zirconia implants: tissue response in rabbits. *Clinical Oral Implants Research* **20**, 844–850 (2009).

[76] Lee, J. et al. Evaluation of nano-technology-modified zirconia oral implants: a study in rabbits. *Journal of Clinical Periodontology* **36**, 610–617 (2009).

[77] Sola, A.; Bellucci, D.; Cannillo, V.; Cattini, A. Bioactive glass coatings: a review. *Surface Engineering* **27**, 560–572 (2011).

[78] Jones, J. R. Review of bioactive glass: From Hench to hybrids. *Acta Biomaterialia* **9**, 4457–4486 (2013).

[79] Stojanovic, D. et al. Bioactive glass-apatite composite coating for titanium implant synthesized by electrophoretic deposition. *Journal of the European Ceramic Society* **27**, 1595–1599 (2007).

[80] Braem, A. et al. Biofunctionalization of porous titanium coatings through sol-gel impregnation with a bioactive glass-ceramic. *Materials Science & Engineering C-Materials for Biological Applications* **32**, 2292–2298 (2012).

[81] Koller, G. et al. Surface modification of titanium implants using bioactive glasses with air abrasion technologies. *Journal of Materials Science-Materials in Medicine* **18**, 2291–2296 (2007).

[82] Comesana, R. et al. Laser cladding of bioactive glass coatings. *Acta Biomaterialia* **6**, 953–961 (2010).

[83] Borrajo, J. P. et al. In vivo evaluation of titanium implants coated with bioactive glass by pulsed laser deposition. *Journal of Materials Science-Materials in Medicine* **18**, 2371–2376 (2007).

[84] Drnovsek, N. et al. Bioactive glass enhances bone ingrowth into the porous titanium coating on orthopaedic implants. *International Orthopaedics* **36**, 1739–1745 (2012).

[85] Krajewski, A.; Ravaglioli, A.; Mazzocchi, M.; Fini, M. Coating of ZrO_2 supports with a biological glass. *Journal of Materials Science: Materials in Medicine* **9**, 309–316 (1998).

[86] Rahaman, M. N.; Li, Y.; Bal, B. S.; Huang, W. Functionally graded bioactive glass coating on magnesia partially stabilized zirconia (Mg-PSZ) for enhanced biocompatibility. *Journal of Materials Science: Materials in Medicine* **19**, 2325–2333 (2008).

[87] Bosetti, M. et al. In vitro characterisation of zirconia coated by bioactive glass. *Biomaterials* **22**, 987–994 (2001).

[88] Torricelli, P. et al. Biological glass coating on ceramic materials: in vitro evaluation using primary osteoblast cultures from healthy and osteopenic rat bone. *Biomaterials* **22**, 2535–2543 (2001).

[89] Ferraris, M. et al. Coatings on zirconia for medical applications. *Biomaterials* **21**, 765–773 (2000).

[90] Brovarone, C. V.; Verne, E.; Krajewski, A.; Ravaglioli, A. Graded coatings on ceramic substrates for biomedical applications. *Journal of the European Ceramic Society* **21**, 2855–2862 (2001).

[91] Martorana, S.; Fedele, A.; Mazzocchi, M.; Bellosi, A. Surface coatings of bioactive glasses on high strength ceramic composites. *Applied Surface Science* **255**, 6679–6685 (2009).

[92] Kim, C. Y.; Jee, S. S. Hydroxyapatite formation on bioactive-glazed alumina. *Journal of the European Ceramic Society* **23**, 1803–1811 (2003).

[93] Liu, J. L.; Miao, X. G. Sol-gel derived bioglass as a coating material for porous alumina scaffolds. *Ceramics International* **30**, 1781–1785 (2004).

[94] Rosengren, A. et al. Protein adsorption onto two bioactive glass-ceramics. *Biomaterials* **24**, 147–155 (2003).

[95] Stanic, V. et al. Osteointegration of bioactive glass-coated zirconia in healthy bone: an in vivo evaluation. *Biomaterials* **23**, 3833–3841 (2002).

[96] Oliva, J.; Oliva, X.; Oliva, J. Five-year success rate of 831 consecutively placed zirconia dental implants in humans: a comparison of three different rough surfaces. *International Journal of Oral and Maxillofacial Implants* **25**, 336–344 (2010).

[97] Schickle, K. et al. Towards osseointegration of bioinert ceramics: Introducing functional groups to alumina surface by tailored self assembled monolayer technique. *Journal of the European Ceramic Society* **32**, 3063–3071 (2012).

[98] Pelaez-Vargas, A. et al. Isotropic micropatterned silica coatings on zirconia induce guided cell growth for dental implants. *Dental Materials* **27**, 581–589 (2011).

[99] Liu, Y. T.; Lee, T. M.; Lui, T. S. Enhanced Osteoblastic Cell Response on Zirconia by Bio-Inspired Surface Modification. *Colloids and Surfaces B: Biointerfaces* **106**, 37–45 (2013).

[100] Elliot, J. C. Structure and Chemistry of the Apatites and other Calcium Orthophophates. Studies in Inorganic Chemistry (Elsevier, Amsterdam, 1994).

[101] Pan, H.; Darvell, B. W. Effect of Carbonate on Hydroxyapatite Solubility. *Crystal Growth & Design* **10**, 845–850 (2010).

[102] Rey, C.; Combes, C.; Drouet, C.; Somrani, S. Tricalcium phosphate-based ceramics. In: *Bioceramics and their clinical applications*. 326–366 (Woodhead Publishing 2008).

[103] Bian, J. J.; Kim, D. W.; Hong, K. S. Phase transformation and sintering behavior of Ca2P2O7. *Materials Letters* **58**, 347–351 (2004).

[104] Slater, C. et al. Enhanced stability and local structure in biologically relevant amorphous materials containing pyrophosphate. *Journal of Materials Chemistry* **21**, 18783–18791 (2011).

[105] Rosenthal, A. K.; Ryan, L. M. Crystal arthritis: Calcium pyrophosphate

deposition[mdash]nothing 'pseudo' about it! *Nat Rev Rheumatol* **7**, 257–258 (2011).

[106] Zhou, X.; Cui, Y.; Han, J. Phosphate/pyrophosphate and MV-related proteins in mineralisation: discoveries from mouse models. *Int J Biol Sci* **8**, 778–790 (2012).

[107] Bäeuerlein, E.; Behrens, P.; Epple, M. Handbook of Biomineralization: . Medical and clinical aspects (Wiley-VCH, 2007).

[108] Combes, C.; Rey, C. Amorphous calcium phosphates: synthesis, properties and uses in biomaterials. *Acta Biomaterialia* **6**, 3362–3378 (2010).

[109] Champion, E. Sintering of calcium phosphate bioceramics. *Acta Biomaterialia* (2012).

[110] Berry, E. E. The structure and composition of some calcium-deficient apatites. *Journal of Inorganic and Nuclear Chemistry* **29**, 317–327 (1967).

[111] Fowler, B. O.; Moreno, E. C.; Brown, W. E. Infra-red spectra of hydroxyapatite, octacalcium phosphate and pyrolysed octacalcium phosphate. *Archives of Oral Biology* **11**, 477–492 (1966).

[112] Ishikawa, K.; Ducheyne, P.; Radin, S. Determination of the Ca/P ratio in calcium-deficient hydroxyapatite using X-ray diffraction analysis. *Journal of Materials Science: Materials and Medicine* **4**, 165–168 (1993).

[113] Mortier, A.; Lemaitre, J.; Rouxhet, P. G. Temperature-Programmed Characterization of Synthetic Calcium-Deficient Phosphate Apatites. *Thermochimica Acta* **143**, 265–282 (1989).

[114] Nelson, D. G. A.; McLean, J. D. High-resolution electron microscopy of octacalcium phosphate and its hydrolysis products. *Calcified Tissue International* **36**, 219–232 (1984).

[115] LeGeros, R. Z.; LeGeros, J. P. Hydroxyapatite. In: *Bioceramics and their clinical applications*. (Woodhead Publishing Cambridge, 2008).

[116] Leeuwenburgh, S. C. G.; Wolke, J. G. C.; Jansen, J. A. Calcium phosphate coatings. In: *Bioceramics and their clinical applications*. 464–484 (Woodhead Publishing Cambridge, 2008).

[117] León, B.; Jansen, J. Thin Calcium Phosphate Coatings for Medical Implants (Springer, New York, 2009).

[118] Junker, R.; Dimakis, A.; Thoneick, M.; Jansen, J. A. Effects of implant surface coatings and composition on bone integration: a systematic review. *Clinical Oral Implants Research* **20**, 185–206 (2009).

[119] Sarikaya, M. An introduction to biomimetics: a structural viewpoint. *Microscopy Research and Technique* **27**, 360–375 (1994).

[120] Sarikaya, M. et al. Molecular biomimetics: nanotechnology through biology. *Nature Materials* **2**, 577–585 (2003).

[121] Tamerler, C.; Sarikaya, M. Molecular biomimetics: nanotechnology and bionanotechnology using genetically engineered peptides. *Philosophical transactions. Series A, Mathematical, physical, and engineering sciences* **367**, 1705–1726 (2009).

[122] Tamerler, C.; Sarikaya, M. Molecular biomimetics: utilizing nature's molecular ways in practical engineering. *Acta Biomaterialia* **3**, 289–299 (2007).

[123] Abe, Y.; Kokubo, T.; Yamamuro, T. Apatite coating on ceramics, metals and polymers utilizing a biological process. *Journal of Materials Science: Materials in Medicine* **1**, 233–238 (1990).

[124] Jessel, N. et al. Bioactive coatings based on a polyelectrolyte multilayer architecture functionalized by embedded proteins. *Advanced Materials* **15**, 692–695 (2003).

[125] Kokubo, T.; Matsushita, T.; Takadama, H.; Kizuki, T. Development of bioactive materials based on surface chemistry. *Journal of the European Ceramic Society* **29**, 1267–1274 (2009).

[126] Hata, K.; Kokubo, T.; Nakamura, T.; Yamamuro, T. Growth of a Bonelike Apatite Layer on a Substrate by a Biomimetic Process. *Journal of the American Ceramic Society* **78**, 1049–1053 (1995).

[127] Müller, L.; Müller, F. Preparation of SBF with different HCO3- content and its influence on the composition of biomimetic apatites. *Acta Biomaterialia* **2**, 181–189 (2006).

[128] Tas, A. C. Synthesis of biomimetic Ca-hydroxyapatite powders at 37 degrees C in synthetic body fluids. *Biomaterials* **21**, 1429–1438 (2000).

[129] Habibovic, P. et al. Biomimetic hydroxyapatite coating on metal implants. *Journal of the American Ceramic Society* **85**, 517–522 (2002).

[130] Tanahashi, M. et al. Apatite coated on organic polymers by biomimetic process: improvement in adhesion to substrate by HCl treatment *Journal of Materials Science: Materials in Medicine* **6**, 319–326 (1995).

[131] Tanahashi, M. et al. Apatite coated on organic polymers by biomimetic process: improvement in its adhesion to substrate by glow-discharge treatment. *Journal of Biomedical Materials Research* **29**, 349–357 (1995).

[132] Qu, H. B.; Wei, M. Improvement of bonding strength between biomimetic apatite coating and substrate. *Journal of Biomedical Materials Research Part B-Applied Biomaterials* **84B**, 436–443 (2008).

[133] Rigo; Carrodeguas; Zavaglia; Boschi Characterization of biomimetic calcium phosphate coatings on Ti6Al4V alloy. *Revista CENIC Ciencias Químicas* **37**, (2006).

[134] Uchida, M. et al. Structural dependence of apatite formation on titania gels in a simulated body fluid. *Journal of Biomedical Materials Research. Part A* **64**, 164–170 (2003).

[135] Leonor, I. B. et al. Apatite-forming ability of polymers with SO3H groups in SBF.

18th Meeting of the European Society For Biomaterials, Stuttgart, Germany, T027. (2003).

[136] Toworfe, G. K.; Composto, R. J.; Shapiro, I. M.; Ducheyne, P. Nucleation and growth of calcium phosphate on amine-, carboxyl- and hydroxyl-silane self-assembled monolayers. *Biomaterials* **27**, 631–642 (2006).

[137] Himeno, T. et al. Surface structural changes of sintered hydroxyapatite in terms of surface charge. *Bioceramics* **15**, 457–460 (2002).

[138] Kim, H. M. et al. Surface potential change in bioactive titanium metal during the process of apatite formation in simulated body fluid. *Journal of Biomedical Materials Research. Part A* **67**, 1305–1309 (2003).

[139] Mullin, J. W. Crystallization (Butterworth-Heinemann, Woburn, 2001).

[140] Bunker, B. C. et al. Ceramic Thin-Film Formation on Functionalized Interfaces Through Biomimetic Processing. *Science* **264**, 48–55 (1994).

[141] Heughebaert, J. C.; Nancollas, G. H. Mineralization kinetics: The role of octacalcium phosphate in the precipitation of calcium phosphates. *Colloids and Surfaces* **9**, 89–93 (1984).

[142] Koutsoukos, P. G.; Nancollas, G. H. Crystal growth of calcium phosphates - epitaxial considerations. *Journal of Crystal Growth* **53**, 10–19 (1981).

[143] Koutsoukos, P.; Amjad, Z.; Tomson, M. B.; Nancollas, G. H. Crystallization of calcium phosphates. A constant composition study. *Journal of the American Chemical Society* **102**, 1553–1557 (1980).

[144] Nancollas, G. H.; Tomazic, B. Growth of calcium phosphate on hydroxyapatite crystals. Effect of supersaturation and ionic medium. *The Journal of Physical Chemistry* **78**, 2218–2225 (1974).

[145] Wu, W.; Nancollas, G. H. Kinetics of Heterogeneous Nucleation of Calcium Phosphates on Anatase and Rutile Surfaces. *Journal of Colloid and Interface Science* **199**, 206–211 (1998).

[146] Christoffersen, M. R.; Dohrup, J.; Christoffersen, J. Kinetics of growth and dissolution of calcium hydroxyapatite in suspensions with variable calcium to phosphate ratio. *Journal of Crystal Growth* **186**, 283–290 (1998).

[147] Cheng, P.-T.; Pritzker, K. H. Solution Ca/P ratio affects calcium phosphate crystal phases. *Calcified Tissue International* **35**, 596–601 (1983).

[148] Wang, L.; Nancollas, G. H. Calcium orthophosphates: crystallization and dissolution. *Chemical Reviews* **108**, 4628–4669 (2008).

[149] Wu, W.; Nancollas, G. H. Kinetics of nucleation and crystal growth of hydroxyapatite and fluorapatite on titanium oxide surfaces. *Colloids and Surfaces B: Biointerfaces* **10**, 87–94 (1997).

[150] Chow, L. C.; Eanes, E. D. Octacalcium Phosphate (Karger Publishers, Berlin, 2001).

[151] Kališnik, M. Temelji stereologije (Stereologija Yugoslavia, Ljubljana, 1982).

[152] Gonczy, S. T.; Randall, N. An ASTM Standard for Quantitative Scratch Adhesion Testing of Thin, Hard Ceramic Coatings. *International Journal of Applied Ceramic Technology* **2**, 422–428 (2005).

[153] Ofir, P. B.; Lippman, R. G.; Garti, N.; Furedi-Milhofer, H. The Influence of Polyelectrolytes on the Formation and Phase Transformation of Amorphous Calcium Phosphate. *Crystal Growth & Design* **4**, 177–183 (2004).

[154] Fowler, B. O.; Markovic, M.; Brown, W. E. Octacalcium Phosphate .3. Infrared and Raman Vibrational-Spectra. *Chemistry of Materials* **5**, 1417–1423 (1993).

[155] Mortier, A.; Lemaitre, J.; Rodrique, L.; Rouxhet, P. Synthesis and thermal behavior of well-crystallized calcium-deficient phosphate apatite. *Journal of Solid State Chemistry* **78**, 215–219 (1989).

[156] Garvie, R. C.; Nicholson, P. S. Phase Analysis in Zirconia Systems. *Journal of the American Ceramic Society* **55**, 303–305 (1972).

[157] Eanes, E. D.; Chow, L. C. Octacalcium Phopsphate (Karger, Gaithersburg, 2001).

[158] Lu, X.; Leng, Y. Theoretical analysis of calcium phosphate precipitation in simulated body fluid. *Biomaterials* **26** 1097–1108 (2005).

[159] Reiner, T.; Gotman, I. Biomimetic calcium phosphate coating on Ti wires versus flat substrates: structure and mechanism of formation. *Journal of Materials Science: Materials in Medicine* **21**, 515–523 (2010).

[160] Barrere, F.; Van Blitterswijk, C. A.; De Groot, K. Bone regeneration: molecular and cellular interactions with calcium phosphate ceramics. *International Journal of Nanomedicine* **1**, 317–332 (2006).

[161] Ducheyne, P.; Qiu, Q. Bioactive ceramics: the effect of surface reactivity on bone formation and bone cell function. *Biomaterials* **20**, 2287–2303 (1999).

[162] LeGeros, R. Z. Biodegradation and bioresorption of calcium phosphate ceramics. *Clinical Materials* **14**, 65–88 (1993).

[163] Quéré, D. Rough ideas on wetting. *Physica A: Statistical Mechanics and its Applications* **313**, 32–46 (2002).

[164] Donos, N. et al. Gene expression profile of osseointegration of a hydrophilic compared with a hydrophobic microrough implant surface. *Clinical Oral Implants Research* **22**, 365–372 (2011).

[165] He, B.; Wan, Y.; Bei, J.; Wang, S. Synthesis and cell affinity of functionalized poly(l-lactide-co-β-malic acid) with high molecular weight. *Biomaterials* **25**, 5239–5247 (2004).

[166] Ber, S.; Torun Köse, G.; Hasirci, V. Bone tissue engineering on patterned collagen films: an in vitro study. *Biomaterials* **26**, 1977–1986 (2005).

[167] Elias, C. N. Factors Affecting the Success of Dental Implants. In: *Implant Dentistry*

- A Rapidly Evolving Practice. 319–366 (InTech, Turkyilmz, 2011).

[168] Sarin, V. K. Micro-scratch test for adhesion evaluation of thin films. *Journal of Adhesion Science and Technology* **7**, 1265–1278 (1993).

[169] Wang, J.; Layrolle, P.; Stigter, M.; De Groot, K. Biomimetic and electrolytic calcium phosphate coatings on titanium alloy: physicochemical characteristics and cell attachment. *Biomaterials* **25**, 583–592 (2004).

[170] Rohanizadeh, R.; LeGeros, R. Z.; Harsono, M.; Bendavid, A. Adherent apatite coating on titanium substrate using chemical deposition. *Journal of Biomedical Materials Research. Part A* **72**, 428–438 (2005).

[171] Arias, J. L. et al. Micro- and nano-testing of calcium phosphate coatings produced by pulsed laser deposition. *Biomaterials* **24**, 3403–3408 (2003).

[172] Liu, Y. et al. Proteins incorporated into biomimetically prepared calcium phosphate coatings modulate their mechanical strength and dissolution rate. *Biomaterials* **24**, 65–70 (2003).

[173] Barrère, F.; Layrolle, P.; Van Blitterswijk, C. A.; De Groot, K. Physical and chemical characteristics of Plasma-sprayed and Biomimetic Apatite coating. *Bioceramics* **12**, 125–128 (1999).

[174] Kim, H. M.; Miyaji, F.; Kokubo, T.; Nakamura, T. Bonding strength of bonelike apatite layer to Ti metal substrate. *Journal of Biomedical Materials Research* **38**, 121–127 (1997).

[175] Chen, X.; Li, Y.; Hodgson, P. D.; Wen, C. Microstructures and bond strengths of the calcium phosphate coatings formed on titanium from different simulated body fluids. *Materials Science and Engineering C* **29** 165–171 (2009).

[176] Leeuwenburgh, S. C. G. et al. Mechanical properties of porous, electrosprayed calcium phosphate coatings. *Journal of Biomedical Materials Research Part A* **78A**, 558–569 (2006).

[177] Hagi, T. T. et al. Mechanical insertion properties of calcium-phosphate implant coatings. *Clinical Oral Implants Research* **21**, 1214–1222 (2010).

[178] Tanahashi, M. et al. Apatite Coated on Organic Polymers by Biomimetic Process - Improvement in Adhesion to Substrate by Hcl Treatment. *Journal of Materials Science-Materials in Medicine* **6**, 319–326 (1995).

[179] Tanahashi, M. et al. Apatite Coated on Organic Polymers by Biomimetic Process - Improvement in Its Adhesion to Substrate by Naoh Treatment. *Journal of Applied Biomaterials* **5**, 339–347 (1994).

[180] Tanahashi, M. et al. Apatite Coated on Organic Polymers by Biomimetic Process - Improvement in Its Adhesion to Substrate by Glow-Discharge Treatment. *Journal of Biomedical Materials Research* **29**, 349–357 (1995).

[181] Oliveira, A. L. et al. Surface modification tailors the characteristics of biomimetic coatings nucleated on starch-based polymers. *Journal of Materials Science-Materials in Medicine* **10**, 827–835 (1999).

[182] Liu, Y. Introduction of ectopic bone formation by BMP-2 incorporated biomimetically into calcium phosphate coatings of titanium-alloy implants. *Bioceramics* **15**, 667–670 (2002).

[183] Yonggang, Y.; Wolke, J. G.; Yubao, L.; Jansen, J. A. The influence of discharge power and heat treatment on calcium phosphate coatings prepared by RF magnetron sputtering deposition. *Journal of Materials Science: Materials in Medicine* **18**, 1061–1069 (2007).

[184] van Dijk, K.; Schaeken, H. G.; Wolke, J. G. C.; Jansen, J. A. Influence of annealing temperature on RF magnetron sputtered calcium phosphate coatings. *Biomaterials* **17**, 405–410 (1996).

[185] Yang, Y.; Kim, K. H.; Ong, J. L. A review on calcium phosphate coatings produced using a sputtering process-an alternative to plasma spraying. *Biomaterials* **26**, 327–337 (2005).

[186] Forsgren, J.; Svahn, F.; Jarmar, T.; Engqvist, H. Structural change of biomimetic hydroxyapatite coatings due to heat treatment. *Journal of Applied Biomaterials & Biomechanics* **5**, 23–27 (2007).

[187] Barrere, F.; Layrolle, P.; Van Blitterswijk, C. A.; De Groot, K. Biomimetic coatings on titanium: a crystal growth study of octacalcium phosphate. *Journal of Materials Science: Materials in Medicine* **12**, 529–534 (2001).

[188] Reiner, T.; Klinger, L. M.; Gotman, I. Biomimetic Calcium Phosphate Growth over Differently Shaped Ti Substrates: Modeling the Effect of Surface Curvature. *Crystal Growth & Design* **11**, 190–195 (2011).

[189] Raynaud, S.; Champion, E.; Bernache-Assollant, D.; Thomas, P. Calcium phosphate apatites with variable Ca/P atomic ratio I. Synthesis, characterisation and thermal stability of powders. *Biomaterials* **23**, 1065–1072 (2002).

[190] Vasant, S. R.; Joshi, M. J. Synthesis and Characterization of Nanoparticles of Calcium Pyrophosphate. *Modern Physics Letters B* **25**, 53–62 (2011).

[191] Raynaud, S.; Champion, E.; Bernache-Assollant, D.; Thomas, P. Calcium phosphate apatites with variable Ca/P atomic ratio I. Synthesis, characterisation and thermal stability of powders. *Biomaterials* **23**, 1065–1072 (2002).

[192] Ning, C. Q.; Greish, Y.; El-Ghannam, A. Crystallization behavior of silica-calcium phosphate biocomposites: XRD and FTIR studies. *Journal of Materials Science-Materials in Medicine* **15**, 1227–1235 (2004).

[193] Choi, J. et al. Calcium phosphate coating of nickel–titanium shape-memory alloys. Coating procedure and adherence of leukocytes and platelets. *Biomaterials* **24**, 3689–3696 (2003).

[194] Barrere, F. et al. Osteogenecity of octacalcium phosphate coatings applied on porous metal implants. *Journal of Biomedical Materials Research. Part A* **66**, 779–788 (2003).

[195] Barrere, F. et al. Osteointegration of biomimetic apatite coating applied onto dense and porous metal implants in femurs of goats. *Journal of Biomedical Materials*

Research. Part B, Applied Biomaterials **67**, 655–665 (2003).

[196] Habibovic, P. et al. Biological performance of uncoated and octacalcium phosphate-coated Ti6Al4V. *Biomaterials* **26**, 23–36 (2005).

[197] Habibovic, P. et al. Influence of octacalcium phosphate coating on osteoinductive properties of biomaterials. *Journal of Materials Science: Materials in Medicine* **15**, 373–380 (2004).

[198] Webster, T. J. et al. Specific proteins mediate enhanced osteoblast adhesion on nanophase ceramics. *Journal of Biomedical Materials Research* **51**, 475–483 (2000).

[199] Preissner, K. T. Structure and Biological Role of Vitronectin. *Annual Review of Cell Biology* **7**, 275–310 (1991).

[200] Pankov, R.; Yamada, K. Fibronectin at a glance. *Journal of Cell Science* **115**, 3861–3863. (2002).

[201] Kondo, N. et al. Osteoinduction with highly purified beta-tricalcium phosphate in dog dorsal muscles and the proliferation of osteoclasts before heterotopic bone formation. *Biomaterials* **27**, 4419–4427 (2006).

[202] Wennerberg, A.; Albrektsson, T. Structural influence from calcium phosphate coatings and its possible effect on enhanced bone integration. *Acta Odontologica Scandinavica* **67**, 333–340 (2009).

[203] Wennerberg, A.; Albrektsson, T. On implant surfaces: a review of current knowledge and opinions. *International Journal of Oral and Maxillofacial Implants* **25**, 63–74 (2010).

[204] Kim, H.-W. et al. Sol–gel derived fluor-hydroxyapatite biocoatings on zirconia substrate. *Biomaterials* **25**, 2919–2926 (2004).

[205] Piveteau, L.-D.; Gasser, B.; Schlapbach, L. Evaluating mechanical adhesion of sol–gel titanium dioxide coatings containing calcium phosphate for metal implant application. *Biomaterials* **21**, 2193–2201 (2000).

[206] Swain, M. V. Unstable cracking (chipping) of veneering porcelain on all-ceramic dental crowns and fixed partial dentures. *Acta Biomaterialia* **5**, 1668–1677 (2009).

[207] Ravaglioli, A.; Krajewski, A. Bioceramics and biological glasses. In: *Integrated Biomaterials Science*. 189–252 (Springer, New York, 2002).

[208] Hausner, H. H. Modern Developments in Powder Metallurgy (Plenum Press, Michigan, 1971).

[209] Wang, C. X.; Zhou, X.; Wang, M. Influence of sintering temperatures on hardness and Young's modulus of tricalcium phosphate bioceramic by nanoindentation technique. *Materials Characterization* **52**, 301–307 (2004).

[210] Mazel, V.; Busignies, V.; Diarra, H.; Tchoreloff, P. Measurements of elastic moduli of pharmaceutical compacts: A new methodology using double compaction on a compaction simulator. *Journal of Pharmaceutical Sciences* **101**, 2220–2228

(2012).

[211] Liu, D.; Savino, K.; Yates, M. Z. Coating of hydroxyapatite films on metal substrates by seeded hydrothermal deposition. *Surface and Coatings Technology* **205**, 3975–3986 (2011).

[212] Sergo, V.; Sbaizero, O.; Clarke, D. R. Mechanical and chemical consequences of the residual stresses in plasma sprayed hydroxyapatite coatings. *Biomaterials* **18**, 477–482 (1997).

[213] Brown, S. R.; Turner, I. G.; Reiter, H. Residual stress measurement in thermal sprayed hydroxyapatite coatings. *Journal of Materials Science: Materials in Medicine* **5**, 756–759 (1994).

[214] Yang, Y.-C. Influence of residual stress on bonding strength of the plasma-sprayed hydroxyapatite coating after the vacuum heat treatment. *Surface and Coatings Technology* **201**, 7187–7193 (2007).

[215] Yang, Y. C.; Chang, E.; Hwang, B. H.; Lee, S. Y. Biaxial residual stress states of plasma-sprayed hydroxyapatite coatings on titanium alloy substrate. *Biomaterials* **21**, 1327–1337 (2000).

[216] Kim, H.-W.; Yoon, B.-H.; Koh, Y.-H.; Kim, H.-E. Processing and Performance of Hydroxyapatite/Fluorapatite Double Layer Coating on Zirconia by the Powder Slurry Method. *Journal of the American Ceramic Society* **89**, 2466–2472 (2006).

[217] Klopčič, S. B. et al. The Reactivity of $CaTi_4(PO_4)_6$ with Alumina and Y-TZP Ceramics. *Key Engineering Materials* **787**, 361–363 (2007).

[218] Kosmač, T.; Dakskobler, A. The Preparation and Properties of Layered TCP/Y–TZP Composites with Ribbon-Like Microstructures. *Key Engineering Materials* **1145**, 309–311 (2006).

[219] Kokubo, T.; Takadama, H. How useful is SBF in predicting in vivo bone bioactivity? *Biomaterials* **27**, 2907–2915 (2006).

Index of Figures

Index of Tables

Appendix: Publications

[1] Stefanic, M.; Krnel, K.; Pribosic, I.; Kosmac, T. Rapid biomimetic deposition of octacalcium phosphate coatings on zirconia ceramics (Y-TZP) for dental implant applications. *Applied Surface Science* **258**, 4649–4656 (2012).

[2] Stefanic, M.; Krnel, K.; Kosmac, T. Thermal Processing Of Calcium Phosphate Coatings On Zirconia Ceramics. *Key Engineering Materials* **493** 462–466 (2012).

[3] Stefanic, M., Krnel, K., Kosmac, T. Novel method for the synthesis of a bioactive β-tricalcium phosphate coating on a zirconia implant. *Accepted for publication. Journal of the European Ceramic Society* (2013).